

Integrated Microfluidic Liquid-Liquid Extraction for Cocaine Detection in Human Saliva

THÈSE N° 5589 (2012)

PRÉSENTÉE LE 12 DECEMBRE 2012

À LA FACULTÉ DES SCIENCES ET TECHNIQUES DE L'INGÉNIEUR
LABORATOIRE DE CAPTEURS, ACTUATEURS ET MICROSYSTÈMES
PROGRAMME DOCTORAL EN MICROSYSTÈMES ET MICROÉLECTRONIQUE

ÉCOLE POLYTECHNIQUE FÉDÉRALE DE LAUSANNE

POUR L'OBTENTION DU GRADE DE DOCTEUR ÈS SCIENCES

PAR

Philip WÄGLI

acceptée sur proposition du jury:

Prof. J. Brugger, président du jury
Prof. N. de Rooij, Dr A. Homsy, directeurs de thèse
Dr P. Jouy, rapporteur
Dr B. E. Rapp, rapporteur
Prof. H. Shea, rapporteur



ÉCOLE POLYTECHNIQUE
FÉDÉRALE DE LAUSANNE

Suisse
2012

Abstract

On-site drug testing using easily accessible body fluids, such as saliva, has gained a lot of importance both for road safety and forensic applications. However, saliva is a complex, inhomogeneous amalgam with many different compounds, whose concentrations change between people and over time. This leads to a wide range of fluid properties, e.g., viscosity, surface tension, making saliva pretreatment in microfluidic systems extremely challenging. We present the development, fabrication and characterization of a low-cost, portable microsystem to detect cocaine in human saliva. The chip combines multiphase liquid-liquid extraction to transfer the cocaine from the infrared (IR) light absorbing saliva to the IR-transparent solvent, perchloroethylene (PCE), together with on-chip cocaine detection by IR-spectroscopy (IR-laser, waveguide, detector). This miniaturized sensing platform has been developed as part of the Nano-Tera project IrSens.

Saliva is a suitable matrix for the analysis of small molecules such as cocaine, but it is found to be a challenge to process this complex fluid on a microfluidic chip due to the risk of clogging. The characterization of the rheological behavior of saliva is described and then a suitable sample pretreatment method is presented. The low-cost UV-curable polymer NOA81 was chosen as microfluidic chip material and characterized for microfluidic applications. For research applications a new, highly flexible, and low-cost NOA81 rapid prototyping method is presented based on scotch-tape masters. Furthermore, this thesis introduces a microfluidic chip design combining a simple and robust droplet generation method together with a geometry for droplet merging in order to perform continuous droplet-based liquid-liquid extraction. The extraction efficiency of the system was evaluated by state-of-the-art mass spectrometry measurements. The microfluidic chip has been integrated in an optofluidic microsystem transferring cocaine from human saliva to the IR-transparent organic solvent PCE and thereby enabling cocaine detection by IR-spectroscopy.

In this thesis we achieved to develop a simple and robust droplet generation method resulting in precise and controlled droplet sizes, and which allowed to process complex fluids such as human saliva without clogging. Furthermore, a droplet-based liquid-liquid extraction system which transfers the cocaine continuously from human saliva to the organic solvent PCE was established. For these liquids the developed system yielded a two to three times

higher extraction efficiency than state-of-the-art devices. In addition, we demonstrated that our system has the potential for cocaine preconcentration in PCE, which is crucial for IR spectroscopy, our final application.

Keywords: microfluidic, saliva, cocaine, UV-curable adhesive NOA81, rapid prototyping, continuous liquid-liquid extraction, droplet generation, droplet coalescence, IR-spectroscopy

Résumé

Le dépistage sur site de substances psychotropes dans les fluides corporels tels que la salive a gagné en importance de nos jours, car il permet non seulement d'améliorer la sécurité routière, mais aussi les applications en expertises médico-légales. Cependant, la salive est un amalgame complexe et hétérogène avec beaucoup de composants différents, dont les concentrations changent selon les individus et au fil du temps. Cela conduit à une large gamme de propriétés fluidiques, comme par exemple la viscosité ou la tension superficielle, ce qui rend le traitement de la salive dans les systèmes microfluidiques extrêmement difficile. Dans cette thèse, nous présentons le développement, la fabrication et la caractérisation d'un micro-système portable et à faible coût, pour la détection quantitative de la cocaïne dans la salive humaine. Cette puce est la combinaison d'un procédé microfluidique d'extraction multiphasique de la cocaïne à partir de la salive vers un solvant transparent à l'infrarouge (IR), le perchloroéthylène (PCE), avec la détection de la cocaïne par spectroscopie IR (laser IR, guide d'ondes, détecteur). Cette plate-forme miniaturisée de détection a été développée dans le cadre du projet Nano-Tera IrSens.

La salive est une matrice appropriée pour l'analyse de petites molécules telles que la cocaïne, mais le véritable défi consiste à traiter ce fluide complexe dans une puce microfluidique en raison du risque d'obstruction des canaux. Le comportement rhéologique de la salive est présenté ainsi que notre méthode de prétraitement d'échantillons adapté pour notre puce microfluidique. L'adhésif UV photosensible NOA81 a été choisi comme matériau à faible coût pour la puce, et a été caractérisé pour nos applications microfluidiques. Une méthode de prototypage rapide, flexible et à faible coût est présentée sur la base de moules réalisés avec des bandes adhésives. En outre, cette thèse présente une structure simple pour la génération robuste de gouttelettes qui permet de manipuler les liquides complexes sans obstruer nos micro-canaux. Un système microfluidique est présenté, intégrant la génération de gouttelettes et une géométrie pour la coalescence de ces gouttelettes, de façon à effectuer l'extraction liquide-liquide à base des gouttelettes d'une manière continue. L'efficacité d'extraction de notre système a été évaluée par une méthode d'analyse de pointe, le spectromètre de masse. Le système microfluidique présenté a ensuite été intégré dans un système optofluidique qui transfère la cocaïne de la salive humaine au solvant organique PCE et qui permet de détecter la cocaïne par spectroscopie IR.

Dans cette thèse les résultats à souligner sont multiples. Une méthode robuste de génération de gouttelettes résultant sur des tailles de gouttelettes précises et contrôlées a été développée. En particulier cette méthode permet de manipuler les fluides complexes comme la salive humaine, sans obstruction de nos micro-canaux. De plus, un système d'extraction liquide-liquide a été réalisé permettant le transfert continu de la cocaïne à partir de la salive vers le solvant organique PCE. Notre système montre une efficacité d'extraction au moins deux à trois fois supérieure à celle de l'état de l'art. Notre système présente même un potentiel pour la préconcentration, ce qui s'avère crucial pour notre application finale, la spectroscopie IR.

Mots-clés : microfluidique, salive, cocaïne, colle photosensible UV NOA81, prototypage rapide, extraction liquide-liquide continue, génération de gouttelettes, coalescence de gouttelettes, spectroscopie infrarouge

Zusammenfassung

Die Vor-Ort Analyse leicht zugänglicher Körperflüssigkeiten wie Speichel hat sowohl im Zusammenhang mit der Strassenverkehrssicherheit als auch für forensische Anwendungen stark an Bedeutung gewonnen. Allerdings ist Speichel eine komplexe, inhomogene Flüssigkeit, bestehend aus vielen verschiedenen Bestandteilen, deren Konzentrationen zeitlich und zwischen verschiedenen Personen variieren. Dies führt zu starken Veränderungen der Flüssigkeitseigenschaften, wie zum Beispiel der Viskosität oder der Oberflächenspannung, was das Analysieren von Speichel in einem Mikrofluidiksystem extrem erschwert. Wir präsentieren hier die Entwicklung, Herstellung und Charakterisierung eines kostengünstigen, portablen Mikrosystems zum Nachweis von Kokain im menschlichen Speichel. Der hier vorgestellte Mikrofluidikchip verbindet dazu eine mehrphasen Flüssig-Flüssigextraktion (um das Kokain vom Infrarotlicht absorbierenden Speichel in das infrarottransparente Lösungsmittel Perchloroethylen (PCE) zu transferieren), mit einer auf dem Mikrochip integrierten Kokaindetektion mittels Infrarotspektrometrie (Infrarotlaser, Wellenleiter, Detektor). Diese miniaturisierte Sensorplattform wurde im Rahmen des Nano-Tera Projektes IrSens entwickelt.

Der menschliche Speichel bietet zwar eine leicht zugängliche Matrix zur Analyse kleiner Moleküle wie Kokain, stellt aber gleichzeitig auf Grund des Verstopfungsrisikos der Mikrofluidik-Kanäle auf dem Chip durch diese komplexe Körperflüssigkeit eine grosse Herausforderung bei der Verarbeitung dar. Das rheologische Verhalten des Speichels wurde analysiert und ein geeignetes Verfahren zur Vorbehandlung von Speichelproben definiert. Das kostengünstige und UV-härtende Polymer NOA81 wurde als Chipmaterial gewählt und spezifisch für mikrofluidik Anwendungen charakterisiert. Für dieses Polymermaterial wird hier eine schnelle, hochflexible und günstige Methode zur Prototypenherstellung präsentiert, welche auf simplen Klebeband-Abformvorlagen basiert. Zudem wurde ein Mikrofluidikchip entwickelt, welcher eine neue, absolut einfache und robuste Technik der Tröpfchenerzeugung mit einer Geometrie zur Tröpfchenzusammenführung vereint um somit eine kontinuierliche, tröpfchenbasierte Flüssig-Flüssigextraktion durchführen zu können. Die Extraktionseffizienz dieses Chips wurde mit einem Massenspektrometer neuester Generation evaluiert. Der entwickelte Fluidikchip ist Teil eines optofluidischen Mikrosystems, welches das Kokain aus dem menschlichen Speichel in das infrarottransparente organische Lösungsmittel PCE transferiert und somit überhaupt die Kokaindetektion mittels Infrarotspektrometrie erlaubt.

Während dieser Doktorarbeit ist es gelungen eine einfache Methode zur Erzeugung von Tröpfchen mit kontrollierter Grösse zu entwickeln, welche ohne zu verstopfen komplexe Flüssigkeiten wie den menschlichen Speichel verarbeiten kann. Zudem wurde ein tröpfchenbasiertes Flüssig-Flüssigextraktionsverfahren entwickelt, welches das Kokain aus dem menschlichen Speichel in das organische Lösungsmittel PCE transferiert. Das geschaffene System hatte eine mindestens zwei- bis dreimal höhere Extraktionseffizienz als diejenige gängiger mikrofluidik Extraktionssysteme. Weiter konnten wir aufzeigen, dass unser System das Potential zur Kokain-Vorkonzentration im organischen Lösungsmittel hat, was entscheidend ist für unsere Endanwendung, die Infrarotspektrometrie.

Schlüsselwörter: Mikrofluidik, Speichel, Kokain, UV-härtender Klebstoff NOA81, Prototypenherstellung, kontinuierliche Flüssig-Flüssigextraktion, Tröpfchenerzeugung, Tröpfchenzusammenführung, Infrarotspektrometrie

Contents

Abstract (English/Français/Deutsch)	iii
Table of Contents	xii
1 Introduction	1
1.1 Microfluidics	1
1.2 Microfluidic Systems Involved in Real Sample Analysis	5
1.2.1 Commercialized Microfluidic Systems	5
1.2.2 Saliva Analysis with Microfluidic Devices	7
1.2.3 Microfluidic Chips used in Combination with IR-Detection	9
1.3 Project IrSens	10
1.3.1 Objectives & Concept of the Project	10
1.3.2 Relevance of the Project	11
1.3.3 Involved Partners and their Roles	11
1.4 Objectives of this Thesis	11
2 Materials & Methods	15
2.1 Human Saliva	15
2.1.1 Composition of Human Saliva	15
2.1.2 Cocaine in Human Saliva	16
2.1.3 Collection and Preparation of Human Saliva Samples	19
2.1.4 Saliva Samples in the IrSens Project	26
2.1.5 Adjustment of the pH-Value of Human Saliva	27
2.1.6 Rheological Characteristics of Human Saliva	28
2.2 Reference System for Cocaine Measurements	31
2.2.1 Sample Preparation for Mass Spectrometry	31
2.3 Materials used for Microfluidic Devices	33
2.3.1 Comparison of relevant Properties for Microfluidic Applications between Glass and Polymer	34
2.3.2 Material Requirements for Microfluidics	35
2.3.3 Polymer Materials used in this Work	35
2.4 Rapid Prototyping of Microfluidic Devices	36
2.4.1 Master Fabrication	36
2.4.2 Fabrication & Assembly of the Microfluidic Device for the project IrSens	39

Contents

2.5	Microfluidic Measurement Setup	40
2.6	Discussion	41
2.7	Summary	42
3	Characterization of Microfluidic Channels Made of UV-Curable Adhesive	43
3.1	Chemical Resistance Against Mid-IR-Transparent Organic Solvents	44
3.1.1	Method	44
3.1.2	Results	45
3.2	Cocaine Adsorption	46
3.2.1	Method	46
3.2.2	Results	47
3.3	Adjustable Wetting Behavior	48
3.3.1	Method	48
3.3.2	Results	49
3.3.3	Application	52
3.4	UV-Characteristics	54
3.4.1	Method	55
3.4.2	Results	55
3.4.3	Application	55
3.5	Low-Cost Rapid Prototyping	57
3.5.1	Replication Capability	58
3.5.2	Bonding Strength	59
3.6	Summary	60
4	Robust Droplet Generation Based on a Simple Geometry	63
4.1	Introduction	63
4.2	Theory & Fundamental Principles	66
4.2.1	Basic Conditions for Droplet Generation Based on Dimensionless Numbers	66
4.2.2	Droplet Generation at a Step Between a Shallow and a Deep Microfluidic Channel	67
4.3	Design	68
4.4	Results	68
4.4.1	Basic Conditions for PCE Droplet Generation in Saliva	69
4.4.2	Robust Droplet Generation	70
4.4.3	Investigations on the Droplet size	70
4.4.4	Flow Field Characteristics during Droplet Generation	71
4.4.5	Parallelization of the Droplet Generation	74
4.5	Discussion	74
4.6	Summary	75

5	Passive Phase Coalescence of Organic Solvent Droplets Dispersed in Saliva	77
5.1	Introduction	77
5.1.1	Surfactants and Interfacial Tension	77
5.1.2	Different Approaches for Microfluidic Passive Coalescence	78
5.2	Theory & Fundamental Principles	81
5.2.1	Droplet Coalescence Stages	81
5.2.2	Compressive Merging	81
5.2.3	Decompressive Merging	81
5.2.4	Avalanche Coalescence	82
5.3	Design	82
5.3.1	Chemically Assisted Merging Approaches	82
5.3.2	Physically Assisted Merging Approach	83
5.4	Results	86
5.5	Discussion	87
5.6	Summary	87
6	Liquid-Liquid Extraction of Cocaine from Human Saliva	89
6.1	Introduction	89
6.1.1	Microfluidic H-filter	90
6.1.2	Slugs in a Capillary	91
6.1.3	Droplet-Based Liquid-Liquid Extraction	92
6.2	Theory & Fundamental Principles	93
6.3	Design	94
6.3.1	Principle of the Microfluidic System for Droplet-Based Liquid-Liquid Extraction	94
6.3.2	Design Variations	95
6.4	Results	95
6.4.1	pH Value Optimized Extraction Conditions	96
6.4.2	Influence of the Flow Rates on the Extraction Efficiency	97
6.4.3	Influence of the Geometrical Dimensions on the Extraction Efficiency	98
6.4.4	Extraction Efficiency at Different Concentrations	100
6.4.5	Influence of the Induced Turbulences on the Extraction Efficiency	100
6.5	Discussion	101
6.5.1	Improvements of the extraction efficiency	101
6.5.2	Changes from the First to the Second Extraction System	102
6.5.3	Comparison with the State of the Art	102
6.6	Summary	103
7	Integrated Cocaine Sensor for Saliva Samples based on IR-Spectroscopy	105
7.1	Introduction	105
7.2	Theory & Fundamental Principles	106
7.3	Design	107
7.3.1	Optical Waveguide	107

Contents

7.3.2	Integration with the Microfluidic System	108
7.3.3	Optical Experimental Setup	109
7.3.4	Microfluidic Experimental Setup	109
7.4	Results	111
7.5	Discussion	113
7.6	Summary	116
8	Summary & Outlook	117
8.1	Summary	117
8.2	Outlook	119
A	Appendix:	
	UPLC-MS Cocaine Calibration Curve	121
	Bibliography	140
	Glossary	141
	Acknowledgements	145
	Curriculum Vitae	149
	List of Publications	151

1 Introduction

Handling fluids on the micro scale involves very different phenomena from what we are used to in our daily life. Some physical effects, neglectable at the macro scale, become predominant. Although nowadays many of these effects are observable, mastering them well is not so straightforward and building complex microfluidic systems involving several effects is even more challenging. On the other hand these phenomena open up a huge variety of new possibilities. Now the whole trick is to take advantage of these high-potential micro scale effects for every day applications and integrate them in commercial products. This is one of the key drivers behind the growth in the field of microfluidics during the last years [1, 2]. Furthermore there is a wide range of applications in the areas such as cosmetics, pharmaceuticals, medical applications, food industry, and drug testing in forensics, where the sample volumes are limited.

In this chapter some microfluidic basics are explained, an overview of real sample analysis systems is given, and the project IrSens as well as the goal of this thesis are presented.

1.1 Microfluidics

Microfluidics is a multidisciplinary field interconnecting physics, chemistry, engineering, micro-, and biotechnology. Microfluidics is also called the art of precisely controlling microliter volumes of fluids. This implies the size of channels and other features on a microfluidic chip are in the millimeter to micrometer range. The dimensions are demonstrated with the volume and the side length of a cube in Table 1.1.

In microfluidics typically different liquids are mixed, separated, moved or used themselves as transport medium to handle small particles or even biological cells. The fluid flow is either passively controlled by e.g. capillary forces or by using active techniques such as centrifugal forces, pumps, and valves. Commonly used pumps for microfluidics provide fluids at constant pressure or constant flow rate.

Table 1.1: Typical dimensions of microfluidic systems.

Volume		Side length of the cube
1 nL	10^{-3} mm^3	100 μm
1 μL	1 mm^3	1 mm
1 mL	1 cm^3	1 cm

Surface-to-volume ratio

Reducing the dimensions of a fluidic system to the micro scale increases the surface-to-volume ratio. Consequently the relative importance of surface forces (e.g. surface tension, shear stress) increases as well versus body forces (e.g. gravitational forces, centrifugal forces, inertial forces) which is expressed by [1] as

$$\frac{\text{surface forces}}{\text{volume forces}} \propto \frac{\ell^2}{\ell^3} \xrightarrow{\ell \rightarrow 0} \infty. \quad (1.1)$$

The relatively larger surface also affects strongly the energy transfer (e.g. heat exchange) and matter transfer (e.g. diffusion) through surfaces.

Diffusion in a semi-infinite slab

According to Fick's first law of diffusion, the flux j of a matter per area [$\text{kg} \cdot \text{m}^{-2} \cdot \text{s}^{-1}$] from an interface in direction z [m] into a semi-infinite slab is given by [3]

$$j = -D \frac{\delta c}{\delta z}, \quad (1.2)$$

whereas c is the concentration of the matter [$\text{kg} \cdot \text{m}^{-3}$] and D the diffusion constant [$\text{m}^2 \cdot \text{s}^{-1}$]. The diffusion constant scales roughly with the inverse of the size of the molecule and also depends on its shape. Therefore, small molecules have a large diffusion constant and are able to move a longer average distance per time than a large molecule.

Rewritten using the mass balance on a infinite small slab ($\Delta z \rightarrow 0$) the diffusion law reads

$$\frac{\delta c}{\delta t} = D \frac{\delta^2 c}{\delta^2 z}. \quad (1.3)$$

For the following boundary conditions the time-dependent flux becomes

$$j = \sqrt{\frac{D}{\pi t}} \exp\left(\frac{-z^2}{4Dt}\right) (c_0 - c_\infty) \quad (1.4)$$

$$\begin{aligned} t = 0, & \quad \text{all } z: & c = c_\infty \\ t > 0, & \quad z = 0: & c = c_0 \\ & \quad z = \infty: & c = c_\infty \end{aligned}$$

and at the interface ($z = 0$)

$$j = \sqrt{\frac{D}{\pi t}}(c_0 - c_\infty). \quad (1.5)$$

The root mean square distance, x , traveled by a molecule in solution in a time interval, t , is given by [3] as

$$x \sim \sqrt{D \cdot t}. \quad (1.6)$$

Interfacial tension

Another important parameter is the interfacial tension γ , a force per unit length [Nm^{-1}]. As a result of the interfacial tension, the surface area of a liquid is minimized and so the free energy of the interface reduced. The minimum area for a given free volume of a liquid is a sphere, which is the shape always taken by an isolated droplet. Normally in microfluidic systems droplets have limited space available and are confined by walls or neighboring droplets, which is changing their shape. These introduced curvatures introduce a pressure jump, known as the Laplace pressure Δp [Nm^{-2}], between the inside and the outside of the droplet.

$$\Delta p = \gamma \left(\frac{1}{R_1} + \frac{1}{R_2} \right), \quad (1.7)$$

where R_1 [m] and R_2 [m] are the two principal radii of the curvature of the interface [4].

The interfacial tension between two liquids γ_{12} can be calculated by using Antonov's rule [5]

$$\gamma_{12} = |\gamma_1 - \gamma_2|, \quad (1.8)$$

where γ_1 and γ_2 are the surface tensions of the liquids measured against air.

Reynolds number

Mainly based on small dimensions and lower velocities in microfluidics the relative importance of inertial forces and viscous forces is reduced on the micro scale. In fluid dynamics their ratio is described by the Reynolds number [1], which is defined as

$$\text{Re} = \frac{\text{inertial forces}}{\text{viscous forces}} = \frac{\rho v_0 L_0}{\eta}, \quad (1.9)$$

Chapter 1. Introduction

where ρ is the fluid density [$kg \cdot m^{-3}$], v_0 and L_0 are the characteristic fluid velocity [$m \cdot s^{-1}$] and the characteristic length [m] of the system, and η is the dynamic viscosity [$N \cdot m^{-2} \cdot s$] of the fluid. If $Re \gg 1$, then the inertial forces dominate which results in chaotic flows. If $Re \ll 1$, viscous forces are predominant resulting in laminar flows, where streamlines never cross.

Based on the small dimensions of micro systems, the Re of microfluidic systems is usually less than 1 representing the conditions of perfect laminarity. This allows finely control of the flow trajectories and parallel flow even of miscible liquids. This is of advantage for many microfluidic systems for chemical applications such as the microfluidic H-filter [6] or the field of optofluidics [7–9]. On the other hand, the laminar flow conditions allow mixing only by diffusion, which is much slower than what we expect in such confined volumes. Fast mixing of liquids in microfluidic devices asks for special geometries [10, 11].

Capillary number

On the micro scale the relative effect of viscous forces and surface tension forces acting across an interface between two immiscible fluids becomes important. Their ratio is described by the capillary number [1], which is defined as

$$Ca = \frac{\text{viscous forces}}{\text{surface tension forces}} = \frac{\eta v_0}{\gamma}, \quad (1.10)$$

where η is the dynamic viscosity [$N \cdot m^{-2} \cdot s$], v_0 the characteristic fluid velocity [$m \cdot s^{-1}$] and γ is the interfacial tension [$N \cdot m^{-1}$].

For $Ca \ll 1$ the flow is dominated by capillary forces and interfacial tension. Droplet generation in a continuous two-phase flow becomes feasible [1, 12]. A critical capillary number for droplet generation of 10^{-3} was given by [4].

Bond number

Another dimensionless number is the Bond number, which compares gravity to interfacial tension. The Bond number is defined as [1]

$$Bo = \frac{\text{gravitational forces}}{\text{surface tension forces}} = \frac{\Delta\rho g L_0^2}{\gamma}, \quad (1.11)$$

where $\Delta\rho$ is the difference of the densities of the involved liquids, g the gravitational acceleration, L_0 a characteristic length, and γ the interfacial tension.

For $Bo \ll 1$ the flow is dominated by interfacial tensions and the gravity can be ignored.

1.2 Microfluidic Systems Involved in Real Sample Analysis

Since complete microfluidic systems for analysis were first presented [13], they have been called miniaturized total-analysis-systems (μ TAS) or more general lab-on-a-chip (LOC) devices. Typically they include a system of fluidic channels, sites for chemical or biological reactions and detections, alongside with pumping elements and electronics for data acquisition and control. Balslev et al. of MIC-DTU Denmark presented a nice example of an integrated LOC system for optical analysis of chemical reactions (see Figure 1.1) [14]. This system is a hybrid polymer/silicon device based on a silicon substrate containing integrated photo diodes, while the laser, the waveguides, a mixer, and the microfluidic channels are made in a SU-8 polymer film on top of the substrate. This section will give an overview of commercially available devices, a more specific state of the art of microfluidic devices for saliva analysis and a list of examples of microfluidic chips used together with IR-detection.

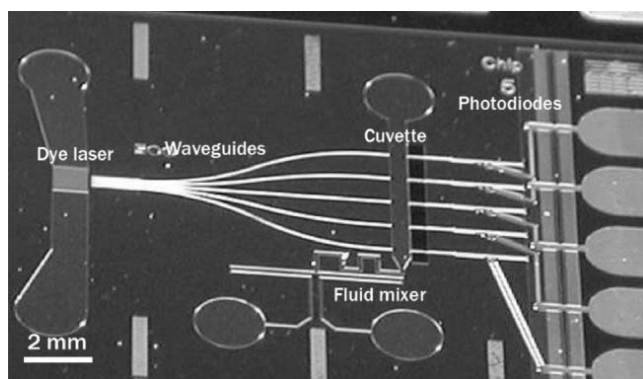
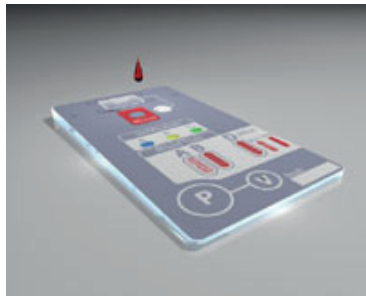


Figure 1.1: LOC device with integrated microfluidic dye laser, optical waveguides, microfluidic network, and photodiodes. [14]

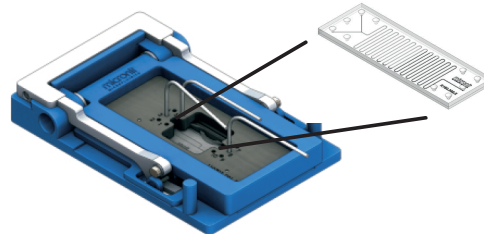
1.2.1 Commercialized Microfluidic Systems

For several microfluidic applications – mostly in biology – devices have been commercialized. Here we like to highlight some examples: Caliper Life Sciences has focused much energy on providing microfluidic chips for separation and analysis of DNA [15]. BioTrove developed a device to perform thousands of nanoliter-volume PCRs [16]. Some companies have moved away from DNA-and protein-based microfluidics. Cellix, founded in 2004, provides a chip with microfluidic channels which mimic the in vivo conditions of blood vessels [17]. An overview of companies which entered successfully the microfluidic market is presented in [18].

There are systems available which use for pumping the capillary effect such as the autonomous chip "ABORh-Card" of Micronics [19] shown in Figure 1.2a. The fully-integrated, credit card sized device is used to determine the presence of human blood group antigens during blood transfusions. Otherwise also complete systems with disposable microfluidic chips together with a chip holder and external pumping are provided as for example the "Fluidic Connect Pro" of Micronit Microfluidics [20] presented in Figure 1.2b.



(a) ABORh-Card of Micronics based on capillary pumping [19].

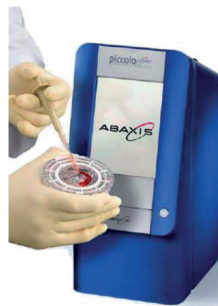
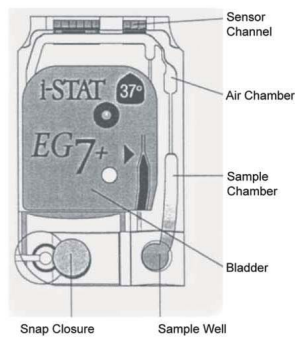


(b) Chip holder for external pumping of Micronit Microfluidics with disposable microfluidic part [20].

Figure 1.2: Commercialized microfluidic devices with active and passive pumping.



(a) iSTAT system for detection of electrolyte levels and limited immunoassays [22].



(b) Disc-based microfluidic system for blood analysis sold by Abaxis [23].

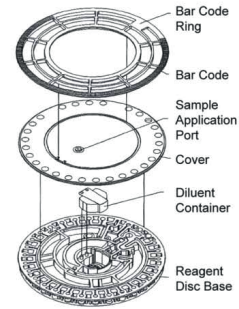


Figure 1.3: Commercialized POC devices with readout unit and disposable microfluidic part.

Microfluidic point-of-care diagnostic devices represent a large part of commercialized systems. Here most popular are the lateral flow tests, which use a membrane or paper strip to indicate the presence of protein markers in a liquid. They also work with capillary action, they form a visible band and are interpreted by eye only e.g. the product of Diagnostics For All [21] which is in development. Otherwise the systems commonly include a readout unit and a low-cost disposable microfluidic chip as presented in Figure 1.3. The iSTAT system was one of the first commercially available LOC products. It combines miniature fluidics and electrochemical detection of electrolyte levels and limited immunoassays [22]. Abaxis used the compact disc-based approach for blood chemistry analysis to test for small molecule and protein markers for different diseases [23]. In [2] a broad review of commercialized point-of-care diagnostic devices together with potential systems in development is presented.

Although a large part of the excitement behind microfluidics is in its potential for practical applications, surprisingly only few LOC-based systems have been successfully introduced in

the market so far [2]. There is a huge growth over the last years [1], but the so called "killer application" as the accelerometers in MEMS, has not been established yet. George Whitesides of Harvard University believes the solution will be found through an application: "We need to find applications where it is the result that is the value, not the device." [18]

1.2.2 Saliva Analysis with Microfluidic Devices

Saliva can be collected easily in a non invasive way and drugs have a well defined ratio between the concentration in blood plasma and saliva [24]. That is why many research groups work with saliva as diagnostic fluid in microfluidic devices. They look for various analytes, but mainly for small molecules dissolved in saliva. Different detection techniques like optical, electrophoretic, chromatographic, electrochemical, immunochemical, or preencoded microbead-based techniques are investigated. Table 1.2 provides an overview of the reported techniques together with the associated analytes and the research group working on this technique.

The Groups of Yager and Wong focus on surface plasmon resonance imaging (SPRI) [25–27]. Researchers around Singh, Niki and Landers explore electrophoretic techniques [28–31] and Bhansali is using electrochemical detection. The group of Bau approaches the topic with chromatography [32–34]. Several other groups functionalize microarrays or microbeads and choose optical detection also using fluorescence.

Nowadays, there are already quite a number of different (mainly immunoassay based), lateral flow tests or so called drug test strips commercially available for saliva, e.g. DrugWipe[®], Cozart[®], OraSure[®] (see section 1.2.1).

These lateral flow tests are lacking on reliability. Evanescent field spectroscopy (SPRI) seems to be the most promising technique to detect molecules in saliva. This technique is independent of the charge/polarizability of the sample (unlike electrophoretic methods), generates a directly detectable signal without time delay (unlike chromatographic techniques), does not need any functionalization (unlike immunoassays) and is label-free (unlike fluorescent label based optical techniques). Evanescent field methods are favored to techniques where the light is sent through the sample due to the high absorption of IR radiation in water (see Figure 1.6 in section 1.4).

There are also research groups detecting cocaine in microfluidic devices. Scheller and Stemme are using mass sensitive piezoelectric/amperometric sensors, called quartz crystal microbalance (QCM) in combination with an immunoassay. They are able to detect $10^{-7} - 10^{-9} M$ of cocaine in water or buffers within 20min [35, 36]. Wang presented an electrochemical device based on functionalized nanoparticles to detect cocaine in centrifuged saliva with a limit of detection of $10^{-7} M (= 40 ng/mL)$ [37]. Techniques using functionalization show a good limit of detection but not with a reasonable time-to-result.

Chapter 1. Introduction

Table 1.2: Techniques of saliva analysis in microfluidic devices.

Detection Technique <i>Saliva Preparation</i>	Analytes in Saliva	Channel dim. [μm] depth/with/length	Res. Group
Surface Plasmon Resonance Imaging - SPRI <i>filtering: syringe filter, ultra filtration, microfluidic H-filter</i>	small molecule analytes (hormones, drugs metabolites, pathogens and markers of oral cancer, protein markers of systemic disease, drug monitoring of antiepileptic drugs)	62/3600/60000	Yager [25, 26]
Surface Plasmon Resonance Imaging - SPRI <i>adding protease inhibitors for sample preservation, centrifugation</i>	interleukin-8 (protein secreted by cells)	50/500/2400	Wong [27]
Electrophoretic immunoassay with fluorescence detection readout <i>off-chip: centrifugation, on-chip: filtration</i>	protein bio-markers of periodontal disease	~70/~70/n.a.	Singh [28]
Electrophoresis <i>membrane filtration</i>	bio-markers for oral diseases (pathogens like porphyromonas gingivalis, tanerella forsythensis, treponema denticola)	25/100/n.a.	Singh [29]
Electrophoresis <i>diluting: 10% saliva in distilled water</i>	NO-metabolites	n.a./n.a./25000	Niki [30]
Capillary Electrophoresis <i>preconcentration, centrifugation, filtration, diluting: 25% saliva, 10% 0.1M HCl</i>	hydroxyl radical bio-markers	250/1500-2000/2800 (trapezoidal shape)	Landers [31]
Chromatography with optical detection (UpLink reader) <i>on-chip: cell lysis</i>	bacterial pathogens	250-500/250-500/n.a.	Bau [32]
Chromatography with optical detection using UPT (Upconverting Phosphor Technology) <i>some filtration by using OraSure[®] collector</i>	pathogens	n.a.	Bau [33]
Chromatography using immobilized proteins with fluorescence detection readout <i>dilution</i>	antibodies of HIV	380/var./var.	Bau [34]
Magnetic bead-based microfluidic platform with fluorescence detection readout <i>cell lysis</i>	gDNA (genetic detection)	n.a.	Lee [38]
Preencoded microbead-based detection with fluorescence detection readout <i>dilution</i>	interleukin-8	380/var./var.	Bau [34]
Microsphere-based antibody array with fluorescence detection readout <i>centrifugation</i>	bio-markers (inflammatory cytokines)	chamber	Walt [39]
Electrochemical detection using functionalized electrodes <i>freeze-thawing, centrifugation</i>	cortisol	chamber	Bhansali [40]
Electrochemical detection using functionalized nanoparticles <i>centrifugation</i>	cocaine	chamber	Wang [37]
Pattern-based microarrays with optical readout <i>analysis in aqueous solution</i>	peptides	array of wells	Anslyn [41]
Test strip based optical fiber microarray <i>n.a.</i>	bio-markers for renal and pulmonary disease	test strips	Walt [42]
Gel-based microarray <i>n.a.</i>	microbial species	diffusion system	Stahl [43]
Quantum dot bioconjugate microarray with fluorescence detection readout <i>dilution 25% in PBS</i>	proteins (cancer markers)	n.a.	McDevitt [44]
Immunochemical-based test strip, DrugWipe [®] <i>n.a.</i>	cocaine	n.a.	Samyn [45, 46]
Enzyme immunoassay, Cozart [®] <i>n.a.</i>	cocaine and its metabolites	n.a.	Cooper [47]
Enzyme-linked immunoassay, OraSure [®] <i>n.a.</i>	cocaine metabolites	n.a.	Kidwell [48]

1.2. Microfluidic Systems Involved in Real Sample Analysis

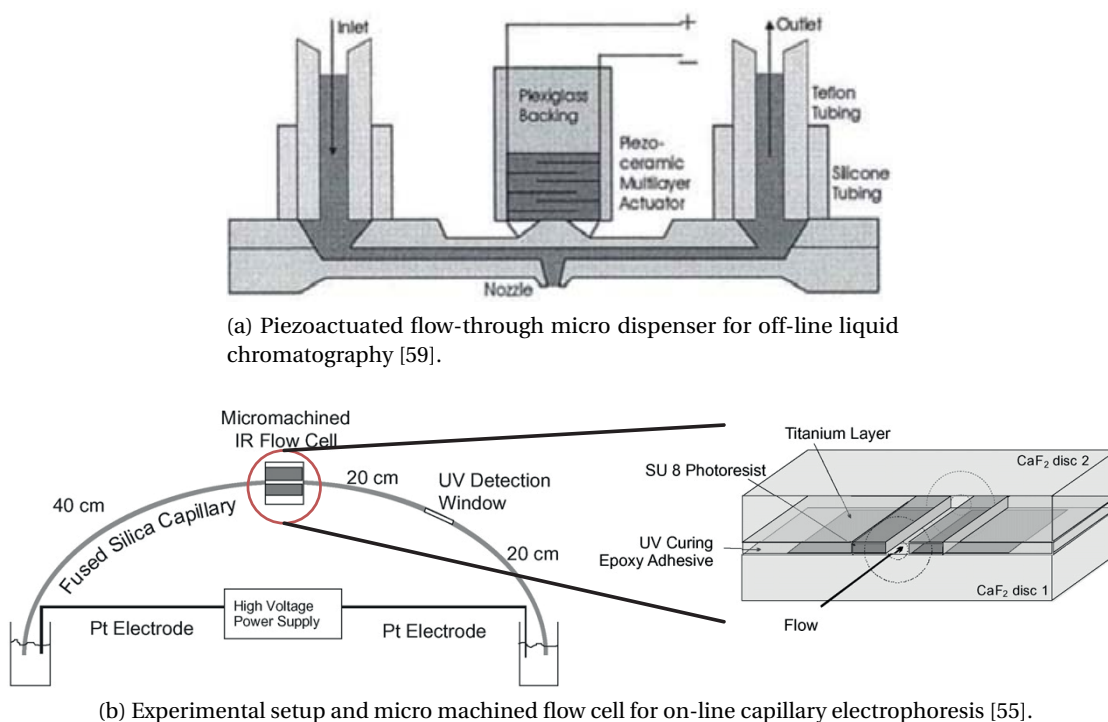


Figure 1.4: Microfluidic sample preparation used in combination with IR detection.

1.2.3 Microfluidic Chips used in Combination with IR-Detection

The combination of IR-light-based analyte detection with microfluidic systems represents an extraordinary effort, mainly due to the poor availability of materials for microfluidic chips which are transparent at wavelengths of the required IR spectra. However, this combination would result in strong qualitative analyte identification and complement the separation information [49].

Microfluidic separation techniques have been combined with IR detection methods such as IR spectroscopy, Fourier transformed IR spectroscopy (FT-IR), attenuated total reflection IR spectroscopy (ATR-IR) or the related surface enhanced Raman spectroscopy (SERS). Chromatography based separation techniques such as liquid chromatography, high performance liquid chromatography or size exclusion chromatography, are the mostly applied separation methods [50–53]. The chromatography approach looks promising, but it is hard to integrate the long channels on a small microfluidic chip. Also electrophoretic separation techniques such as capillary electrophoresis (CE) and sequential-injection-capillary electrophoresis (SI-CE) are tested [53–58].

The separation method is either performed off-line with an independent system such as the piezoactuated flow-through micro dispenser shown in Figure 1.4a or on-line integrated together with the detection device such as the presented capillary electrophoresis system in Figure 1.4b.

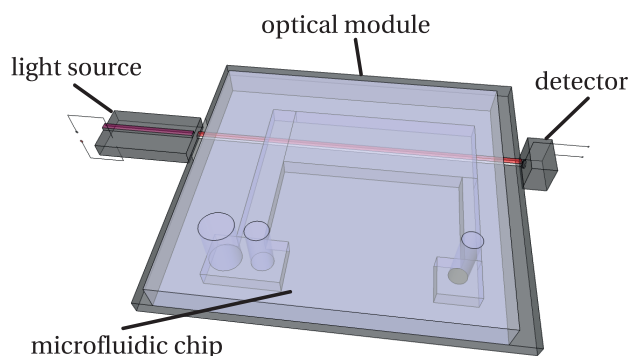


Figure 1.5: Concept of the integrated sensing platform for fluids based on IR spectroscopy.

1.3 Project IrSens

The work of this thesis is part of the integrated project IrSens, which is scientifically evaluated by the Swiss National Science Foundation (SNSF), financed by the Swiss Confederation and funded by Nano-Tera. The project started in 2009 for a duration of four years under the full title "Integrated sensing platform for gases and liquids in the near and mid-infrared range". This section provides an overview of the project including a short description of the objectives and the concept, the project relevance and a list of involved partners (adapted from the project description). Further information can be found on www.nano-tera.ch.

1.3.1 Objectives & Concept of the Project

The IrSens project aims to design and build an integrated optical sensor platform with high performance and reliability which will leverage on the new source, detector and interaction cell technologies to create a new sensor element with improved performance and lowered cost. The improvements will be demonstrated by two pilot applications, the first one sensing in the gas phase, the second one sensing in the liquid phase.

The compact sensing platform for gases is based on a multi path absorption cell with various compact semiconductor light source and detector types. Infrared absorption spectroscopy can be used to detect a wide variety of gases. To demonstrate its suitability for breath analysis, the first part of this project is focused on the detection of exhaled CO_2 .

The integrated sensing platform for fluids is based on IR laser spectroscopy as well. The idea is to couple the light source and the detector to an optical module where the analyte in liquid will flow through a built-in microfluidic channel as shown in Figure 1.5. The microfluidic system will take care of the on-chip sample pretreatment as well. To improve the limit of detection and increase the analyte concentration the analyte has to be transferred to a less absorbing solvent by liquid-liquid extraction. This sensing platform is intended to be used mainly in bio-medical applications with an emphasis on detection of drugs and doping agents

in human body fluids: specifically, a first targeted demonstrative application for this sensor would be the cocaine detection in human saliva.

1.3.2 Relevance of the Project

There is an increasing demand for sensitive, selective, and portable detectors to trace components in gases and liquids, e.g. due to increasing concerns about atmospheric pollutants, and a need for improved medical screening capabilities for early detection of diseases and abuse of drugs. In this context, the project IrSens aims building a platform based on optical spectroscopy in the near and mid-infrared range. This method allows probing the vibrational frequencies of the targeted molecules - most of which are located in the near and mid-infrared range, and to obtain an unambiguous signature of the investigated gas or liquid. Section 1.2 already highlighted the advantages of a microfluidic system for integrated sample preparation such as portability, automation, reduction of the sample and reagent volume. Furthermore, this section also presented the huge pool of new available techniques as well as the potential for commercialization of microfluidic systems.

1.3.3 Involved Partners and their Roles

In the Nano-Tera project IrSens nine groups of five Swiss research institutes are involved working towards two pilot applications for a gas and liquid sensing platform. Table 1.3 gives an overview of their main tasks.

1.4 Objectives of this Thesis

As mentioned in section 1.3, the aim of this research in the framework of the project IrSens is to develop a portable microfluidic system for cocaine detection in human saliva by IR-spectroscopy.

A low-cost, disposable chip is required which is easy to fabricate. Therefore, the chip material is chosen to be a polymer. Polymers are challenging materials and require specific characterization. Not only the material itself, but also the fabrication process should be simple and low-cost, thus rapid prototyping is investigated.

The cocaine is detected by absorption IR-spectroscopy. Unfortunately saliva (99% water) is strongly absorbing where the characteristic absorption peak of the cocaine molecule is located (shown in Figure 1.6). So one of the tasks has been to come up with a microfluidic sample pretreatment design to bring the cocaine from saliva to an IR-transparent solvent by liquid-liquid extraction.

For better extraction efficiency due to the larger liquid-liquid interface I followed the approach of droplet-based liquid-liquid extraction. Therefore, I produced first droplets of the organic solvent (acceptor phase) tetrachloroethylene (PCE) in saliva (donor phase) containing cocaine

Chapter 1. Introduction

Table 1.3: IrSens project partners and their tasks.

Main task	Partner
Development of near- and mid-infrared optical sources Development of quantum cascade laser (QCL) Development of vertical-cavity surface-emitting laser (VCSEL)	Group of Jérôme Faist, ETHZ Group of Eli Kapon, EPFL
Development of the detection system Development of quantum cascade detectors (QCD) Signal analysis	Groupe of Daniel Hofstetter, UniNe Group of Edoardo Charbon, EPFL Herbert Looser, FHNW
Development of a compact and portable optical sensor for human breath analysis Benchmark setup Demonstrator device	Group of Markus Sigrist, ETHZ Group of Lukas Emmenegger, EMPA
Development of a compact and portable optical sensor for liquids Benchmark setup Waveguide based optical detection Microfluidic sample preparation	Group of Markus Sigrist, ETHZ Group of Hans Peter Herzig, EPFL Group of Nico de Rooij, EPFL

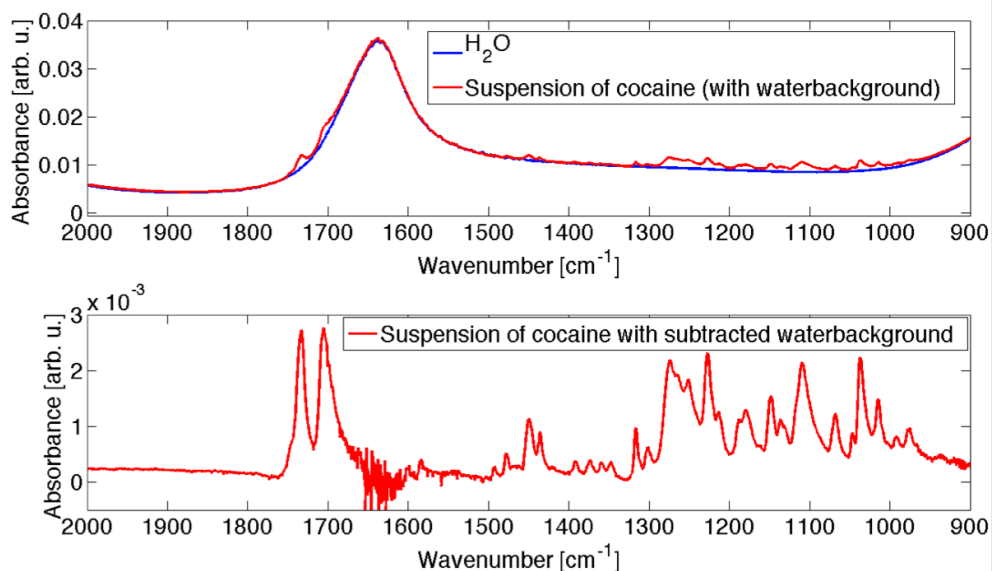


Figure 1.6: Top: Absorption spectra of water and overlapping an over-saturated suspension [1.3 mg/mL] of cocaine in water. Bottom: Absorption spectra of the cocaine suspension with subtracted water background. Cocaine shows two strong absorptions peaks at around wave number 1700 cm^{-1} , but only the left one at 1750 cm^{-1} is characteristic. The other overlaps with an absorption peak of caffeine.

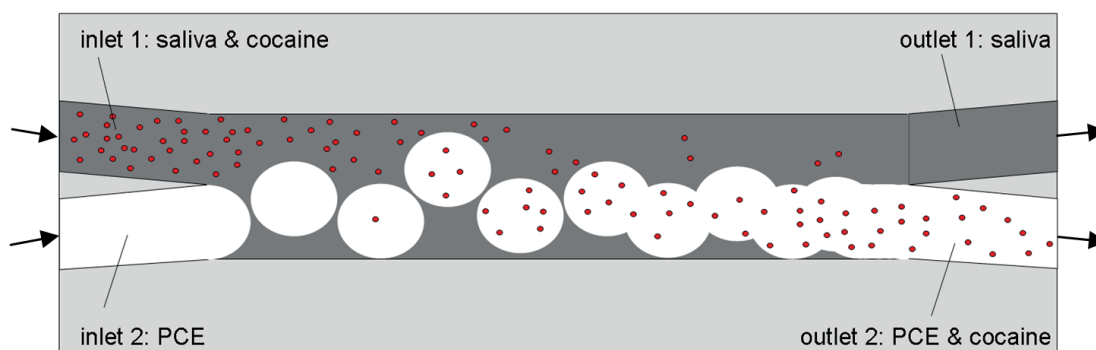


Figure 1.7: Principle of the droplet-based liquid-liquid extraction method to transfer efficiently cocaine from human saliva to the IR-transparent organic solvent tetrachloroethylene (PCE).

for the efficient extraction. As shown in Figure 1.7 these droplets had to be merged again to a continuous phase for the optical detection.

Furthermore, the microfluidic system has to be compact, portable, and integrable with the optical waveguide for detection purposes.

The results of our work, implicated by the mentioned goals, is presented in this thesis as follows:

Chapter 2 will give an overview of the not trivial sample fluid human saliva. We will highlight the aspect of cocaine in saliva and present the reference method for cocaine measurements. This chapter will talk as well about the materials used for microfluidic systems and mention the required material properties. We will present our simple and low-cost fabrication process in context with the commonly used rapid prototyping methods applied for microfluidic systems.

Chapter 3 will show the characterization of the polymer microfluidic channels with respect to aspects which are relevant for our application.

Chapter 4 will introduce our robust method to generate droplets of an organic solvent in inhomogeneous human saliva. The simple geometry will be characterized with saliva samples and the influences on the size of the generated droplets investigated.

Chapter 5 will demonstrate how we merge stable organic solvent droplets dispersed in the aqueous saliva to a continuous flowing phase.

Chapter 6 will talk about the microfluidic liquid-liquid extraction or in other words how to transfer efficiently a solute from an aqueous liquid to an organic solvent. We will identify the limitations of the state-of-the-art microfluidic devices. We will present the design and characterization of a new droplet-based system for a more efficient liquid-liquid extraction. Not only the better surface to volume ration of droplets, but also vortexes induced during droplet generation are used for our advantage.

Chapter 1. Introduction

Chapter 7 will present the integrated sensing device for cocaine detection in human saliva. It will show the integration of the microfluidic system for sample pretreatment together with the IR-laser detection by means of an optical waveguide crossing the microfluidic channel.

Chapter 8 will summarize the findings of this research and give an outlook on the future of the developed liquid-liquid extraction system.

2 Materials & Methods

This chapter gives an overview of human saliva. It presents the advantages of this body fluid as a matrix for the analysis of small molecules such as cocaine, but also identifies the numerous challenges we are facing to when using saliva in microfluidic devices. We highlight the aspect of cocaine in saliva and define our reference method for cocaine measurements. This chapter also presents the materials commonly used for microfluidic devices and mentions the required material properties for point-of-care devices. NOA81 is the polymer material we have chosen to work with. Here we present the appropriate, low-cost, highly flexible, and time-efficient rapid prototyping method we developed for this UV-curable polymer to fabricate microfluidic systems for research applications.

2.1 Human Saliva

This section presents background information found in literature about the human body fluid saliva which is the matrix of our analyte cocaine. Of course also some data about cocaine itself are listed. In addition we determined some project relevant characteristics of human saliva before and after pretreatment. Furthermore, the sample collection and preparation is discussed.

2.1.1 Composition of Human Saliva

Basically saliva refers to the complex mixture of body fluids originating from the salivary glands, the gingival fold, oral mucosa transudate, and the mucous of the pharynx (throat) and the nasal cavity. One of the primary function of saliva in the oral cavity is lubrication, which supports eating, swallowing, and speech [60].

Salivary fluid is an exocrine secretion and has been described as a diluted polymer (mucin) solution containing long entangled molecule chains, some of which are bonded by secondary chemical interactions [61, 62]. The composition and consistency of saliva varies greatly

Chapter 2. Materials & Methods

between and also within individuals. The saliva composition changes over time as well as with different levels of physical activity [63, 64].

Saliva consists of approximately 99% water. It contains a variety of electrolytes and proteins, represented by the relatively large mucosal glycoproteins, the enzymes, the immunoglobulins, and some smaller polypeptides and oligopeptides of importance to oral health. In saliva are also enclosed nitrogenous products, such as urea and ammonia, some traces of hormones, non-adherent oral bacteria and human cells like epithelial cells as well as blood cells. Furthermore, you find therein food debris as well as traces of medications or chemical products [65, 66]. The components listed above generally occur in small amounts and their concentration varies with changing saliva secretion flow rate [67].

Table 2.1 shows the composition of human saliva. It is not possible to indicate the exact composition, neither to give a lot of verified concentrations. This domain is not so deeply investigated and the significant inter-subject and intra-subject variations make the characterization difficult.

2.1.2 Cocaine in Human Saliva

Cocaine ($C_{17}H_{21}NO_4$), chemically known as [1*R*-(*exo,exo*)]-3-(*benzoyloxy*)-8-*methyl*-8-*azabicyclo*[3.2.1]*octane* - 2 - *carboxylic acid methyl ester*, is a relatively compact molecule and shows a molecular weight of 303.4Da. Its skeletal model is shown in Figure 2.1. Cocaine exists in several forms: as free base alkaloid or as cocaine hydrochloride (salt form). One gram of the free base cocaine dissolves in 600mL water, 6.5mL alcohol or 0.7mL chloroform. The hydrochloride form is much more soluble. One gram dissolves in 0.4mL water, but it is also much less stable and decomposes fast. The hydrochloride is not heat- and light-resistant.[68]

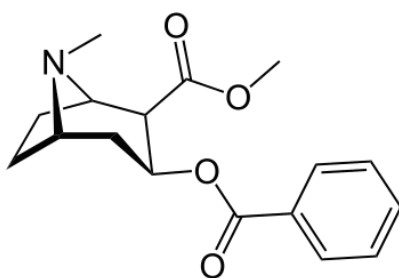


Figure 2.1: Skeletal model of a cocaine molecule [68].

At human physiological pH (7.35–7.45), the tertiary amine group of cocaine would be protonated resulting in a net positive charge. The pKa(15°C) of cocaine is at a pH value of 8.61. In the human body, the active cocaine degenerates. The primary metabolites of cocaine are called benzoylecgonine, norcocaine, ecgonine methyl ester, and are formed in the liver. Parallel consumption of cocaine and alcohol results in a still active molecule called cocaethylene.

Table 2.1: Composition of human saliva with cocaine.

component		weight	unstimulated concentration	stimulated conc.	radius	
water		18Da [69]	99% [65]			
electrolytes	sodium Na ⁺	0.022kDa [69]	2 – 26mmol/L [24]	13 – 80mmol/L [24]	1.02Å [69]	
	potassium K ⁺	0.039kDa [69]	13 – 40mmol/L [24]	13 – 38mmol/L [24]	1.51Å [69]	
	calcium Ca ²⁺	0.040kDa [69]	0.5 – 2.8mmol/L [24]	0.2 – 4.7mmol/L [24]	1.12Å [69]	
	chloride Cl ⁻	0.035kDa [69]	n.a.	n.a.	0.08Å [69]	
	magnesium Mg ²⁺ bicarbonate HCO ₃ ⁻	0.024kDa [69] 0.061kDa [69]	0.15 – 0.6mmol/L [24]	n.a.	0.72Å [69]	
	phosphate PO ₄ ³⁻	0.094kDa [69]	n.a.	1.5 – 25mmol/L [24]	n.a.	
proteins	enzymes	α-amylase	46 – 60kDa [70]	+++ 0.4g/L (0.008mmol/L) [24]	n.a.	n.a.
		lysozyme	14kDa [70]	+	n.a.	n.a.
		kallikrein	n.a.	+	n.a.	n.a.
	statherins		5.400kDa [71]	++	n.a.	n.a.
	cystatins		n.a.	++	n.a.	n.a.
	proline-rich proteins PRPs (proline C ₅ H ₉ NO ₂)		6 – 36kDa [70]	++++	n.a.	n.a.
	immunoglobulins	secretory immunoglobulin A/sIgA	155kDa [70]	+++ 194mg/L (0.001mmol/L) [24]	n.a.	n.a.
		immunoglobulin G/IgG	144kDa [70]	+	n.a.	53Å [24]
		immunoglobulin M/IgM	70kDa [72]	+	n.a.	n.a.
		immunoglobulin D/IgD	n.a.	+	n.a.	n.a.
		immunoglobulin E/IgE	n.a.	+	n.a.	n.a.
	glycoproteins	mucosal glycoproteins/MG1, MG2	2 – 40 * 10 ³ kDa [73], 150 – 200kDa [70]	++++ 0.001% [24]	n.a.	n.a.
		extra-parotid glycoprotein	18 – 20kDa [70]	+	n.a.	n.a.
		haptocorrin	60 – 80kDa [70]	+	n.a.	n.a.
		zinc-α2-glycoprotein	41kDa [70]	+	n.a.	n.a.
	albumin	67.500kDa [70]	+	n.a.	36Å [24]	
	β-microseminoprotein	11kDa [70]	+	n.a.	n.a.	
	nitrogenous products	urea CO(NH ₂) ₂	60.060kDa [69]	3.4mmol/L [74]	n.a.	n.a.
ammonia NH ₃		17.031kDa [69]	2 – 6mmol/L [75]	n.a.	n.a.	
hormones	estrogens	0.270 – 0.288kDa	n.a.	n.a.	n.a.	
	progestins	n.a.	100 – 800pmol/L [24]	n.a.	n.a.	
	androgens	n.a.	n.a.	n.a.	n.a.	
	corticosteroids	n.a.	9 – 27nmol/L [24]	n.a.	n.a.	
lipids		n.a.	8 – 10mg/100mL [24]	n.a.	n.a.	
cells	human	n.a.	~ 8million/mL	n.a.	2 – 25μm [76]	
	bacterial	n.a.	~ 500million/mL 3.75 * 10 ⁵ colony forming units/mL [77]	n.a.	0.1 – 2.5μm [76]	
cocaine		0.303kDa [78]	> 1μg/mL [45, 79, 80]	n.a.	n.a.	

n.a.: no certified values found

(+) <1%, (++) 1–5%, (+++) 5–15%, (++++) >15% of total protein amount in saliva [70]

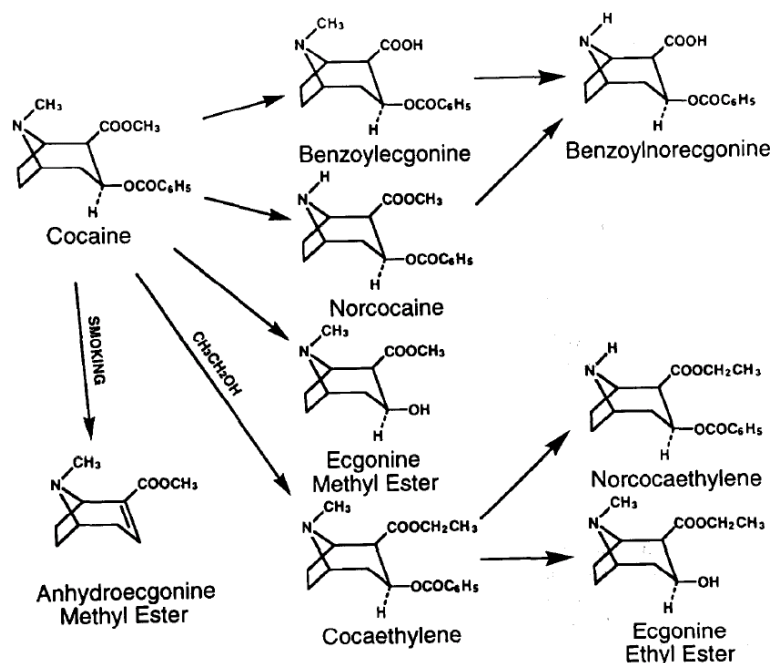


Figure 2.2: Metabolites of cocaine [82].

When smoking cocaine (pyrolysis) anhydroecgonine methyl ester is formed. Figure 2.2 presents the different metabolites resulting from cocaine degeneration. [81, 82]

Cocaine is produced from the leaves of the plant *Erythroxylon coca* or by synthesis. Today Colombia is the world's leading producer of cocaine. More than three-quarters of the world's annual yield of cocaine has been produced in Colombia, both from cocaine base imported from Peru or Bolivia, and from locally grown coca plants.

There are different ways of consumption. Cocaine is swallowed, smoked, injected or sniffed. It is an appetite suppressant, an anesthetic and a powerfully addictive stimulant drug that increases the level of dopamine, a brain chemical associated with pleasure and movement, in the brain's reward circuit. It makes the consumers feeling really euphoric. After this first effect, the consumers fall into a depression. This behavior is mostly responsible for the addiction already after the first contact. Abusing cocaine has a variety of effects on the human body, such as constricted blood vessels, dilated pupils, and increased body temperature, heart rate, and blood pressure.

In Switzerland cocaine is an illegal drug and a zero tolerance policy is followed [83]. The American Substance Abuse and Mental Health Services Administration (SAMHSA) has proposed an oral fluid screening cutoff of 20ng/mL with cocaine as the target analyte [84, 85].

Samyn et al. showed in an on-site study of 6 subjects (3 smoking, 3 intranasal applications) that for cocaine users, the saliva concentrations of cocaine exceeded 1000ng/mL (2–4 hours after the last drug abuse) [45]. Cooper et al. found $28 - 360\text{ng/mL}$ cocaine and $18 - 263\text{ng/mL}$ of

the metabolite benzoylecgonine in saliva samples of cocaine users [47]. To test drug detectors Wang et al. prepared sample concentrations of 12.5 – 1000 *ng/mL* [82]. In general drugs have a well defined ratio between the concentration in blood plasma and saliva [24]. For cocaine the oral fluid to blood concentration ratio is about 3, slightly increasing with time [86, 87].

Up to three hours after consumption traces of cocaine remain in the mouth (not when injected). Already after one hour, cocaine is extracted from blood by saliva glands and secreted again into the oral cavity. The half-life of cocaine is roughly 0.7 – 1.5 *h*. The time, which cocaine remains detectable can vary depending on factors like the weight, age, health of the consumers and frequency of use of the drug. Generally speaking it is detectable in saliva, blood, and urine for some days and in hair even for months [79, 88].

2.1.3 Collection and Preparation of Human Saliva Samples

This section explains the background of saliva sample collection, reports on its advantages and disadvantages, and presents the conditions under which samples are usually collected. Different methods to collect bigger amounts of saliva are explained and compared in terms of the flow rate. An overview on the most important saliva collector types for lab analysis is given and some commercially available tools are listed. The last section presents the state of the art of commonly used saliva sample preparation steps.

Why Collecting Saliva Samples?

To date, oral fluid screening systems for the detection of drugs of abuse have been used in only a few countries, but now an increasing number of countries are planning to introduce them as a legal screening device [89].

Collecting saliva as diagnostic fluid brings along many amenities. The main advantage is the non-invasive and painless collection of samples. Therefore, they can be obtained more frequently than it would be practical with blood tests. To monitor the patient's health and the disease state in shorter time intervals is a highly desirable goal for health care research and health promotion.

Compared with other techniques as blood sampling, saliva is easy to handle, because it does not clot. Only minimal trained personal is required (cost factor). Depending on the application even the ability for self-collection outside of the clinical setting exists.

Small and simple devices can be used for saliva collection and the hygienic standards are less demanding than for blood tests, which facilitates point-of-care (POC) testing. For on-site drug testing, the police can take saliva and urine samples. Saliva is preferred to get a snap shot view of the analyte concentration in the body to probe recent consumption whereas urine gives more information about consumption some days ago, which is more interesting for workplace testing and doping tests in sports.

Furthermore, an increasing number of systemic diseases and conditions have been shown to be reflected diagnostically in saliva. Some substances may reach saliva by passing from

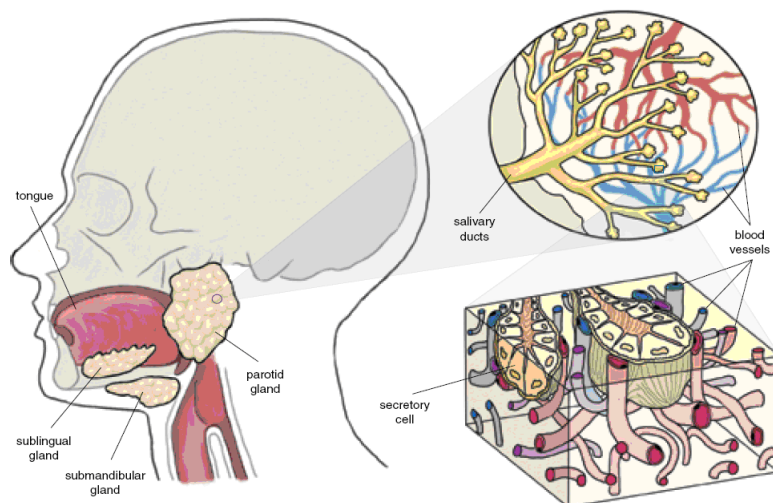


Figure 2.3: Saliva is produced in the sublingual, the submandibular, and the parotid glands. Within each of them, a fine mesh of capillaries surrounds a network of ducts that carry saliva to the mouth. Blood vessels that crowd around the lobed structures make transferring water, salts, and many circulating proteins and molecules. [90]

blood through the spaces between cells (see Figure 2.3). Hence, most compounds found in blood are present in saliva as well. This way, oral fluids can be viewed as a filtrate of blood. Especially, saliva represents a window to the human body for small molecular weight analytes [64]: correlations between salivary and blood serum concentrations have been established for several pharmaceuticals [6]. Also a variety of drugs of abuse levels, including those of marijuana, cocaine, and alcohol, can be monitored [25, 91–93].

In conclusion, saliva is an emergent diagnostic fluid for medical and forensic applications as depicted above, but it also shows some disadvantages. The main drawback is the unstable and low concentration of most analytes in saliva. Finally, it is also a matter of the acceptance in public. There are behavioral perception and cultural reservations against using saliva. In western countries, for example, the act of spitting is taken as an insult, whereas in some other cultures it can be considered a blessing. [92]

Conditions for the Saliva Collection

The conditions in the oral cavity (influenced by smoking, meals, and drinks) strongly have an impact on the composition and behavior of saliva. In addition the composition varies with the saliva flow as explained in section 2.1.1.

Therefore, conditions of collection as similar as possible have to be taken into consideration to get comparable measurements. Common guidelines for saliva sample collection do not exist. Different studies follow different instructions, but over all the rules are within the same scope: saliva samples are usually collected before brushing teeth and applying make-up (lipstick). The subjects should refrain from smoking, eating, and drinking for 1–2 hours.

As a preparation step the mouth is rinsed with cool water to remove food debris and other non-salivary contaminants. [27, 40, 94]

Methods for Collecting Whole Saliva Samples

Traditionally several methods are used for the collection of large quantities of whole mouth saliva (the liquid with all ingredients as it appears in the oral cavity). Usually for all of them the subjects are instructed to tilt their heads forward, keep the eyes open and make as few movements as possible. [94]

Draining Method The saliva drains out between parted lips into a receptacle held near the mouth.

Spitting Method The saliva is collected in the oral cavity behind closed lips and is expectorated repeatedly into a receptacle.

Suction Method A tube can be used to suck saliva from under the tongue, the floor of the mouth into a vessel.

Swab Method Cotton (or synthetic) swabs are inserted under the tongue to absorb saliva collection on the floor of the mouth.

Stimulated versus Non-Stimulated Collection

The average of total daily flow of saliva ranges from 0.5 – 1.5L, depending on the individual [65]. There are daily and annual variations of the flow rate. Low flow rates occur during sleep, whereas peaks occur during high activity or stimulation periods. In general, in summer the flow is much smaller compared to the flow rate in winter time [67, 95]. Also opened/closed eyes, the position and angle of the head, as well as the extent of movements influence the salivary flow rate [94].

Gustatory and masticatory stimuli increase the salivary flow at the collection. For detection of analytes in saliva non-stimulated samples are preferred due to the higher concentration of the molecules of interest. Navazesh et al. measured the flow rate of stimulated and non-stimulated saliva collection methods [94]. In a study they compared the different collection methods and found that resting salivary flow values were roughly equivalent for all the mentioned collection techniques (see Table 2.2).

Based on the spitting technique, different methods of salivary stimulation were evaluated; two gustatory methods (drops and filter paper) and one masticatory method (chewing). The first gustatory stimulus was a 0.1M citric acid solution (0.17g) applied as droplets on the tongue. For the filter paper method, 0.1mL of the citric acid solution was applied on a filter paper disc (diameter = 2cm) which was then gently pressed on the tongue. As masticatory stimulus a polyvinyl acetate gum base was used for chewing at a rate of 20strokes/min.

Chapter 2. Materials & Methods

Table 2.2: Whole mouth salivary flow rates for different collection methods. [94]

Collection Methods	Flow Rate (<i>g/min</i>)
Draining Method	0.47 ± 0.06
Spitting Method	0.47 ± 0.06
Suction Method	0.54 ± 0.12
Swab Method	0.52 ± 0.08

Table 2.3: Whole mouth salivary flow rates for different methods of salivary stimulation. [94]

Stimulation Methods	Flow Rate (<i>g/min</i>)
Drops Method	2.64 ± 0.22
Filter Paper Method	1.51 ± 0.21
Chewing Method	2.38 ± 0.52

The stimuli induce significantly higher salivary flow rates compared to resting levels, but also the between- and within-subject variances were higher. As shown in Table 2.3 stimulation produced a remarkable higher flow rate, whether individual resting flow rates at the beginning were low or high.

After around five minutes stimulating the flow, saliva gets highly diluted. Due to this dilution, stimulating will inevitably also change the pH and concentration of the analyte in the oral fluid. For instance for cocaine, the concentration lowers about five-fold [96].

To conclude the way of saliva collection is not crucial. The quantity is given by the natural flow rate of saliva and is independent of the collection method [94]. The flow rate (rate of secretion) can be stimulated but that tends to dilution after a few minutes of collection (lower analyte concentration).

Commercially Available Saliva Collection Tools

Whole saliva collected as mentioned in the section "Methods for Collecting Whole Saliva Samples" is often contaminated with food and other debris from the mouth, and is also relatively viscous. This is why it can be difficult to work with saliva in the laboratory. In addition, the collected volume will often be less than 1 mL. To handle these challenges the following three general saliva collecting methods got established: wipe collectors, swab collectors, and collectors on device. In the following subsections, each type is described and illustrated with an example. Table 2.4 presents a selection of commercially available collectors reported in

literature. Most of them are used for immunoassay based drug tests. The detection limit for cocaine is also reported in Table 2.4 as well.

Wipe Collectors The subject wipes or just places a cotton or foam pad collector mounted on a stick in the mouth and let it draw oral fluid. Usually a container is also provided for the later transport to the lab. Some of these containers are empty and only seal against contamination, sometimes they contain liquid preservatives to stabilize and dilute the samples. As an example Figure 2.4 shows the wipe saliva collector OraSure[®].



Figure 2.4: Wipe saliva collection tool: OraSure[®]; white pad collector on blue stick provided with transportation bag containing liquid preservatives. [97]

Swab Collectors Using the swab collectors the subject is asked to chew for a certain time on the swab which draws saliva. The masticatory motion stimulates the salivary flow primarily and in addition the swabs are also available prepared with citric acid for gustatory stimulation (refer to section 2.1.3). Figure 2.5 shows the commonly available swab collector called Salivette[®]. Here the subject places the cotton swab in the mouth, chews it for about 1 minute, and put it then into the Salivette[®] tube within a closable insert. After saliva extraction in the lab (e.g. by centrifugation), this closed inner tube containing the swab can be hygienically disposed.



Figure 2.5: Swab saliva collection tool: Salivette[®] system with stopper, swab, insert, and Salivette[®] tube (left to right). [98]

Collector on device Collection and testing are here integrated in one device. During the test (holding or wiping in mouth), saliva is collected directly at the collection pad on the device, which eliminates sample adulteration or contamination. As an example of such an integrated collector the device OraTect[®] is presented in Figure 2.6.



Figure 2.6: Collection on device tool: OraTect[®]. [97]

Chapter 2. Materials & Methods

Table 2.4: Selection of collectors reported in literature (roughly split into the presented methods; wipe collectors, swab collectors, and collectors on device) [64, 99, 100]. For immunoassay based drug tests the detection limit for cocaine is indicated.

Name of collector	Method of operation	cocaine det. limit
OraSure [®]	wipe and preservative diluent	1.5ng/mL [48]
Oracol	absorbent foam swab which is then centrifuged	n.a.
DrugWipe [®]	wipe only (tongue or skin)	50ng/mL [101, 102]
Cozart [®] collector	absorbent foam pad plus diluent	10 – 300ng/mL [103]
Dräger Drug Test [®]	absorbent foam pad with diluent	n.a.
Intercept [®]	absorbent foam pad with diluent	n.a.
OralScreen [®]	absorbent foam pad only, drops applied to device	15ng/mL [104]
Quantisal [™]	absorbent foam pad plus diluent	n.a.
SalivaScreen [®]	absorbent foam pad, drops applied to device	30 – 40ng/mL [46]
Salivette [®]	cotton wool swab which is then filtered and centrifuged	n.a.
Toxiquick [®]	absorbent bud, saliva squeezed in syringe to apply on device	50ng/mL [105]
OralLab [®]	collector squeezed to apply saliva in test cartridge	10 – 20ng/mL [46, 106]
Transorb [®] wicks	absorbent, filtering devices	n.a.
Mini-UniPrep [™]	collection and integrated filtration	n.a.
OraTect [®]	absorbent directly connected to device	20ng/mL [102, 107]
UpLink [™]	absorbent directly connected to device	200ng/mL [102]
OraLine [®]	direct application to oral cavity, or use of other collectors	25ng/mL [108]

Depending on the application only the most important challenges mentioned at the beginning of this section are solved. The problem of contamination is reduced by a provided sealed container or by collecting directly onto the device. To overcome the low sample volumes, the collected sample can be mixed with a dedicated diluter (reduction of the analyte concentration), which also can take over the function of a preservative. In general the viscosity of the saliva samples can be reduced by the common freeze-thaw-centrifugation (FTC) technique. During this process the long protein chains are broken and then separated.

To sum up, there are many different collectors commercially available (Table 2.4). Three general methods got established: wipe collectors, swab collectors, and collectors on device. Detection devices integrated on the collector show reliabilities of 60 – 80% [109].

The problem of contamination can be reduced by collecting directly onto the device. To overcome the low sample volumes, the collected sample can be mixed with a dedicated diluter, which can also take over the function of a preservative. Using swab or some kinds of wipe collectors reduces the viscosity directly, because debris and some bulky proteins remain in the swab tissue. Actually all techniques influence in some way the composition of saliva due to different transfer efficiencies of the different components. [99, 110]

Regardless of the collection method for the subsequent analysis, the samples are usually filtered or centrifuged to further reduce the viscosity. For filtration, often syringe filters showing a pore size of $0.2\mu m$ are used [26]. Centrifugation to remove bulky proteins is typically performed in a small tube at 4000 times g for around $10min$ [64].

Preparation of Saliva Samples

The tiny microfluidic channels, junctions, and nozzles are at high risk of clogging, because whole saliva samples show a high viscoelasticity and often contain food debris and cells as mentioned in section 2.1.1. Therefore, some basic sample preparation steps are inevitable. Here, we present a list of state-of-the-art techniques applied to whole saliva samples as sample preparation steps prior to be used as liquid in microfluidic devices:

- filtration:
 - * syringe filter
 - * ultra filtration
 - * microfluidic H-filter
- centrifugation
- dilution
- freeze-thawing
- cell lysis

For our application the filtration preparation method presented among others by Yager et al. seems to be the most interesting. It is a flexible, portable, and low-cost technique. Centrifugation already needs a machine in the lab. Dilution is not applicable in our case due to the

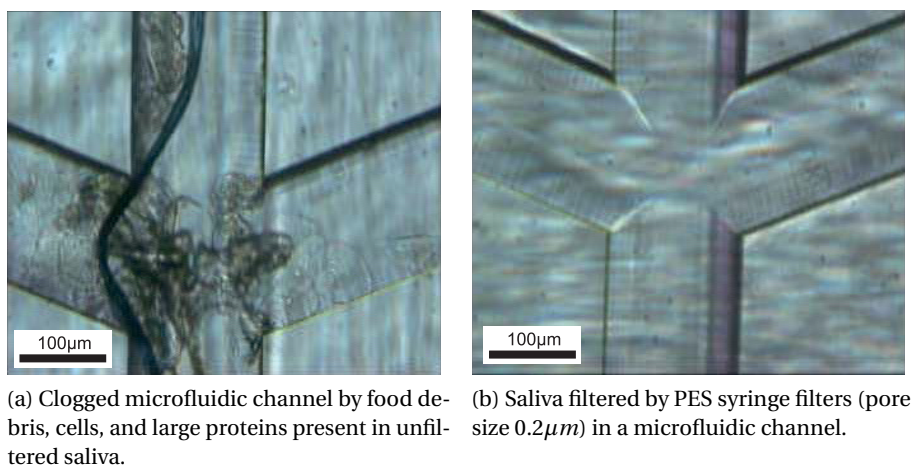


Figure 2.7: Effect of saliva filtration.

already low analyte concentration in saliva. Freeze-thawing and cell lysis are rejected because they alter the cocaine molecule.

2.1.4 Saliva Samples in the IrSens Project

Saliva donors were chosen randomly with good variation of gender and age. Prior the sample collection, the donors were asked to refrain from eating, drinking, and smoking for at least one hour and to rinse their mouth with water. We collected human saliva samples using the spitting method (see section 2.1.3). No stimulation, neither mechanical (chewing) nor a chemical stimulant, was applied to avoid dilution and consequently a decrease of the analyte concentration.

Saliva samples were processed individually for the saliva characterization experiments. To get a more representative, averaged sample, the saliva collected from different donors was mixed together for all the other experiments such as the absorption or extraction measurements.

The samples were filtered to remove food debris and a big part of the long glycoproteins (see Figure 2.7) as suggested in [26]. We used PES (polyethersulfone) syringe filters showing a pore size of $0.2\mu\text{m}$ (Carl Roth GmbH, Karlsruhe, Germany). This filtering step reduced the saliva volume by a factor of around 2. The small cocaine molecules passed through the filter. No change of the cocaine concentration in saliva was observed comparing the concentration in filtered and unfiltered samples.

The pH value of the sample was adjusted and stabilized at pH 9 by adding 10% of a buffer concentrate (Titrisol[®] buffer concentrate, Merck, Switzerland). This pH value was chosen to be higher than the pKa value of cocaine for better extraction conditions, but still as low as possible, since components of the buffer may attack the substrate of the optical waveguide of the final integrated system (hydroxide OH^- attacks silicon).

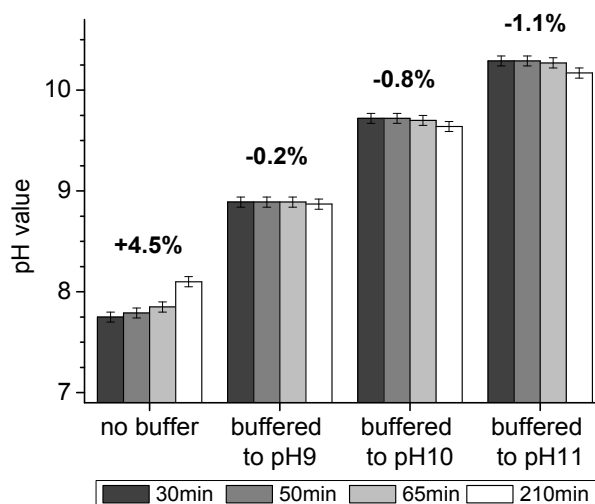


Figure 2.8: Time evolution of the pH value (in %) of natural and buffered (10% buffer concentrate) human saliva samples. pH measurements were performed by an ISFET-based sensor in $500\mu\text{g}/\text{mL}$ cocaine spiked saliva samples. Error bars indicate the standard deviation for 19 samples of different donors.

Finally saliva samples were spiked with powder of free base cocaine (purity higher than 98%, Lipomed, Switzerland). The cocaine was purchased with the permission of the Cantonal Drug Administration of Neuchâtel.

2.1.5 Adjustment of the pH-Value of Human Saliva

Saliva is slightly acidic in steady state, showing a normal pH value of 6 to 7. The pH value in salivary flow can be in the range from 5.3 at low flow conditions up to 7.8 at the peak flow. [66]

Saliva has a certain buffering capacity to buffer to the physiological pH value of around 7. There are three main buffering systems involved (see Table 2.1):

- phosphate buffer, stable
- protein buffering system, stable mostly active to buffer acids
- bicarbonate buffer system, changes when exposed to air

The bicarbonate buffer system is no more balanced, when saliva is exposed to air. CO_2 escapes, which decreases the H_3O^+ concentration in saliva and results in a higher pH value. [111]

Adding cocaine (base) to saliva, the pH value slightly increases. In our study with samples of 19 donors the pH value increased from 7.44 to 7.75 by adding $500\mu\text{g}/\text{mL}$ of cocaine. The pH value then further increased (4.5%) over time mainly due to the unbalanced bicarbonate buffer system. The value can be stabilized by adding 10% of Titrisol[®] buffer concentrate, whereas smaller concentrations of buffer (1%) were not able to stop the raise of the pH value (see Figure 2.8).

2.1.6 Rheological Characteristics of Human Saliva

In this section we present the basic theory, some references as well as our own measurements of some important rheological characteristics of saliva samples such as the viscosity, the viscoelasticity, and the surface tension.

Viscosity

Viscosity is the measure of the internal friction of a liquid. This internal friction becomes apparent when a layer of a liquid is moved in relation to another layer. The friction is larger, when the amount of force (shear stress) required to cause this movement (shear rate) is larger. Viscosity is defined as the ratio of shear stress to shear rate, which is given by

$$\eta = \frac{\text{shear stress}}{\text{shear rate}} = \frac{\tau}{|\dot{\xi}|} [Pa \cdot s], \quad (2.1)$$

where τ is the shear stress [Pa] and $|\dot{\xi}|$ the shear rate [s^{-1}]. Water at 20°C has a viscosity of $1.002 mPa \cdot s = 1.002 cP$ [68].

Ostwald-de Waele model This model is a two-parameter power-law model, a simplification of the Carreau-Yasuda model. The Ostwald-de Waele model describes the viscosity as a function of the shear rate.

$$\eta(|\dot{\xi}|) = m \cdot |\dot{\xi}|^{n-1} [1], \quad (2.2)$$

whereas m is a parameter called flow consistency index and n is the flow behavior index:

$$\begin{aligned} n < 1, & \quad \text{non-Newtonian shear-thinning,} \\ n = 1, & \quad \text{Newtonian fluid with } \eta=m, \\ n > 1, & \quad \text{non-Newtonian shear-thickening.} \end{aligned}$$

Water is an example of a Newtonian fluid, where the shear stress is directly proportional to the shear rate. So called pseudo-plastic, or non-Newtonian shear-thinning fluids show lower viscosity at higher shear rates, and are usually solutions of large, polymeric molecules in a solvent with small molecules.

Shear-thinning Saliva Saliva is a shear-thinning, non-Newtonian fluid. High molecular weight glycoproteins (mucins)(see section 2.1.1) are responsible for this complex rheological behavior [62]. At rest or low shear rates the long protein chains are in irregular order, and therefore a resistivity against flow is observed (i.e. high viscosity). At higher shear rates the mucins disentangle and become aligned in parallel to the driving force, what allows them to slip on each other more easily. In conclusion, the viscosity of saliva decreases with increasing

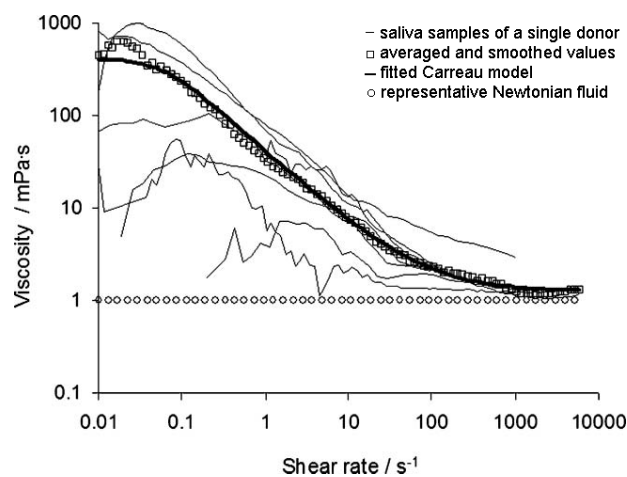


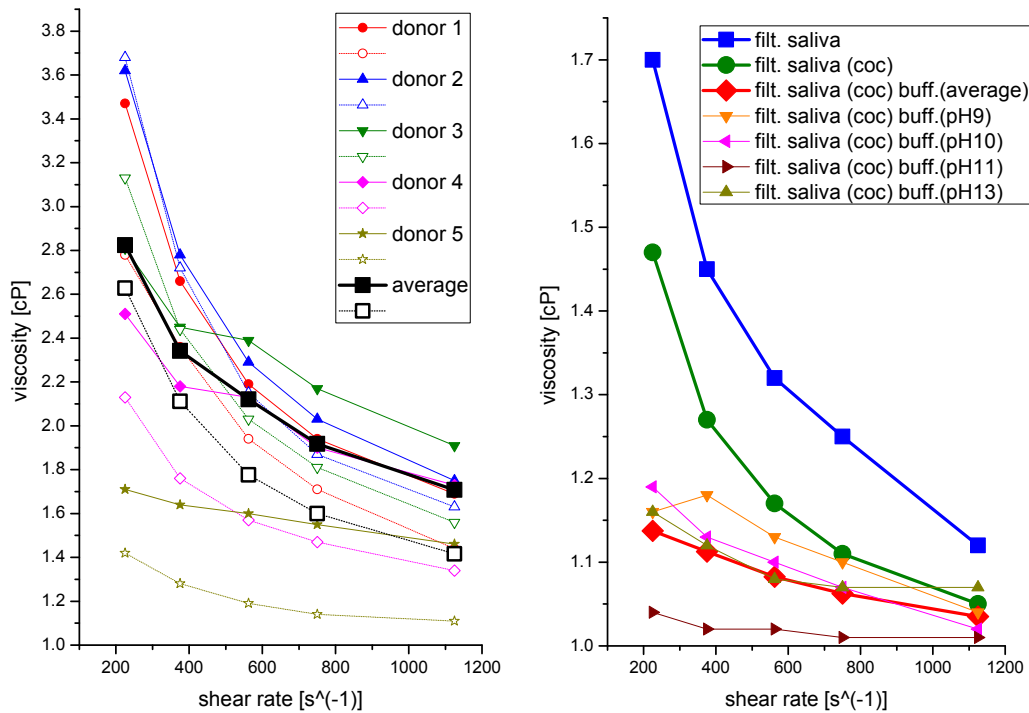
Figure 2.9: Shear rate-dependent viscosities of several human saliva samples of a single donor on different days (fine lines), averaged and smoothed values (boxes), the fitted Carreau-Yasuda model (bold line), and as comparison a representative Newtonian fluid (circles) [73].

shear rates as presented in Figure 2.9. Helton and Yager measured at shear rates up to 0.02s^{-1} almost constant viscosity of around $400\text{mPa}\cdot\text{s}$. In the range of 0.02s^{-1} to 1000s^{-1} they observed the transition region. For higher shear rates saliva is in the Newtonian regime [73]. Waterman et al. derived for saliva a dynamic viscosity of $10^4\text{Pa}\cdot\text{s}$ [60]. Davis concludes saliva is a highly viscoelastic fluid and shows viscosity values of $0.01\text{Pa}\cdot\text{s}$ to $40\text{Pa}\cdot\text{s}$ in a frequency range of $2.5 \cdot 10^{-3}\text{Hz}$ to 10Hz [112]. This demonstrates the high inter-subject and intra-subject variations what is also confirmed by Rantonen, Panu [110] and our own measurements (see Figure 2.10).

We measured the viscosity of saliva as well, but in a smaller range of shear rate. These results correspond well with the measurements of Helton and Yager [73] (compare Figure 2.10a and 2.9). Furthermore, we investigated the effects of sample preparation on the viscosity. Our viscosity measurements presented in Figure 2.10 are recorded with a Brookfield Viscosimeter LV DV-II+Pro (Brookfield, Germany) using a spindle CPE-40. The measuring inaccuracy was around 2% (max 9%). Samples were prepared as described in section 2.1.4. Filtration (removing some of the large glycoproteins) reduced the viscosity overall, but the shear-thinning behavior remained as shown in Figure 2.10a. Spiking with cocaine and dilution with buffer reduced obviously the shear-thinning behavior. But the effect was considered as pH-value independent as presented in Figure 2.10b.

The curves of Figure 2.10 describing the shear rate dependent viscosity can be fitted well to the Ostwald-de Waele model showing R-square values > 0.97 (see Table 2.5).

Studies in literature report considerable reduction of the salivary viscosity by 17 – 50% within only three hours, caused by proteolytic degradation of mucins by the bacteria present in our mouth [62].



(a) Influence of filtration on the viscosity. Solid symbols represent the measured values before filtration and empty symbols the values after filtration.

(b) Influence of spiking filtered saliva (mixture of 19 donors) with 500 μg/mL of cocaine and the effect of additional buffering on the viscosity.

Figure 2.10: Shear rate dependent viscosity measurements of human saliva samples.

Table 2.5: Fitting parameters of the Ostwald-de Waele model for the curves presented in Figure 2.10.

curve	m	n
Figure 2.10a: unfiltered saliva	15.05	0.6893
Figure 2.10a: filtered saliva	22.52	0.6020
Figure 2.10b: filtered saliva	6.76	0.7433
Figure 2.10b: filtered saliva with cocaine	4.65	0.7846
Figure 2.10b: buffered, filtered saliva with cocaine	1.567	0.9414

Viscoelasticity

The viscoelasticity is described by the frequency dependent dynamic moduli G' (elastic storage modulus, representing the solid-like component) and G'' (viscous loss modulus, representing the liquid-like component). In the frequency range of $0.5 - 10\text{ Hz}$ values < 1 were determined for the ratio of G'' to G' , which indicates saliva to be a more elastic and gel-like solution [73].

Surface Tension

The surface tension of different human saliva samples was measured with a Kibron AquaPi (EZ-Pi) (Krüss, Germany). Samples were prepared as described in section 2.1.4. Filtration did not influence the surface tension (see Figure 2.11a), whereas adding cocaine or buffer solution to saliva reduced its surface tension (see Figure 2.11b). Bases (cocaine or buffer) introduced in water disturb the hydrogen bonds between water molecules, which resulted in this lower surface tension.

2.2 Reference System for Cocaine Measurements

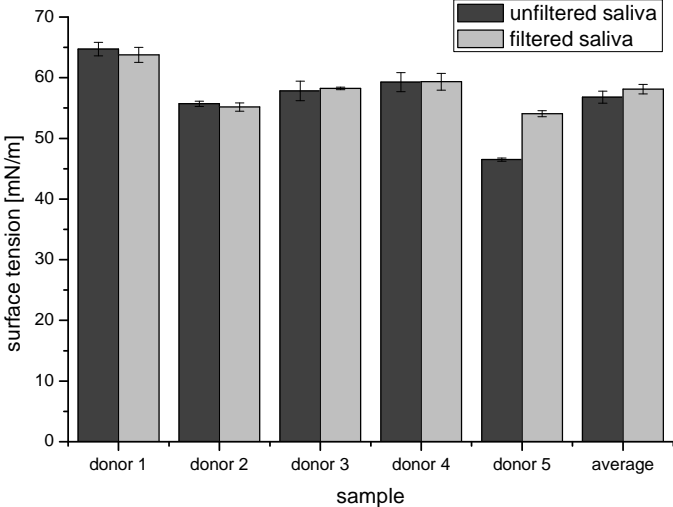
The method commonly used to detect cocaine in human body fluids is mass spectrometry (MS). The machine used is a heavy, non-portable laboratory apparatus (Figure 2.12). Our reference measurements were performed by the Swiss Laboratory for Doping Analyses (LAD) at the Centre Hospitalier Universitaire Vaudois (CHUV) in Lausanne. This laboratory is accredited by the World Anti-Doping Agency since 1991 and ISO 17025 certified. The samples were measured with a class leading ultra performance liquid chromatography - mass spectrometer (UPLC-MS). The machine Xevo TQ-S from Waters is designed for the most demanding quantitative UPLC-MS applications [113]. It features an off-axis ion source technology, known as StepWave, for accurate, robust, and reproducible measurements with an overall measurement uncertainty of 5%. In the system the column UPLC BEH C18 $1.7\mu\text{m}$ was used.

A calibration curve was recorded using well defined cocaine concentration standards (see Appendix A). Linearity was observed for the concentration range $5 - 2500\text{ ng/mL}$. Higher concentrations had to be diluted for the measurement. Our samples were always analyzed the same day as the microfluidic experiment was performed because it was observed that most of the cocaine in saliva was transformed to its metabolites within 5 days as also observed by [88].

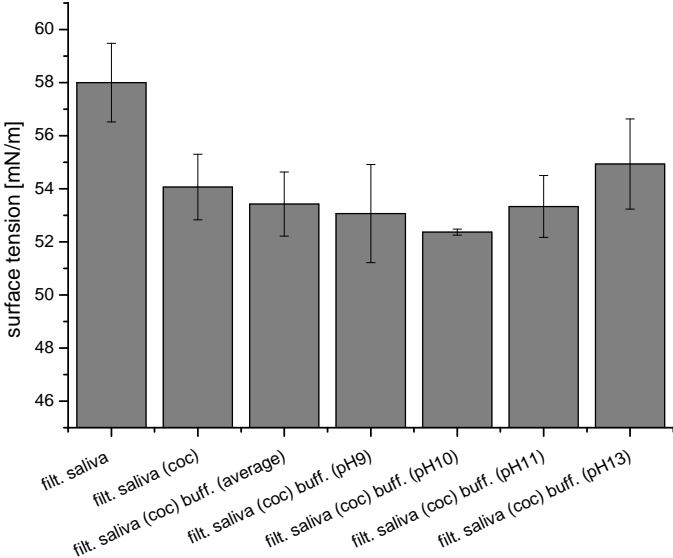
2.2.1 Sample Preparation for Mass Spectrometry

Sample preparation protocol for cocaine detection in human saliva

$100\mu\text{L}$ of the saliva sample was mixed with $500\mu\text{L}$ dilution solution (80% acetonitrile, 20% water) and $400\mu\text{L}$ water. Then $5\mu\text{L}$ of the mixture was injected in the mass spectrometer.



(a) Filtration has no significant influence on the surface tension.



(b) Influence of spiking filtered saliva (mixture of samples of 19 donors) with 500µg/mL of cocaine and the effect of additional buffering on the surface tension.

Figure 2.11: Surface tension measurements of different human saliva samples. Error bars indicate the standard deviation for 3 independent measurements.



Figure 2.12: Ultra performance liquid chromatography - mass spectrometer Xevo TQ-S from Waters [113].

Sample preparation protocol for cocaine detection in PCE

100 μL of the PCE sample was mixed with 900 μL dilution solution (80% acetonitrile, 20% water) and then the liquid completely evaporated. The container containing only the cocaine was refilled with 1 mL of water and well mixed before 5 μL were injected in the spectrometer for the analysis.

2.3 Materials used for Microfluidic Devices

First microfluidic systems were fabricated by the well-developed techniques of the microelectronics and integrated circuit industry. Microfluidic channel networks can be achieved by photolithographic steps and by wet and dry etching: Plasma etching results in nearly vertical channel walls, anisotropic wet etching produces V-shaped grooves and isotropic wet etching produces D-shaped channels. More complex 3D networks of microfluidic channels can be made by bonding several patterned layers together. [114]

These devices made in glass, silicon or quartz, are slowly replaced by cheaper polymer devices mainly because the price of the substrate material is too high for high volume production. Furthermore, for glass, silicon or quartz are too many fabrication steps involved, which raises the time and cost of fabrication and the geometrical designs are limited.

Much work has been focused on creating inexpensive, disposable polymer devices for high-throughput production. Most commercially available devices are fabricated in polymers such as polycarbonate (PC) and polymethylmethacrylate (PMMA). Micronics (founded in 1996 and acquired by Sony in 2011) was one of the first companies who recognized the importance of

Chapter 2. Materials & Methods

Table 2.6: Comparison between polymers and glass properties with respect to their use for microfluidic applications.

	Polymer	Glass
Manufacturing costs	low relative to glass, especially for mass production	higher in cost, especially for large-area substrates and due to clean-room facilities
Fabrication complexity	simpler than for glass	time consuming and expensive wet chemistry
Clean-room facilities	not necessary	often required
Material properties	wide selection of polymers with different properties	less variability
Operation temperature	limited because of low glass transition temperature	higher relative to polymers
Optical properties	optical transparency lower than glass	excellent optical properties, very low autofluorescence
Bonding	different options: adhesives, thermal fusion, plasma, ultrasonic and mechanical clamping	time consuming compared to polymers: thermal, adhesive and anodic bonding
Surface treatment	available, but not yet well established	established using silanes
Compatibility with organic solvents or strong acids	generally not compatible with most organic solvents and strong bases or acids	good resistance
Geometrical flexibility	many different channel cross-sections possible	limited
Permeability to gasses	generally higher permeability relative to glass	no permeability

plastics in developing POC diagnostics. They developed thin-film laminate-techniques and injection-molding for microfluidic chips (see Figure 1.2a) [19, 115].

An overview of the most commonly used materials and developed fabrication methods for polymers such as hot embossing, injection molding, and different casting methods was presented by C.E. White in 2003 [116].

2.3.1 Comparison of relevant Properties for Microfluidic Applications between Glass and Polymer

Glass is an amorphous solid material. Polymer materials show a porous structure and consist of long, high molecular mass polymer chains. This completely different chemical structure results also in different material properties. Table 2.6 compares glass and polymers with respect to relevant properties for microfluidic applications. The presented table was adapted and simplified from [117].

2.3.2 Material Requirements for Microfluidics

Microfluidic material requirements have been discussed by several authors in the literature [117–119] and correspond basically to the points listed in Table 2.6.

Regarding Table 2.6 for some criteria glass shows better material properties. But depending on the final product, the less expensive polymers might be the better choice, because these criteria, for which glass performs better than polymers, are less relevant or even neglectable for a specific application.

For polymers attention has to be paid especially to thermal properties and chemical resistance against certain solvents or strong acids. For observations in microfluidic devices the optical properties (transparency, autofluorescence) play an important role. For sensing applications the adsorption properties definitely have to be investigated.

2.3.3 Polymer Materials used in this Work

The microfluidic devices used in this project were mainly realized using UV-curable adhesive NOA81 from Norland Optical Adhesive (Norland Products Inc, Cranbury, NJ, USA). NOA81 contains among other substances mercapto-esters and its polymerization is a thiol-ene based crosslinking [120]. Compared to polydimethylsiloxane (PDMS), NOA81 has better chemical resistance, is impermeable to air and water vapor, and is less prone to swelling upon contact with fluids [121]. The higher stiffness of the cured polymer (compared to PDMS) of around 1 GPa [122, 123] allows higher clamping pressures, which is needed for droplet generation on a microfluidic chip at high flow rates.

NOA81 was used either in its pure form, or modified by mixing 1 wt% of APTES (Sigma-Aldrich GmbH, Buchs, Switzerland) in the uncured polymer. The surface modifications on the UV-cured polymer were performed either by oxygen plasma or by vapor-phase silanization using the fluoro-silane FOTCS (ABCR GmbH, Karlsruhe, Germany).

This polymer is designed for optical applications, but already in 2008 molding-based fabrication methods for microfluidic chips using NOA81 have been reported. Advantages of this novel material over the commonly used PDMS for low-cost microfluidic devices were presented, but a useful characterization of NOA81 was still missing. [122]

SU-8 from MicroChem (Newton, MA, USA), a negative epoxy resist, was processed by photolithography. SU-8 is a material which is known for very precise prototypes and devices [124]. We used this epoxy to fabricate masters for molding.

PDMS is probably the most commonly used polymer material for microfluidic devices, but it shows poor chemical resistance [125]. Therefore, its use is mainly restricted to aqueous fluids and not a suitable material for the microfluidic channels in our project. We used PDMS (PDMS 184, Sylgard, Dow Corning, Midland, MI, USA) for pattern transfer in context with molding techniques.

2.4 Rapid Prototyping of Microfluidic Devices

The first microfluidic systems were fabricated by the established fabrication technologies of microelectronics and microelectromechanical systems (MEMS) which allow for the development of a wide range of devices with different functionalities [114]. By replacing silicon and glass with polymer materials, new fabrication technologies were developed as presented in this section.

For research applications rapid prototyping methods are used [126]. These methods enable low-cost chip production and facilitate rapid design changes at the cost of high-volume production [127–130]. Rapid prototyping of microfluidic devices commonly implies liquid polymer casting on a structured master, polymer curing, demolding of the structured hard polymer and its bonding to a substrate in order to close the channels.

Here in this section we present methods to make the masters as well as the overall rapid prototyping process we developed for the polymer NOA81 with respect to the IrSens project.

2.4.1 Master Fabrication

Typically masters for rapid prototyping are made in glass or silicon or with a little bit higher geometrical flexibility by photolithographical structuring of an SU-8 epoxy layer. In this section the method using SU-8 is explained and in a second part we present our own master fabrication method based on Scotch-tape which is much more efficient in terms of fabrication time and is really low-cost, since no clean room environment is required. The Scotch-tape can be cut by hand, using a CNC-cutter or with higher precision also by a CNC-laser.

PDMS Master Based on SU-8 Photolithography

Figure 2.13 presents the well established process mainly used for fabrication of microfluidic systems made of soft polymers like PDMS. We applied this method at the beginning of the thesis to build structured PDMS parts, which were then used again as masters for NOA81 molding [131].

Scotch-Tape Master

We developed our own method to build low-cost Scotch-tape based masters for polymer molding inspired by a Chips & Tips article [132].

Common microscope glass slides were cleaned with ethanol and then we stuck gently a film of Scotch-tape on top (avoiding air bubbles being trapped). The negative structure of the desired microfluidic channels was printed on paper which was then put under the glass slide. This pattern was easily transferred to the Scotch-tape film by following the lines (visible through the glass slide) with the scalpel. An advanced example is shown in Figure 2.14.

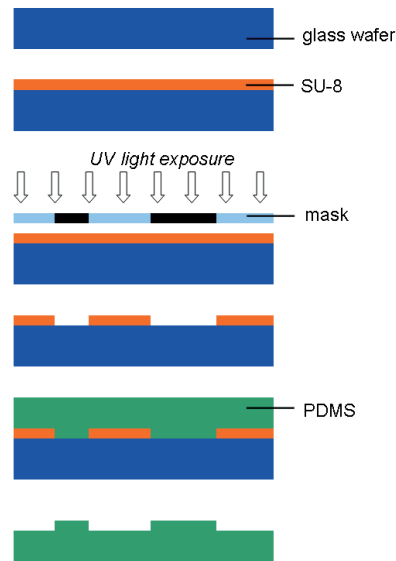


Figure 2.13: PDMS master fabrication: First SU-8 epoxy on a glass substrate was structured by standard photolithography. PDMS was casted and cured on this SU-8 structure and then demolded to be used as a master itself.

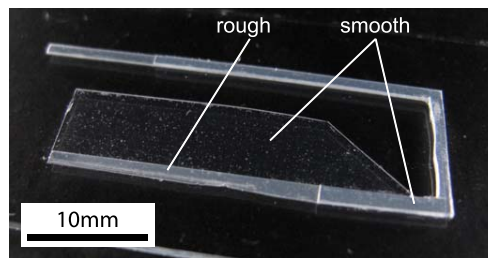


Figure 2.14: Picture of a Scotch-tape master with rough and smooth tape and showing different channel heights realized by different amounts of Scotch-tape layers.

Our method allows building multi-layer masters easily, which is extremely time consuming with the other well established methods. Furthermore, our method makes it possible to adjust the wetting behavior of the channel walls by employing Scotch-tapes with different roughnesses.

Multi-Layer Masters Based on cutting the structures by hand, our method shows quite weak accuracy in lateral dimensions ($\sim 200\mu m$), but the height of the channels was very well controlled. The Scotch-tape we used showed a homogeneous and almost not compressible thickness of $49 \pm 2\mu m$. The fact that the Scotch-tape is not compressible allows building multi-layer masters very precisely in the vertical dimension (unlike other tapes showing variations in the height over more than 50%). The height of stacks with different amounts of layers was measured (Alpha-Step IQ Surface Profiler, KLA-Tencor, error $\pm 2\mu m$) and a linear dependency found as shown in Figure 2.15.

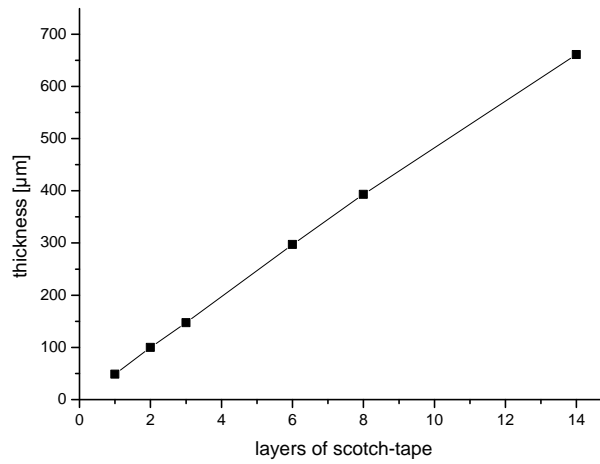
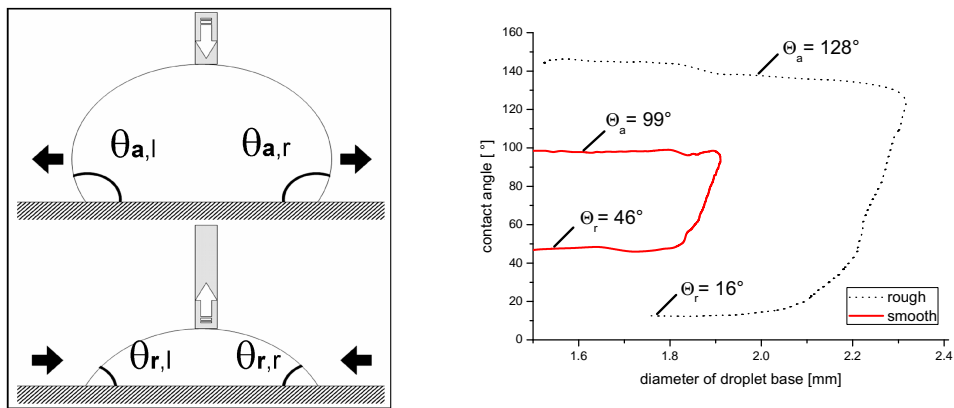
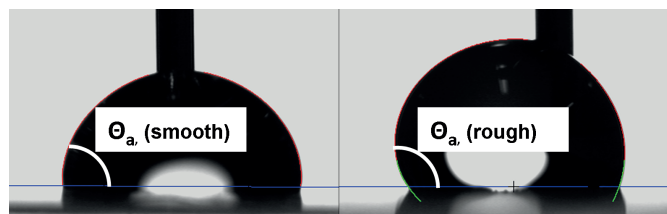


Figure 2.15: Thickness of the stack increases linearly with the amount of Scotch-tape layers.



(a) Principle of dynamic contact angle measurements: The advancing contact angle is measured when the droplet is growing, the receding contact angle when the droplet is shrinking.

(b) The smooth NOA81 surface is more hydrophilic with an advancing contact angle of 99°. It shows better wettability by water than the rough surface with an advancing contact angle of 128°.



(c) Growing water droplets on a smooth and a rough NOA81 surface during the advancing contact angle measurement.

Figure 2.16: Wetting behavior of water on pure NOA81 surfaces molded and cured on rough and smooth Scotch-tape.

Wetting Behavior Using Scotch-tape on the master with different roughness results in different wetting behavior of the replicated microfluidic channel walls. The NOA81 surface molded on the smooth, transparent tape (Transparent Scotch 550, 3M, France) is more hydrophilic than the one molded on the mat tape (Magic Scotch 810, 3M, France). This was investigated by dynamic contact angle measurements with water droplets (see Figure 2.16).

2.4.2 Fabrication & Assembly of the Microfluidic Device for the project IrSens

For the development of the microfluidic system we performed rapid prototyping based on the Scotch-tape masters (presented in section 2.4.1). An overview of the fabrication process is given in Figure 2.17.

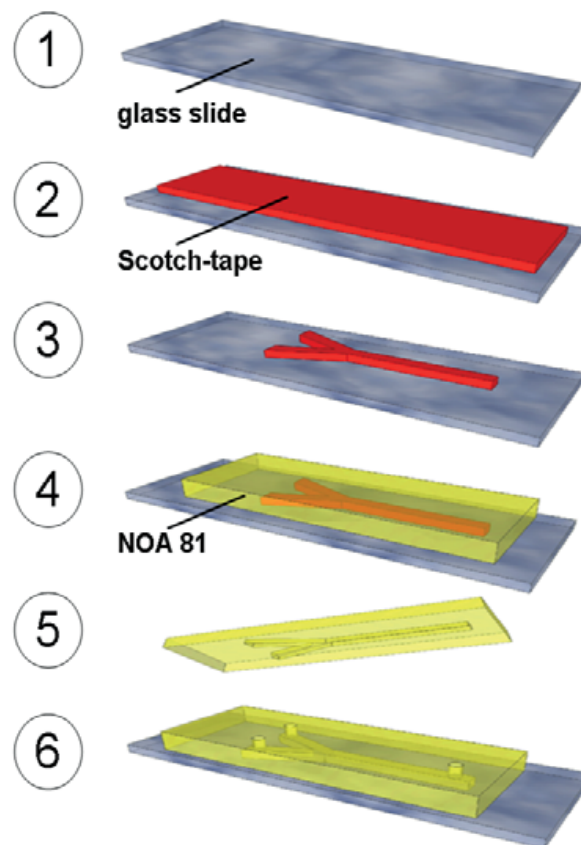


Figure 2.17: Fabrication process for NOA81 chips molded on Scotch-tape masters: A microscope glass slide was cleaned with ethanol first (1), then a Scotch-tape was stuck on top (2) and the desired negative structure of the microfluidic channel was cut out by hand with a scalpel(3). On this Scotch-tape master NOA81 was casted and cured under the UV-lamp (4). The demolded structured NOA81 part (5) was then bonded to a glass or silicon substrate by means of oxygen plasma (6).

NOA81 was casted on the Scotch-tape masters and then cured by exposure to UV-light ($1.5\text{mW}/\text{cm}^2$ at 365nm wavelength for 22min). Then the cured polymer was separated from the master which remained reusable for around 5-10 other molding cycles. Fluidic inlet and outlet holes were drilled into the channels to have later on access to the microfluidic channels. The structured NOA81 part was then exposed to oxygen plasma twice for 15s (400W , 2.45GHz , $500-700\text{mTorr}$, $400\text{cm}^3/\text{min}$ O_2 flow) together with the substrate (silicon or glass) before both parts were pressed together for bonding. Metallic connectors were glued (2 tone epoxy, Devcon) on top of the holes of the microfluidic chip to be able to connect the tubings. For aging of the polymers, the chips were put in the oven at 60°C for at least 12h [123]. A completed microfluidic chip on a glass substrate is shown in Figure 2.18. An additional temperature treatment at 130°C for 1h improved the bonding between NOA and the glass substrate.

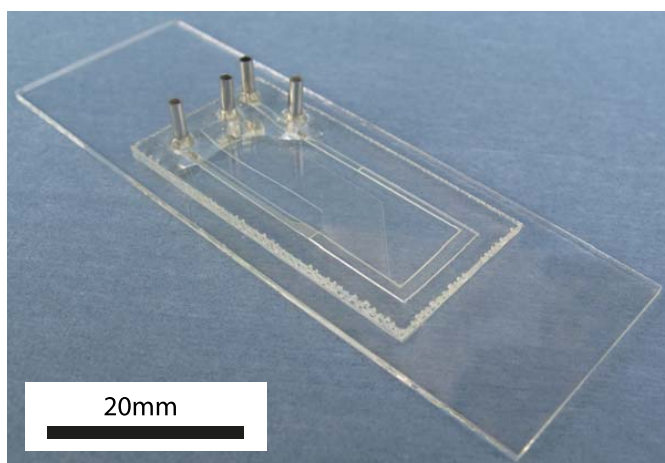


Figure 2.18: NOA81 microfluidic chip bonded on a microscope glass slide with metallic connectors glued on top for the tubing.

2.5 Microfluidic Measurement Setup

Our microfluidic chips (see Figure 2.18) were analyzed upside down under a microscope (Olympus) with the microfluidic measurement setup presented in Figure 2.19. Liquids were provided with two syringe pumps (PHD 2000 Infusion/Withdraw, Harvard Apparatus). If needed, the pressure at the microfluidic outlets was adjusted by the pressure control system (MFCS-8C, Fluigent). Images and video sequences were acquired using a high-speed camera (Phantom V210, Vision Research). To get bright enough pictures at high frame rates (short exposure time), a transmission setup for the illumination was chosen (see Figure 2.19b). The light source was placed under the chip, only separated by a light diffusor.

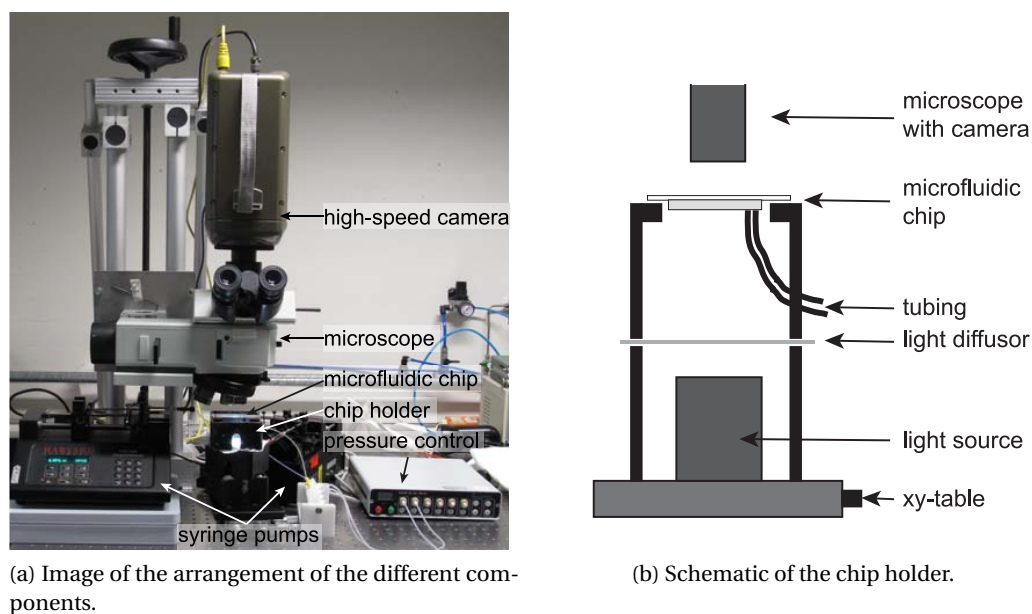


Figure 2.19: Microfluidic measurement setup.

2.6 Discussion

The human body fluid saliva is the perfect matrix for non-invasive, POC detection e.g. for roadside testing. Small molecules present in blood are expressed through the saliva glands and can be found in saliva as well in a fixed ratio [79]. On the other hand, saliva is a really complex fluid showing huge inter- and intra-subject variations. The very fast changing concentrations of the ingredients influence the analyte level, the pH value, and the rheological properties [63, 64]. The latter ask for a highly robust microfluidic systems. Furthermore, saliva is a non-Newtonian fluid, which does not make it impossible to use saliva as a diagnostic fluid in microfluidic devices, but it is definitely challenging [73]. We characterized the rheological properties of saliva before and after the basic sample pretreatment, which includes filtration and pH value stabilization (important for repeatability of our extraction process).

Mass spectrometry is the state-of-the-art method for cocaine detection in human saliva. We used a class leading ultra performance liquid chromatography - mass spectrometer in collaboration with the Swiss Laboratory for Doping Analyses for our cocaine reference measurements.

We presented materials used to build microfluidic devices together with specific material requirements which are important for LOC devices. Polymers are finding their way to microfluidic applications, but still today it is a challenge to find the appropriate polymer material for a complex microfluidic system which fulfills all the relevant material requirements for a specific application. We decided to work with NOA81, a material designed for optical applications, but suggested as a promising material also for microfluidic chip fabrication [122, 133]. Due to the new field of application still many material properties need to be characterized and verified which was done in the framework of this project and will be presented in the next chapter.

A new material asks also for a suitable fabrication method. In research and development, rapid prototyping techniques are popular [125, 128–130]. We developed our own low-cost, highly flexible, and time-efficient rapid prototyping method for NOA81. This method is not as precise as other established ones, but the achieved fabrication accuracy is more than enough for our application. Feature sizes smaller than $\sim 10\mu m$ are anyway not applicable with human saliva samples because of the risk of microfluidic channel clogging. If higher accuracy is needed, the Scotch-tape could be structured by laser cutting, which on the other hand implies higher costs and longer fabrication time.

2.7 Summary

In this chapter we put an emphasis on the nature of saliva and its usage as a sample liquid for the detection of small analytes, e.g. cocaine, in the human body. We explained and characterized the applied saliva sample pretreatment before using the saliva samples on microfluidic chips. We focused on the influence of these pretreatments on the rheological behavior of the human body fluid. Furthermore, the advantages of polymers as chip material for microfluidic systems were explained. We developed our own low-cost, time-efficient, and highly flexible microfluidic chip fabrication method for the UV-curable polymer NOA81. We also present the basic microfluidic measurement setup to analyze the fabricated devices.

3 Characterization of Microfluidic Channels Made of UV-Curable Adhesive

During the last decade polydimethylsiloxane (PDMS) has become one of the most commonly used and reported material in literature for low-cost molding-based fabrication methods of microfluidic systems [127]. However, its application range is limited by poor mechanical strength and chemical resistance against most non-aqueous solvents. The group of Whitesides investigated the solvent compatibility of PDMS-based microfluidic devices [125]. The major problem they observed was swelling. Furthermore, stable surface modifications to adjust the wetting behavior are lacking for PDMS [134, 135].

In 2008, Norland Optical Adhesives (NOA 81 and NOA63) were suggested as a substitute of PDMS for rapid prototyping of microfluidic devices [122, 136]. These UV-curable glues were originally designed to bond optical components or fiber optics, but are also well suited for molding based replication of microfluidic structures [121, 122, 131, 136].

Since NOA is a new material for microfluidic applications, not many material properties are known and need to be investigated. This chapter shows the characterization of NOA81 polymer microfluidic channels with respect to project relevant aspects. The resistance against IR-transparent organic solvents is important, because cocaine will be extracted to such a matrix for IR-spectroscopy. The cocaine absorption has to be investigated since we would not like to lose our analyte in the chip material. Because we are working with a two-phase system (aqueous and organic phase) to control the wetting behavior of channel walls is essential. We also characterize the materials UV-characteristics and its performance for rapid prototyping. Results are always put in relation to values of the commonly used material PDMS.

This chapter is based on a journal publication in *Sensors and Actuators B* [137] as well as on the conference contributions to μ TAS 2010 [138] and the IMCS 2012 [139].

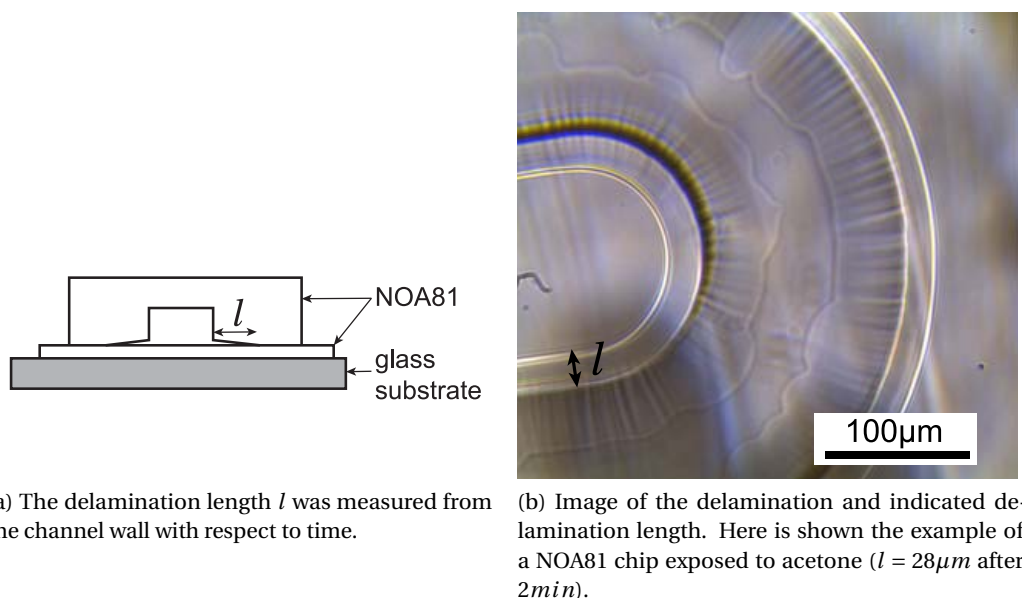


Figure 3.1: Delamination occurring on plasma-bonded NOA81 channels during their exposure to organic solvents.

3.1 Chemical Resistance Against Mid-IR-Transparent Organic Solvents

The compatibility of NOA81 chips with different organic solvents was evaluated with an emphasis on IR-transparent organic solvents, which could be used as carrier medium of the analytes for IR-spectroscopy. The results of this section were published in *Sensors and Actuators B* [137].

3.1.1 Method

In order to test the chemical compatibility, microfluidic chips with a simple meander shaped microfluidic channel were fabricated of NOA81 by rapid prototyping (as explained in section 2.4.2). The structured part as well as a thin film of NOA81 (cover plate) were treated by oxygen plasma, and then bonded together as shown in Figure 3.1a. In this way an all-polymer microfluidic channel made of NOA81 was achieved.

The microfluidic chips were analyzed under the microscope as described in section 2.5. Different organic solvents were pumped through the microfluidic channels at a rate of $1\mu\text{L}/\text{min}$. The solvents attack the bonding site first. The delamination of the microfluidic-channel-part from the flat cover plate (starting at the microfluidic channels) was characterized to quantify the chemical compatibility of the solvents with the microfluidic chip. Measuring from the channel wall, we determined the length of the delamination l with respect to time (see Figure 3.1).

3.1. Chemical Resistance Against Mid-IR-Transparent Organic Solvents

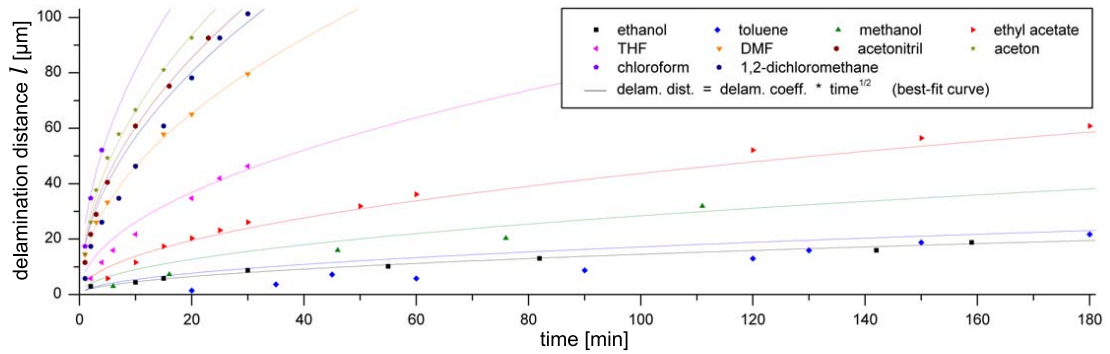


Figure 3.2: Delamination distance of the bonding site of NOA81 chips for exposure to different organic solvents. Measurement data with a measurement uncertainty of $\pm 5\mu m$ is plotted together with the corresponding fitted Washburn equation.

3.1.2 Results

Our samples resisted against the following IR-transparent (mid-infrared range, around a wavelength of $\lambda = 6\mu m$) organic solvents with low polarity: n-pentane, n-hexane, cyclohexane, n-heptane, isopropyl alcohol, and tetrachloroethylene. At least for more than 5 hours no effect, neither swelling, nor delamination, was observed under the microscope. Ethanol, toluene, methanol, and ethyl acetate, which are all as well transparent at a wavelength around $6\mu m$, attacked slowly the bonding site of the NOA81 chips. These solvents will only be suited for microfluidic experiments on NOA81 chips limited in time, e.g. for disposable chips. The delamination front advanced much faster with Tetrahydrofuran (THF) and chloroform, as well as with non-IR-transparent (at $\lambda = 6\mu m$) solvents like dimethylformamide (DMF), 1,2-dichloroethane, acetonitrile, and acetone.

The delamination (Figure 3.1) we observed for some organic solvents is most probably based on swelling of the polymer. For solvents affecting the NOA81 chips the delamination distance is plotted over time in Figure 3.2. The obtained results show a diffusion-limited behavior and are in accordance with the classical Washburn equation [140, 141]. This theory suggest the relation of the diffusion distance l to the time t as

$$l \sim t^{\frac{1}{2}}. \quad (3.1)$$

We fitted our results to the Washburn equation with a linear delamination coefficient, which is given for each solvent in Table 3.1. For these measurements only oxygen plasma bonded chips were studied in detail. A few tests indicated, that the same behavior was valid for microfluidic chips bonded by UV-curing, which also supports the assumption that delamination was caused by swelling. Cracks were never observed in the NOA81 microfluidic chips, unlike for other solvent-resistant polymer materials [142].

Table 3.1: Organic solvents used for compatibility tests in NOA81 chips bonded by oxygen plasma with corresponding delamination coefficient of the Washburn relation and IR-transparency in the midinfrared wavelength range around $6\mu m$.

solvent	delam. coeff.	delamination	IR-transp.
water	0	no	no
n-pentane	0	no	yes
n-hexane	0	no	yes
cyclo-hexane	0	no	yes
n-heptane	0	no	yes
isopropyl alcohol	0	no	yes
tetrachloroethylene	0	no	yes
ethanol	1.45	slow	yes
toluene	1.72	slow	yes
methanol	2.84	slow	yes
ethyl acetate	4.37	slow	yes
THF	8.24	fast	yes
DMF	14.62	fast	no
1,2-dichloroethane	17.96	fast	no
acetonitrile	19.10	fast	no
acetone	20.94	fast	no
chloroform	25.65	fast	yes

3.2 Cocaine Adsorption

PDMS is known as a good adsorbent of cocaine. Because of this adsorption property, PDMS is even commonly used for solid-phase micro-extraction (SPME) of cocaine [143, 144]. Adsorption on our microfluidic channel walls represent a loss. Such a loss of the analyte (cocaine) has to be avoided. So for our sensing project we are looking for a polymer material with preferably low adsorption of the analyte. This section presents the results of the adsorption tests on NOA81 channel walls contributed to the IMCS 2012 [139].

3.2.1 Method

We made all-polymer NOA81 microfluidic channels by means of rapid prototyping using a SU-8 based master as described in section 2.4 and section 3.1.1. The design is shown in Figure 3.3a and consists of a simple serpentine microfluidic channel ($150\mu m$ wide and $40\mu m$ deep). The total surface of the UV-curable adhesive exposed to the liquid, including inlet and outlet ports, was $12.65mm^2$.

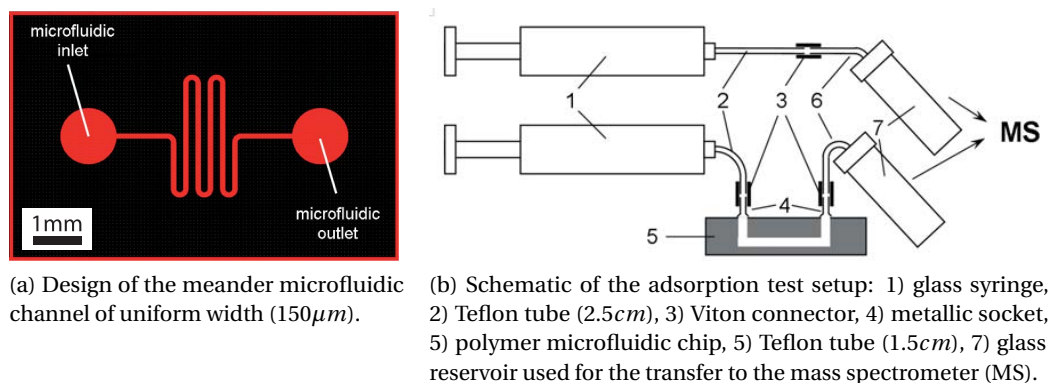


Figure 3.3: Cocaine adsorption measurement setup.

Different cocaine concentrations dissolved in saliva and tetrachloroethylene were flowed through the microfluidic chips at a flow rate of $10 \mu\text{l}/\text{min}$. Saliva was collected from healthy adult volunteers ($\text{pH } 6.8 \pm 0.2$), filtered through a commercially available PES $0.22 \mu\text{m}$ syringe filter, and spiked with cocaine.

The same concentrations were also pumped through a reference system consisting only of the tubing (of equal length) as presented schematically in Figure 3.3b. The cocaine concentration (c) of the samples flowed through the polymer microfluidic chip and the reference system was determined by liquid chromatography - mass spectrometry (see section 2.2) and then used to calculate the recovery rate (r).

$$r = \frac{C_{\text{microfluidicsystem}}}{C_{\text{referencesystem}}} \cdot 100\% \quad (3.2)$$

3.2.2 Results

A very high recovery rate of the cocaine was observed in the aqueous (saliva) and organic (tetrachloroethylene) solvent. Except for the lowest cocaine concentration ($20 \text{ ng}/\text{ml}$), the saliva samples showed recovery rates higher than 92% (see Table 3.2). Low values of the standard deviation confirm stable recovery rates. We observed low adsorption at low flow rates for microfluidic systems. Theoretically, we expect even less adsorption at higher flow rates. The whole adsorption test was repeated with polymer microfluidic chips aged for 3 months. No significant difference between fresh and old chips was measured.

From literature we already know the UV-curable polymer NOA81 shows low adsorption of proteins (interleukins) from blood [145]. Compared to these values, we observed in our study of molecule adsorption an even better, remarkably high recovery rate for the analyte cocaine.

Table 3.2: Mean recovery rate, standard deviation (SD), and coefficient of variation (CV) given in % for the solvents saliva and tetrachloroethylene as function of different cocaine concentrations.

cocaine concentration	human saliva			tetrachloroethylene		
	recovery rate	SD	CV	recovery rate	SD	CV
20ng/mL	85	21	24	86	11	13
2μg/mL	93	4	5	91	12	14
20μg/mL	92	13	14	89	16	18
400μg/mL	101	8	8	100	2	2

3.3 Adjustable Wetting Behavior

In this section different methods to modify the surface properties of NOA81 are investigated and quantitatively characterized by dynamic contact angle measurements. As a new approach to make the surface of the polymerized NOA81 more hydrophobic, we mixed APTES ((3-aminopropyl)triethoxysilane) as an additive to the uncured polymer by the thiol-ene click reaction (efficient, and high yielding addition of functional groups) [146]. This allows homogeneous control over the wetting behavior, which is difficult to achieve with liquid [147] or vapor-phase surface treatments, particularly of those parts located deep within closed microfluidic systems. The common vapor-phase silanization using FOTS ((Tridecafluoro-1,1,2,2-tetrahydrooctyl)trichlorosilane) was applied to NOA81 as a reference treatment. These findings were confirmed by AFM (atomic force microscopy) as well as by XPS (X-ray photoelectron spectroscopy) measurements. We also give examples of multi-phase flow microfluidic systems where the adjustment of the wetting behavior of microfluidic channel walls plays an important role.

The results and applications presented in this section were published in the journal *Sensors and Actuators B* [139].

3.3.1 Method

Sheets of PDMS were cured at room temperature on silicon wafers to achieve homogeneous and flat PDMS surfaces. For the analysis of modified NOA81 surfaces, the UV-glue was cured sandwiched between two of these PDMS sheets (in contact with the PDMS side molded on the silicon wafers). The approximately 1mm thick, cured NOA81 layer was then transferred onto a glass substrate for more convenient handling.

To study the wetting behavior of cured NOA81, dynamic contact angle measurements using water droplets on the sample of interest in ambient air were performed with an optical contact

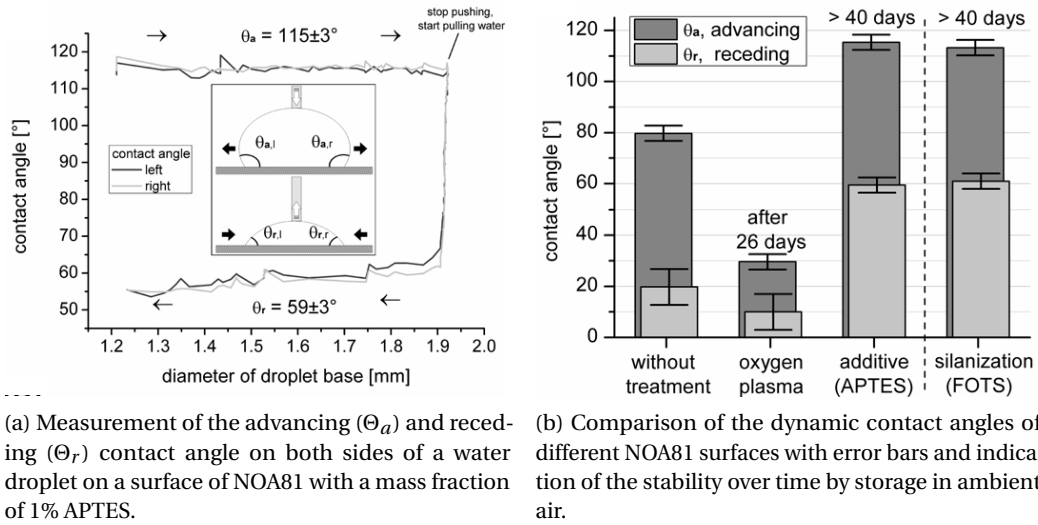


Figure 3.4: Dynamic wetting behavior analysis on different NOA81 surfaces.

angle goniometer (Drop Shape Analysis System DSA 10, Krüss GmbH, Hamburg, Germany). For each sample the advancing (growing droplet) and receding (shrinking droplet) contact angles were measured (see schematic in Figure 3.4a). The static contact angle at equilibrium of the water droplet can be calculated from the dynamic contact angles using the theory of Tadmor [148].

The topography of the NOA81 surfaces was evaluated by surface roughness analysis using an AFM (Veeco Dimension 3100, Digital Instruments, Mannheim, Germany) in the tapping mode on $3\mu\text{m} \times 3\mu\text{m}$ areas.

XPS (Axis Ultra DLD, Kratos Analytical, Manchester, U.K.) was applied to investigate the chemical composition of the surfaces. Depth profiles were achieved by performing ion etching between two different measurements. Measurements were performed at 60° inclination for better surface sensitivity and at 90° for the depth profiles measurements.

3.3.2 Results

A typical dynamic wetting behavior test result is shown in Figure 3.4a. A comparison of all the modified surfaces is presented in Figure 3.4b and Table 3.3. Without any modification NOA81 was hydrophilic, showing an advancing contact angle of $\Theta_a = 80 \pm 3^\circ$ and a receding contact angle of $\Theta_r = 20 \pm 7^\circ$. After oxygen plasma treatment, the surfaces showed a reasonably stable perfect wettability in air (stable at least for 4 days, $\Theta_a = 30 \pm 3^\circ$, $\Theta_r = 10 \pm 7^\circ$ after 26 days). Static contact angle measurements on NOA81 surfaces of Hung et al. confirm these results [121]. Storage of the samples in water further enhanced the hydrophilicity of the plasma-treated surfaces. The plasma treatment on NOA81 was much more stable compared to PDMS. The plasma-treated PDMS surfaces recover fast their hydrophobic character if allowed to react

Chapter 3. Characterization of Microfluidic Channels Made of UV-Curable Adhesive

Table 3.3: Dynamic contact angles (advancing and receding) measured 26 days after fabrication and calculated, corresponding equilibrium contact angles using the theory of Tadmor [148] for different NOA81 surfaces.

NOA81 surface	contact angle [°]		
	advancing	receding	equilibrium
pure	80 ± 3	20 ± 7	48 ± 5
oxygen plasma treated	30 ± 3	10 ± 7	21 ± 5
1% mass fraction of APTES	115 ± 3	59 ± 3	81 ± 3
vapour phase silanisation (FOTS)	113 ± 3	61 ± 3	82 ± 3

with ambient air (change of contact angle from 15° to 79° within $200min$) [134]. Following the concept developed in [149, 150], we added 1 wt% of APTES to uncured NOA81 and unlike vapor-phase silanization using APTES in gas phase, the surfaces were found to be more hydrophobic ($\Theta_a = 115 \pm 3^\circ$, $\Theta_r = 59 \pm 3^\circ$). Samples stored in water recovered their original hydrophilicity after 10 days, but no change was observed (at least for more than 10 days) if the samples were stored in a low polar solvent, like e.g. toluene.

By mixing this additive in NOA81, we obtained similar hydrophobicity, both in terms of contact angle and stability in time (>40 days) as the hydrophobicity originating from a vapor-phase silanization using FOTCS after plasma activation of the surface ($\Theta_{ar} = 113 \pm 3^\circ$, $\Theta_r = 61 \pm 3^\circ$). This reference treatment is a well-known method of chemically modifying silicon, glass, and PDMS surfaces [151].

Adding larger mass fractions of APTES in uncured NOA81 ($> 1\%$) did not increase its hydrophobicity, but inhibited the polymerization of the UV-glue. Probably a competitive reaction with the amine groups in NOA81 runs even before the UV-polymerization. NOA81 with more than 7% APTES by weight was hard to cure completely.

This simple modification using APTES allows easy control over the wetting behavior of micro- and nanoscale parts hidden deep in microfluidic systems, which is hard to achieve by surface modification techniques, e.g. vapor-phase silanizations. The characterization of NOA81 surfaces was performed with a number of samples from different fabrication batches at different times of the year. This assesses the reproducibility of these results.

Generally, changes in wetting behavior stem from modifications of surface topography or chemistry. A roughness analysis was performed by AFM on both NOA81 surfaces and on samples of NOA81 containing APTES. No difference in roughness was found. Samples of pure NOA81 and APTES-modified NOA81 showed height deviations taken from the mean data plane of $0.7 \pm 0.2nm$ (see Figure 3.5). In addition, no differences were found between fresh and 20 days old samples. Therefore, a change in the topography based on the additive

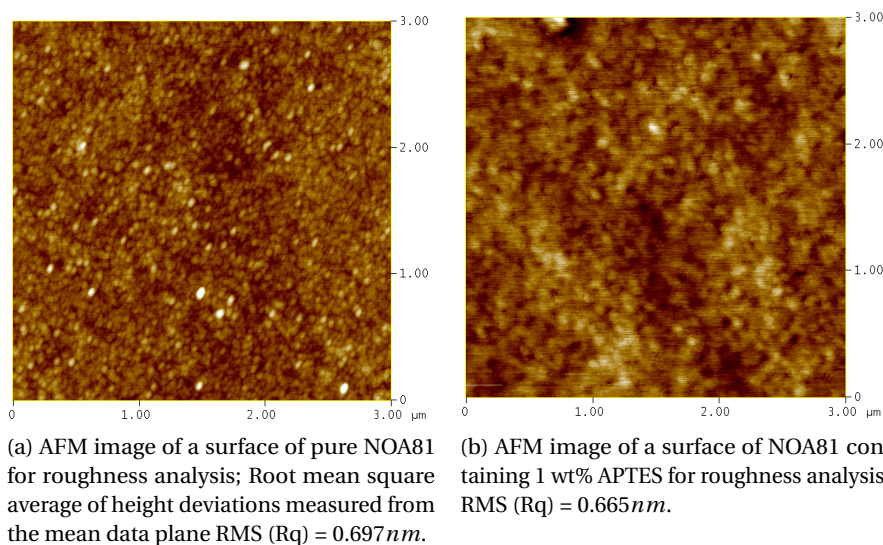


Figure 3.5: AFM roughness evaluation.

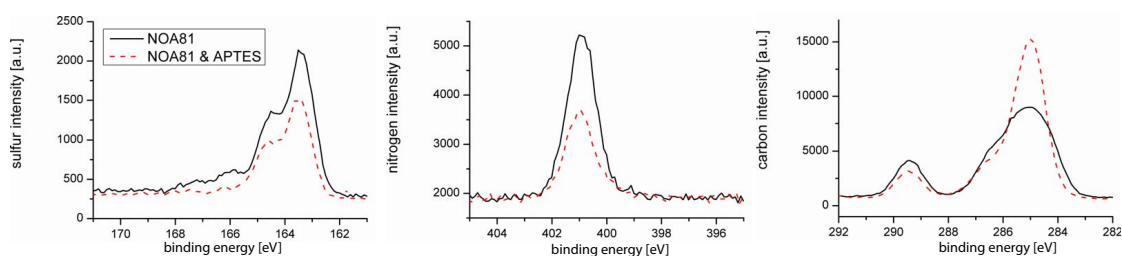


Figure 3.6: Comparison of XPS spectra of pure NOA81 and NOA81 with 1% APTES by weight. Measurements were performed at 60° inclination for better surface sensitivity.

APTES mixed in NOA81 could then be excluded. Images of samples containing APTES were much more difficult to acquire, most probably due to electrostatic forces, which resulted in a blurring effect (as seen when Figure 3.5a and Figure 3.5b are compared).

This phenomenon, together with the fact that the induced hydrophobicity (resulting from the additive APTES) was fading in water, already indicate, that the hydrophobicity of the surfaces of samples containing APTES is based on a chemical modification. Indeed, XPS measurements confirmed a different chemistry on the surfaces (see Figure 3.6). However, our interpretation of XPS measurements could not go deeper in the understanding of the changes in the surface chemistry, since the specific chemical identity of NOA81 is being withheld as a trade secret by the provider. The polymerization of NOA81 is based on thiol-ene crosslinking [120, 121] potentially enhanced by the use of isothiocyanates as the formation of urethanes has been reported to be characteristic for NOA polymers [136]. In the latter case, the formation of a urethane by means of amine-thiocyanate reaction is possible allowing APTES to be chemically bound to the polymer chains [146, 152], which could be confirmed by the lower

sulfur concentration found on samples containing APTES. We expect the ends of the polymer chains holding an APTES molecule to be exposed to the surface for entropy equilibrium reasons. The resulting apolar methyl groups of APTES on the surface (fact supported by the higher carbon concentration measured by XPS) would then be responsible for the more hydrophobic surface.

3.3.3 Application

A method for the fabrication of a closed microfluidic channel with hydrophilic and hydrophobic surfaces was developed and is presented here as an application for the adjustable wetting behavior of NOA81 surfaces.

Fabrication process of closed, all-polymer microfluidic channels with adjustable wetting behavior

Microfluidic channels with adjustable wetting behavior can be fabricated by adapting the process described in section 3.1.1. Completely hydrophilic channels were fabricated by exposing both parts to oxygen plasma before assembly. The joining of two NOA81 parts containing APTES and further UV-curing resulted in an entire hydrophobic channel. With the presented simple rapid prototyping technique, a closed, all-polymer microfluidic channel with hydrophilic and hydrophobic surfaces in the same microfluidic channel can be realized easily. A microfluidic channel with vertically separated wetting properties was achieved by joining two differently modified parts: A hydrophobic thin sheet of NOA81 containing APTES was combined with a hydrophilic structured part (treated with O_2 -plasma) or vice versa (see Figure 3.7, left). Horizontal separation of the wetting properties was obtained, when the two liquid polymers, NOA81 and NOA81 containing APTES, were casted on the same master at the specific places; pure NOA81 at locations, which should be hydrophilic, NOA81 containing APTES at locations, which have to be more hydrophobic in the end (see Figure 3.7, right).

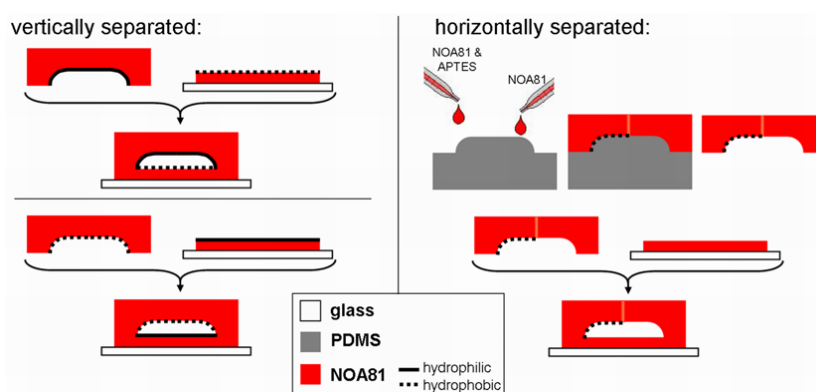


Figure 3.7: Rapid prototyping methods for hybrid chips showing hydrophilic and hydrophobic surfaces in the same microfluidic channel. Vertically (left) and horizontally (right) separated wetting behavior can be achieved.

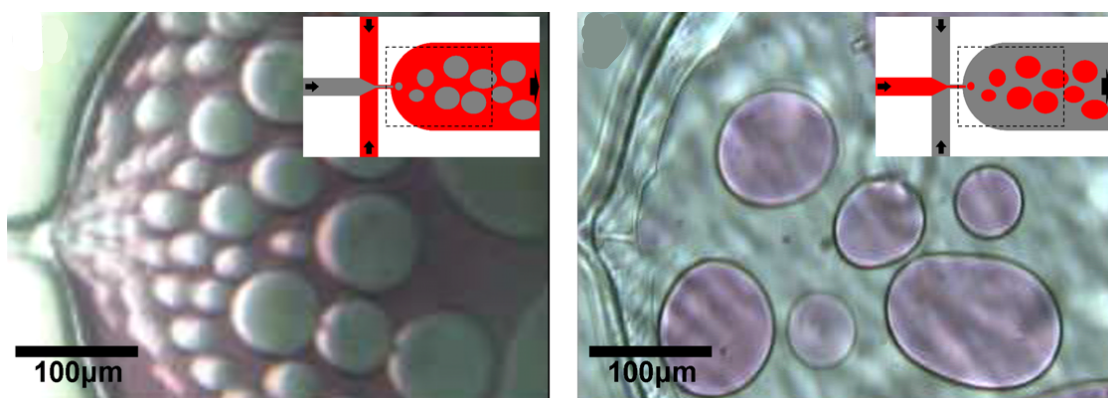


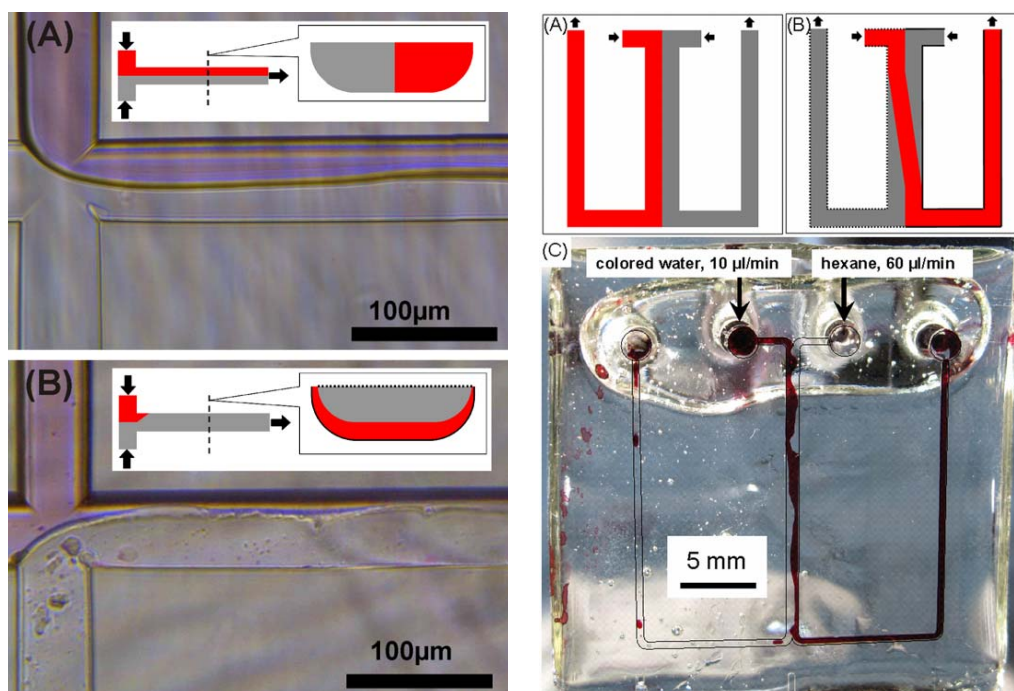
Figure 3.8: Left: Oil-in-water droplet generation: Ethyl acetate droplets generated in saliva (colored with amarant) in a hydrophilic microfluidic channel (flow rates: ethyl acetate $0.3\mu L/min$, saliva $6\mu L/min$). Right: Water-in-oil droplet generation: Saliva (colored with amarant) droplets generated in ethyl acetate in a hydrophobic microfluidic channel (flow rates: saliva $0.5\mu L/min$, ethyl acetate $20\mu L/min$).

Applications for chemical resistant microfluidic chips with adjustable surface properties

As a first example, microfluidic flow-focusing devices (MFFD) were fabricated for oil-in-water and water-in-oil droplet generation (see Figure 3.8). To allow oil droplet generation in an aqueous environment, fully hydrophilic, pure oxygen-plasma treated NOA81 microchannels must be used. First, they were filled completely with the aqueous solvent (saliva colored with amarant) and then the organic solvent (ethyl acetate) was added through the channel located in the middle. By adjusting the ratio of the flow rates of the aqueous to the organic solvent, the droplet sizes can be varied. For water-in-oil droplet generation the opposite is valid, and fully hydrophobic channels were needed. The hydrophobicity of NOA81 surfaces was induced by mixing small amounts of APTES in the uncured polymer before molding as described before. The microfluidic systems were able to withstand a pressure drop of more than 15 bar (flow rate of $360\mu L/min$) without any deformation, which is several times higher than what PDMS based systems allow [122].

For the second application, an all-polymer hybrid channel (hydrophilic and hydrophobic surfaces) was realized to demonstrate the successful handling of a multi-phase flow (see Figure 3.7, left). The microfluidic channels were T-shaped with two inlets and one outlet. For this experiment the two fluids were introduced in the channels at the same flow rate of $1\mu L/min$. In pure, untreated NOA81 samples the organic solvent (toluene, $0.8669g/mL$, similar density as water) flowed next to the water (colored red with $5mM$ amarant). However, when the same fluids flowed in hydrophilic channels with a hydrophobic (NOA81 & APTES) cover, a vertical separation of the laminar flow was established, with the organic solvent flowing preferentially along the hydrophobic surface (see Figure 3.9a). This behavior was confirmed using a so called microfluidic H-filter with two inlets, two outlets, and hydrophilic / hydrophobic side walls (see Figure 3.7, right and Figure 3.9b). In this H-filter configuration, we clearly observe the aqueous

phase (red) separated from the organic phase (transparent) as it follows the hydrophilic walls of the microfluidic channel. Both observations of the applications of the multi-phase flow handling are consistent with previous studies of surface-directed liquid motion control in microfluidic channels [153].



(a) (A) Microscopic top view of the junction of untreated NOA81 channels ($50\mu\text{m}$ wide, $20\mu\text{m}$ deep), where the organic solvent and the colored water meet (same flow rate of $1\mu\text{L}/\text{min}$). The two phases are flowing next to each other. (B) Hybrid NOA81 channel ($50\mu\text{m}$ wide, $20\mu\text{m}$ deep) with a hydrophilic (solid line) bottom side and hydrophobic (dotted line) top side. The organic solvent and the colored water meet with the same flow rate of $1\mu\text{L}/\text{min}$. A vertically separated laminar flow is established, whereupon the organic solvent flows alongside the hydrophobic surface.

(b) Microfluidic H-filter chip with two inlets and two outlets. Water colored with amaranth is introduced on the left-hand side, hexane on the right-hand side. (A) Schematic view of the situation on a chip without surface modification: A parallel laminar flow is established and the liquids stay on their appropriate side. (B) Schematic view on the same situation on a chip with hydrophilic (solid line) and hydrophobic (dotted line) channel walls: The liquids are forced to switch sides and leave the main channel on the opposite side (water on the hydrophilic side, hexane on the hydrophobic side). (C) Picture of the situation on the real chip with modified walls as described in (B).

Figure 3.9: Application of hybrid NOA81 chips.

3.4 UV-Characteristics

For the UV-curable adhesive NOA81, optical characterization for fluorescent based detection systems is missing. In this section we present a comparison of fluorescent emission spectra of various types of NOA as well as the time evolution of the spectra of the most promising one - NOA81. As an application, we show the capillary electrophoresis (CE)-injection of a fluorescent

dye, and its detection by means of fluorescence microscopy. This optical characterization of NOA was presented in the μ TAS 2010 conference [138].

3.4.1 Method

In the visible light range, NOA81 is transparent. For more specific optical characterization of the material, samples of different NOA types were compared with PDMS samples (all of the same uniform thickness, 2mm) using a spectrofluorimeter (Infinite M200, Tecan, Switzerland). NOA samples were cured by exposure to UV-light ($1.5\text{mW}/\text{cm}^2$ at 365nm wavelength for 22min). For the analysis, two different wavelengths were used for excitation (470nm and 546nm).

3.4.2 Results

At the excitation wavelength of 470nm , the fluorescence emission of NOA81 is higher than the one of PDMS (see Figure 3.10a). But the emission intensity is only half of the intensity of NOA63, which is recommended for fluorescence applications [154]. At the excitation wavelength of 546nm , NOA81 has a comparable fluorescence emission as PDMS (see Figure 3.10b). The low auto-fluorescence of NOA81 at 546nm makes it as suitable as PDMS for fluorescence detection based devices. Figure 3.11a shows the evolution of the fluorescent emission spectrum of NOA81 at the excitation of 470nm . The intensity decreased after fabrication and was stable after 8 days. For the excitation at 546nm , the spectra were stable already after 2 days (see Figure 3.11b).

3.4.3 Application

As an application, we present the fluorescence microscopy detection of a CE-injected plug of Rhodamine B in a chip made of NOA81.

Fabrication of a Capillary Electrophoresis Chip

The device for CE consisted of a classical T-channel ($50\mu\text{m}$ wide, $20\mu\text{m}$ deep) and was fabricated by rapid prototyping of NOA81 as explained before in section 2.4. For NOA81 molding, a PDMS master was used, which was a replica of an isotropically etched glass wafer (see Figure 3.12a).

Fluorescence Microscopy Detection through a NOA81 Chip

The CE experiments were performed with a Zeiss Axiovert S100 fluorescence microscope (Carl Zeiss AG, Germany) equipped with a Xenon 100W power light source and a high-sensitivity CCD camera (Kappa AG, Germany). A programmable HVS 448-6000D 8-channel high-voltage

Chapter 3. Characterization of Microfluidic Channels Made of UV-Curable Adhesive

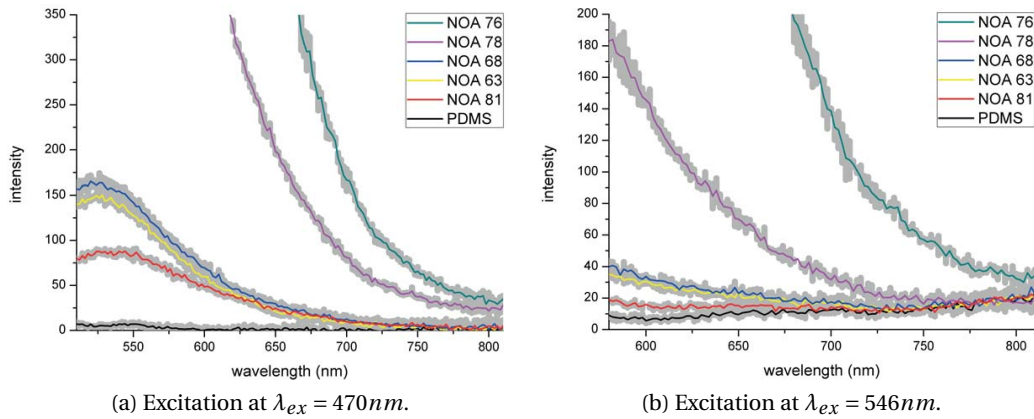


Figure 3.10: Comparison of fluorescent emission spectra of different NOAs and PDMS as reference value. The spectra are recorded 20 days after chip fabrication. The gray region around each plot represents the standard deviation of the measurement.

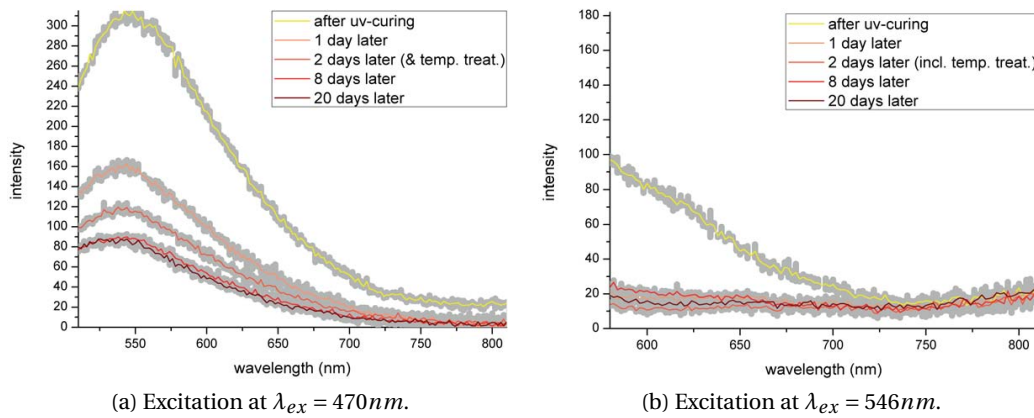
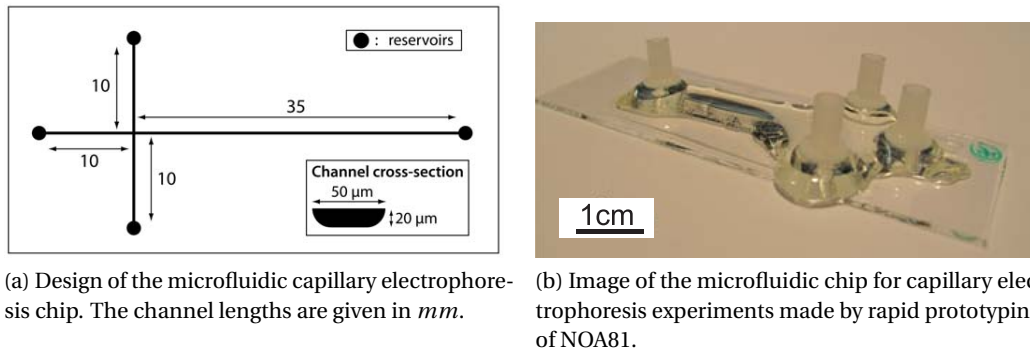


Figure 3.11: Evolution of fluorescent emission spectra of NOA81 for two different excitation wavelengths; directly after the UV-curing, 1 day after the fabrication, 2 days later, and after a temperature treatment of 60°C for 2h , 8 and 20 days later. The intensity is decreasing and stable 8 days after the fabrication. The gray region around each plot represents the standard deviation of the measurement.

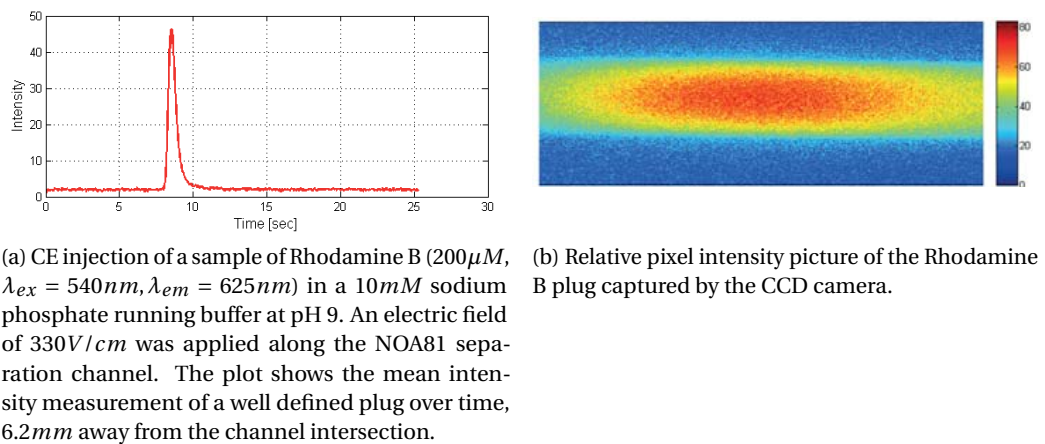
supply (LabSmith, CA, USA) allowed to apply three different voltage sequences for the sample loading and injection inside the separation channel of the microchip. We set the injection method and the corresponding voltages according to [155]. As demonstrated by the intensity profile in Figure 3.13, the fluorescence intensity peak of Rhodamine B was easily detectable in the NOA81 microchannel thanks to the low autofluorescence of this material.



(a) Design of the microfluidic capillary electrophoresis chip. The channel lengths are given in *mm*.

(b) Image of the microfluidic chip for capillary electrophoresis experiments made by rapid prototyping of NOA81.

Figure 3.12: Capillary electrophoresis chip.



(a) CE injection of a sample of Rhodamine B ($200\mu M$, $\lambda_{ex} = 540nm$, $\lambda_{em} = 625nm$) in a $10mM$ sodium phosphate running buffer at pH 9. An electric field of $330V/cm$ was applied along the NOA81 separation channel. The plot shows the mean intensity measurement of a well defined plug over time, $6.2mm$ away from the channel intersection.

(b) Relative pixel intensity picture of the Rhodamine B plug captured by the CCD camera.

Figure 3.13: Capillary electrophoresis experiment in a polymer NOA81 chip.

3.5 Low-Cost Rapid Prototyping

For the rapid prototyping method presented in section 2.4 two things are important: First, the material has to be able to wet the master and flow in between tiny structures to reproduce them. Second, the material needs to show a good bonding strength to a substrate material, which closes the microfluidic channels.

3.5.1 Replication Capability

NOA81 shows a really high replication capability. Even nano structures can be reproduced as proven by the replica of an AFM XYZ-calibration nano-grid (see Figure 3.14). The nano grid CS-20NG (Innovative Solutions, Bulgaria) shows structures of a pitch size of 500nm and a vertical height of 20nm .

In the context of replication, the feature shrinkage from the master to the replica is important as well. Relative to PDMS a neglectable shrinkage of less than 1% was measured for NOA81. Values for the materials PDMS and NOA81 are given in Table 3.4.

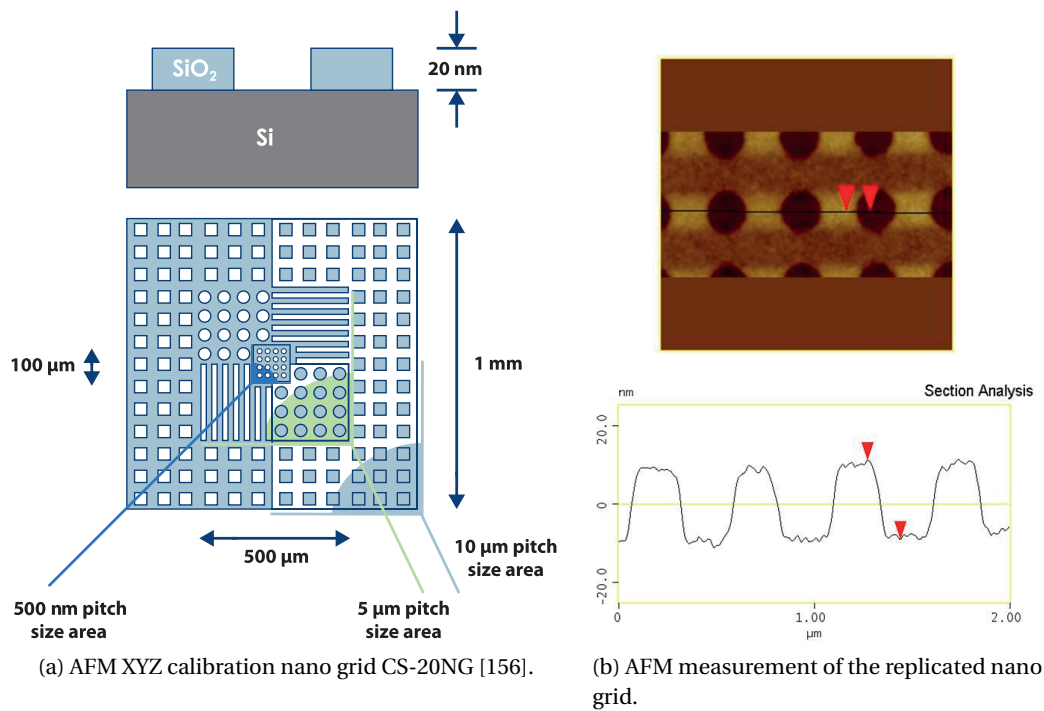


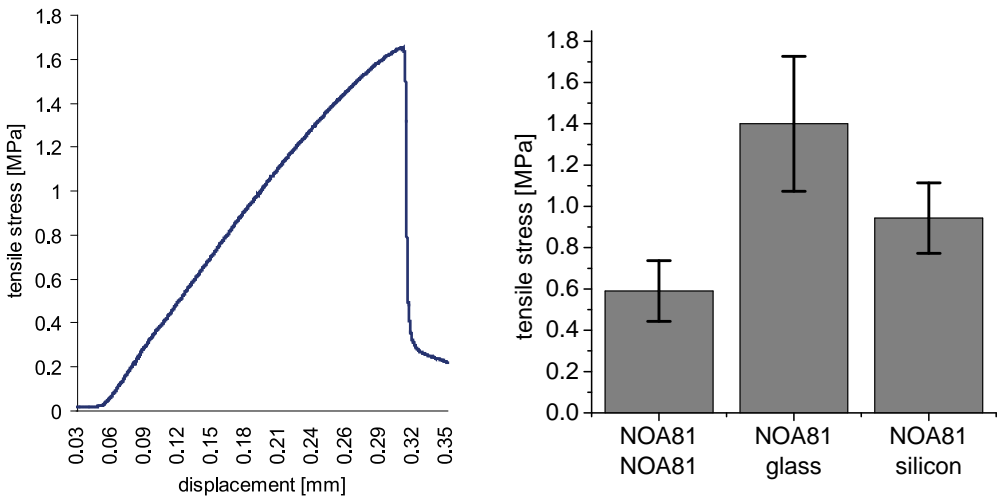
Figure 3.14: Replication of nano structures by NOA81.

Table 3.4: Shrinkage of sizes of nanofeatures from master to replica.

	Silicon-PDMS	PDMS-NOA81
vertical	$37,9 \pm 3,6\%$	$0,4 \pm 0,5\%$
horizontal	$0,4 \pm 0,5\%$	$0,6 \pm 0,7\%$

3.5.2 Bonding Strength

A good bonding strength is important to be able to apply pressure on the liquids in the microfluidic chip. We exposed test samples to oxygen plasma (2x 15s, 400W, 2.45GHz, 500 – 700mTorr, 400cm³/min O₂ flow) for surface activation before bonding. The failure stress was evaluated on 10mm x 10mm test samples with a pull tester (Instron 3344, UK) (see Figure 3.15). NOA81, bonded to a NOA81 surface, failed at 0.59MPa, the combination NOA81-glass at 1.40MPa and NOA81 joined with a silicon substrate separated at 0.94MPa. These values are all higher than the optimized bonding strength achieved with PDMS (see Table 3.5) [157].



(a) Tensile stress measurement until failure (debonding) of a NOA81 test part bonded on a glass substrate. (b) Overview of failure stress for NOA81 test samples bonded to different substrates. Error bars indicate the standard deviation for at least three measurement curves of each material combination.

Figure 3.15: Evaluation of the oxygen plasma bonding strength of NOA81.

Table 3.5: Comparison of the bonding strength of NOA81 and PDMS.

Substrate	NOA81	PDMS[157].
NOA81 / PDMS	0.59MPa	0.40MPa
glass	1.40MPa	0.51MPa
silicon	0.94MPa	n.a.

3.6 Summary

There has been an increasing need for novel materials with better chemical compatibility, easy and more stable surface modifications, and a simple and cost-effective fabrication process. In 2008, Norland Optical Adhesives (NOA81 and NOA63) were suggested as a substitute of PDMS for rapid prototyping of microfluidic devices [122, 136]. These UV-curable glues were originally designed to bond optical components or fiber optics, but are also well suited for molding based replication of microfluidic structures [121, 122, 131, 136].

It was presented that NOA is a solvent-resistant (toluene), biocompatible (culture of HeLa cells) material with native hydrophilicity enabling one to fill microfluidic channels with aqueous solutions by capillary forces [121, 154]. Both NOA81 and NOA63 are transparent in the visual range allowing observation of colored liquids or beads through the material. Besides the activation of the NOA81 surfaces by oxygen plasma, no report about other surface modifications was found in literature.

In conclusion, several interesting aspects of an indeed promising, but widely unknown material were presented. We performed a broad characterization of microfluidic channels to evaluate NOA81 as chip material for the IrSens project.

NOA81 chips showed a much higher chemical resistance against organic solvents compared to PDMS. Our chips were resistant against the IR-transparent (at a wavelength of $6\mu m$) organic solvents n-pentane, n-hexane, cyclo-hexane, n-heptane, isopropyl alcohol, and tetrachloroethylene. Neither swelling, nor delamination was observed after 5 hours of exposure. The solvents ethanol, toluene, methanol, and ethyl acetate showed slow delamination of the chip bonding site (most probably due to swelling), and therefore they would be suited for microfluidic experiments limited in time, e.g. on disposable systems.

Further, we presented a study of the adsorption of cocaine molecules by microfluidic devices made of NOA81. Remarkable low adsorption values (up to 100% recovery rate) were found by mass spectrometry measurements. This makes NOA81 to a potential polymer for forensic applications.

This chapter also presented simple and reasonably stable wettability control procedures for polymerized NOA81 surfaces. As an alternative to the vapor-phase surface treatments, the same modification of the wetting behavior (change to hydrophobic) was achieved by mixing an additive in the uncured, bulk polymer. This allows homogeneous control over the wetting behavior, particularly of those parts located deep within closed microfluidic systems, which is difficult to achieve with vapor-phase treatments. The wetting behavior of APTES-modified NOA81 was due to changes in the surface chemistry and not from a modification in surface topography.

Some aspects important for rapid prototyping were investigated as well. NOA81 was able to reproduce by molding nanostructures with a neglectable feature shrinking. Compared to PDMS, NOA81 showed also better bonding capabilities to substrates such as silicon, glass or the polymer itself.

A new suitable polymer chip material was found meeting all the relevant material requirements given by the application in the project IrSens, such as the compatibility to IR-transparent solvents, the low cocaine adsorption, the adjustable wetting behavior as well as the suitability for low cost prototyping. In this chapter the mentioned material properties were investigated and illustrated by different applications.

4 Robust Droplet Generation Based on a Simple Geometry

This chapter introduces our robust method to generate continuously droplets of an organic solvent in the inhomogeneous saliva without clogging. The robustness of the simple geometry is proofed by using the complex fluid saliva together with the organic solvent PCE to generate droplets. Furthermore, the main influences on the droplet size are investigated.

The results shown here, were presented at the μ TAS 2012 conference in Japan [158].

4.1 Introduction

Besides drop on demand techniques [159], most of the microfluidic methods produce droplets through passive techniques. In order to produce droplets, the dynamic flow field in such passive devices is used to deform the interface between two immiscible liquids and therefore induce interfacial instabilities. Based on the different physical droplet generation mechanisms, the passive devices can be split in three main groups as suggested by [4]: i) breakup in co-flowing streams (Figure 4.1a), ii) breakup in cross-flowing streams (Figure 4.1b) and iii) breakup in elongational strained flows (Figure 4.1c). The droplet size is set by a competition between the pressure caused by external flow and viscous shear stresses on the one hand and the capillary pressure based on the interfacial tension resisting the deformation on the other hand.

i) Breakup in Co-Flowing Streams

For this droplet generation mechanism, a co-axial injection device is used, e.g. a thin cylindrical capillary in a squared microfluidic channel as shown in Figure 4.1a. The dispersed phase is injected through the capillary. The physics responsible for the breakup in droplets is the Rayleigh-Plateau instability [160].

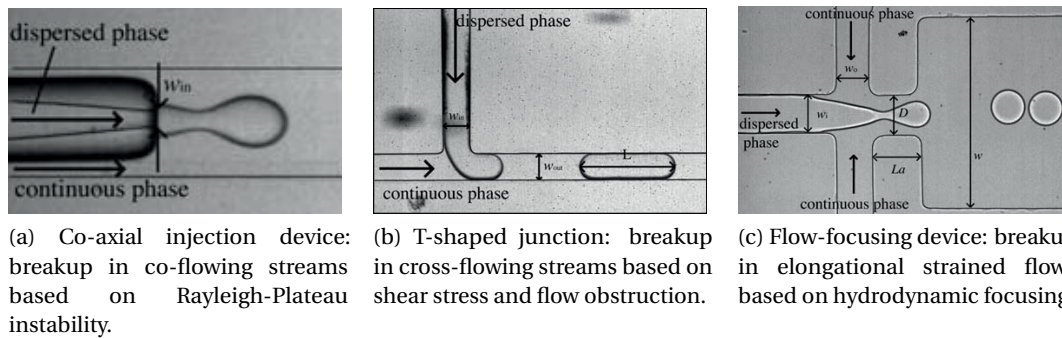


Figure 4.1: State of the art of passive droplet generation devices [4].

ii) Breakup in Cross-Flowing Streams

Droplet generation in a T-junction shown in Figure 4.1b was first reported by [161]. Two different regimes for droplet generation can be distinguished [162]. If the side-channel is smaller than the main channel, droplets rip off at the junction based on shear-stress. If the dimension of the side-channel is comparable to the main channel, the dispersed phase entering through the side-channel blocks the main channel. Pressure is built up by the continuous phase in the main channel behind the plug of the dispersed phase until a droplet is pinched off.

For large scale droplet generation in high-throughput applications, the structures used for droplet generation are arranged in parallel. For breakup in cross-flowing streams two different mechanisms were reported. Firstly, the microchannel emulsification (MCE) was introduced by [163] and applied by [164, 165] (see Figure 4.2a). They inject the dispersed phase through an array of small side channels (orthogonal, in plane), over a terrace, into the main channel containing the continuous phase. The droplets are generated upon entering the main channel due to shear-stresses and Laplace pressure gradients (between the side and the main channel) [166].

Secondly, droplets are produced using only shear-stresses when the dispersed phase is pushed from perpendicular side channels into the main channel (see Figure 4.2b). These systems were called straight-through microchannel emulsification devices (SMCE) [167, 168] or micro-sieve devices [169].

iii) Breakup in Elongational Strained Flows

Hydrodynamic Focusing The flow focusing device for droplet generation shown in Figure 4.1c was first presented by [171, 172]. Here the dispersed phase is squeezed by two counter-flowing streams of the continuous phase and focused through a nozzle (hydrodynamic focusing). Droplets are generated after relaxation in a wider collection channel also based on the Rayleigh-Plateau instability. Here four different main regimes of droplet generation can be observed: squeezing, dripping, jetting, and thread formation. Droplet diameters depend on

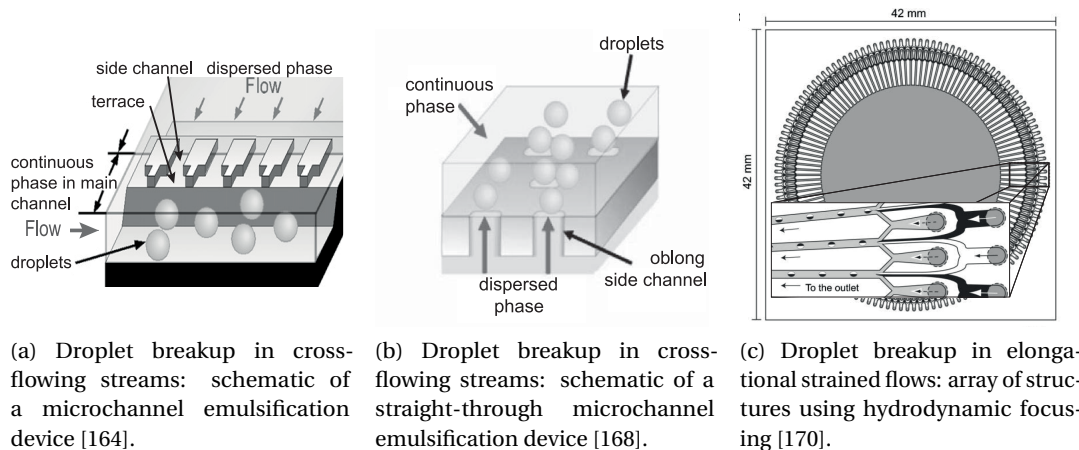


Figure 4.2: Parallelization of droplet generation features for high-throughput applications.

many parameters, but also depend linearly on the flow rates. For the different regimes as well as for the prediction of the droplet size no clear laws are available [4].

For high-throughput applications, parallelization of many droplet-generating features using hydrodynamic focusing was introduced by [170] (see Figure 4.2c).

Capillary Focusing Droplet generation by capillary focusing is another physical mechanism to break up droplets in elongational strained flows. Here the devices called nano-terrace (shown in Figure 4.3), consist of a nano-scale channel (nano-terrace) ending up in a deeper and larger microfluidic channel (reservoir) as first reported by [12, 173]. Both fluids are flowing in parallel over the nano-terrace separated by a meniscus which induces a cross-stream pressure difference (laplace pressure, see section 1.1). The fluids are forced to balance their pressures when arriving at the reservoir, meaning the dispersed phase has to move locally faster. Based on the insufficient supply of the dispersed phase, the droplets are snapped-off. The droplet size was reported to be linearly related to the nanochannel height [12].

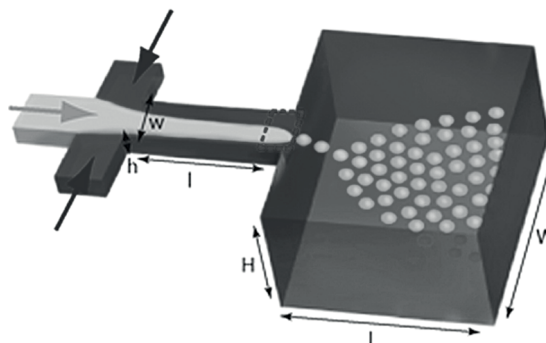


Figure 4.3: Nano-terrace device: breakup in elongational strained flows based on capillary focusing [12].

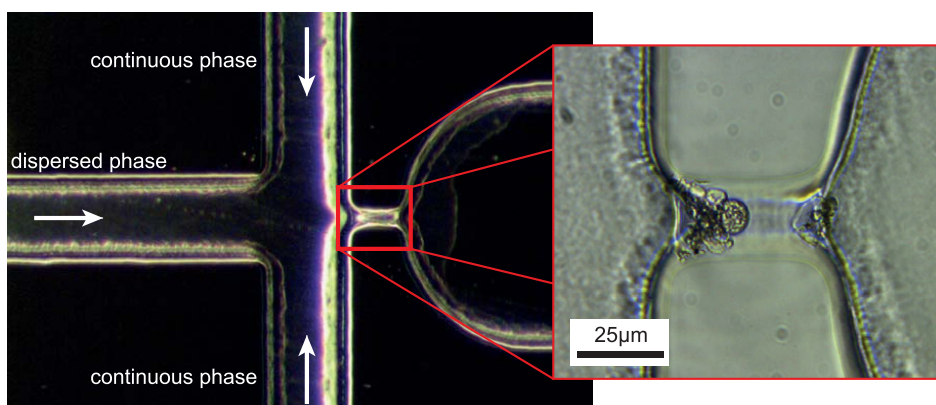


Figure 4.4: Particles in saliva such as cells or proteins tend to clog the small microfluidic structures on droplet generation devices. Here a clogged microfluidic flow focusing device with a $20\mu\text{m}$ wide nozzle is shown.

The here presented state-of-the-art droplet generation systems were found not to be robust enough to be used with inhomogeneous, non-Newtonian liquids such as saliva. Furthermore, to produce small droplets, unfortunately all of the presented devices show small feature sizes which got easily clogged by large saliva components (see Figure 4.4). We present here a new developed method, based on the idea of nano-terrace devices [12, 173] which can process the complex liquid saliva without clogging. In addition the device is easy to fabricate by our low-cost rapid prototyping technique presented in section 2.4.1.

4.2 Theory & Fundamental Principles

In this section we explain the basic conditions for droplet generation with the help of dimensionless numbers and also give a theoretical description of the droplet formation process using our method.

4.2.1 Basic Conditions for Droplet Generation Based on Dimensionless Numbers

Laminar flow conditions are assumed for a passive microfluidic structure, in which the flow deforms the interface between two liquids for droplet generation. Therefore, the Reynolds number (see section 1.1) is supposed to be small. Another requirement for successful droplet generation is a low value of the capillary number (see section 1.1) of the overall system. This indicates that the interfacial tension dominates the viscous stresses. Plugs of one liquid in another one stay compact. Drops formed under such conditions are really stable and try to minimize their surface area by producing spherical ends [4]. On the other hand, in systems showing high values of the capillary number, viscous effects are stronger than the interfacial tension. Large deformations of plugs, as well as asymmetric shapes can be observed at high capillary numbers. Flow focusing devices produce a thin tread instead of droplets. For high

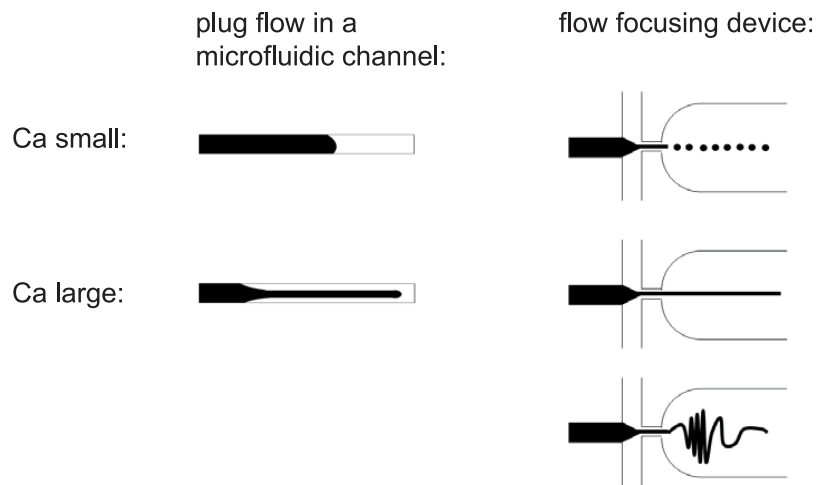


Figure 4.5: The schematics illustrate the influence of a small or large value of the capillary number (Ca) on a plug flow and the flow behavior in a flow focusing device. At low capillary numbers a plug remains compact and highly spherical droplets can be produced by a flow focusing device. At large capillary numbers, plugs get deformed and show asymmetric shapes. Under such conditions a flow focusing device produces a thin (sometimes piling) tread instead of droplets.

viscous core-annular flows also piling of the tread was observed [174]. The mentioned flow characteristics are visualized in Figure 4.5.

Small values of the Reynolds number and the capillary number of a microfluidic system do not exclude inertial effects in certain situations of local high-speed flows such as the droplet breakup situations [4].

4.2.2 Droplet Generation at a Step Between a Shallow and a Deep Microfluidic Channel

The droplet generation at a step between a shallow and a deep microfluidic channel can be explained theoretically by the capillary focusing effect. A quantitative theory for this effect was developed to explain the droplet generation in nano-terrace devices (see Figure 4.3) [12].

The continuous phase and the dispersed phase are brought together in a microfluidic channel. The two liquids flow side by side in the shallow channel before the step. They are separated by a meniscus which induces a cross-stream pressure difference between them (Laplace pressure, hydrodynamic constraints). The two liquids are forced to balance their pressures when they arrive at the larger volume of the deeper channel (pressure drop of approximately $\frac{2\gamma}{h}$, where h is the inlet channel (also refer to Figure 5.6) height and γ the interfacial tension [173]). This pressure drop causes an acceleration of the dispersed phase, leading to a thread thinning (tongue-like shape) and subsequent a snap-off of the droplet due to the insufficient supply by the dispersed phase (see droplet generation sequence in Figure 4.6).

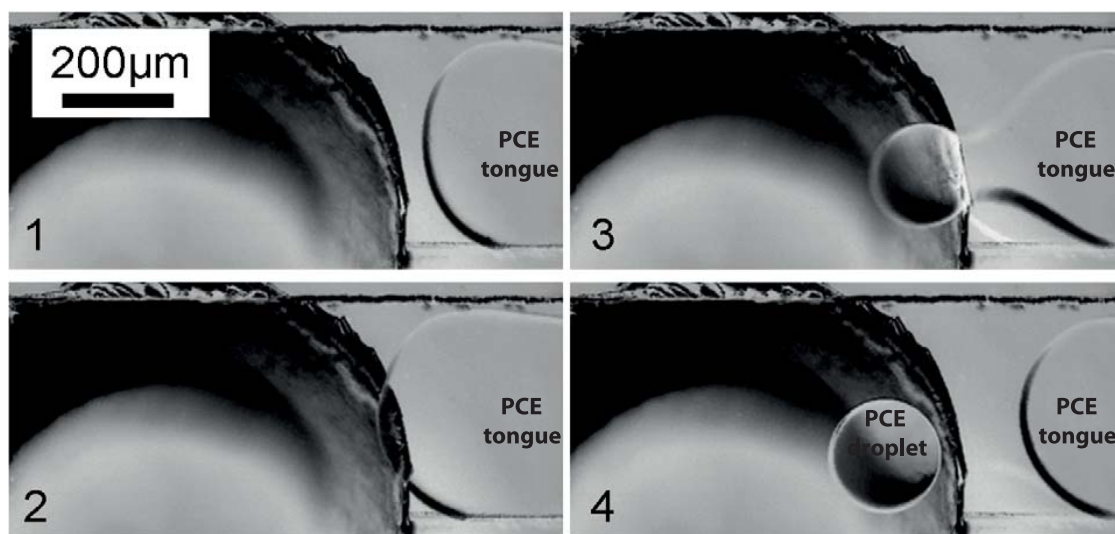


Figure 4.6: PCE droplet generation in saliva by the capillary focusing effect at the step down after the $50\mu\text{m}$ deep microfluidic inlet channel. The liquids flow from right to the left over the step: $8\mu\text{L}/\text{min}$ saliva, $2\mu\text{L}/\text{min}$ PCE. Droplet generation with a period of $\sim 30\text{ms}$.

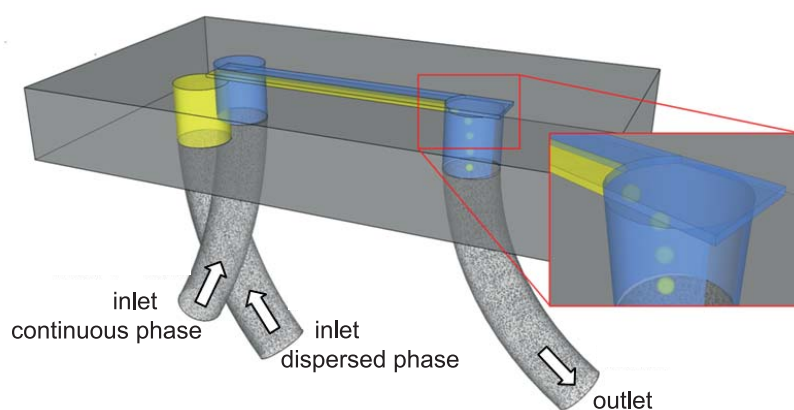
4.3 Design

For our droplet generation method only a simple step in the microfluidic channel was required. Figure 4.7 provides a 3D schematic of the droplet generation devices. Droplets were generated from a microfluidic channel into the microfluidic outlet of the chip as shown in Figure 4.7a. If the droplets needed to be further processed on the microfluidic chip, the generation took place at the step between a shallow and a deep part of the microfluidic channel (see Figure 4.7b).

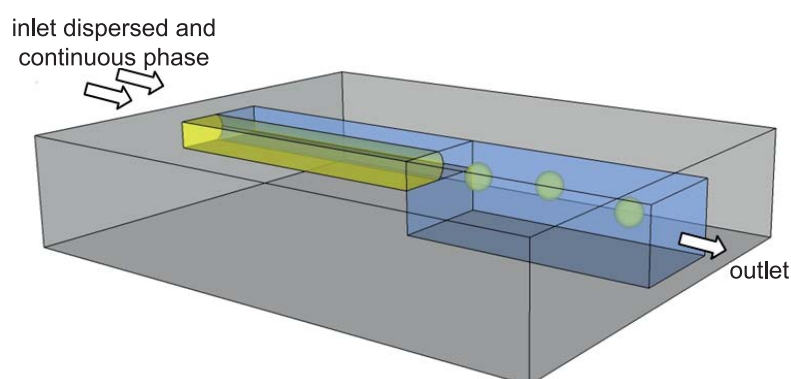
Such a simple step was easy to build with the developed rapid prototyping technique using multilayer scotch-tape masters as presented in section 2.4.1, because the lateral dimensions were found not to be of critical importance (see section 4.4.3). However, for well controlled droplet generation a clearly defined edge of the step is required (straight cut with a scalpel), otherwise the PCE tongue could split into two filaments (symmetric or asymmetric) producing droplets in parallel (satellite droplets) as also observed in nano-terrace device by [173].

4.4 Results

In this section we first verify the basic conditions for PCE droplet generation in saliva by checking the values of the dimensionless numbers. Then the droplet generation mechanism is presented. The influences on the droplet size are investigated and the flow field during the generation process is described by observations using fluorescent beads mixed in saliva. Also the potential for high-throughput droplet generation is demonstrated.



(a) Droplet generation at the outlet of a microfluidic channel.



(b) Droplet generation at the step down between a shallow and a deep microfluidic channel.

Figure 4.7: Schematic of the droplet generation devices.

4.4.1 Basic Conditions for PCE Droplet Generation in Saliva

The Reynolds number (see equation 1.9 in section 1.1) as well as the capillary number (see equation 1.10 in section 1.1) of the microfluidic system need to show a low value to allow droplet generation. Both were calculated here for our system according to the theory given in section 1.1 with the values listed in table 4.1. For comparison, the capillary number was also calculated by a specific formula for the nano-terrace device given by [12]. All calculated values are low (< 1), which indicates good conditions for droplet generation.

$$Re = \frac{\rho v_0 L_0}{\eta} = 0.1987$$

$$Ca = \frac{\eta v_0}{\gamma} = 0.0005$$

$$Ca_{nano-terrace} = \frac{6\eta v_0 w_{nano-terrace}}{\gamma h_{nano-terrace}} = 0.0283$$

Chapter 4. Robust Droplet Generation Based on a Simple Geometry

Table 4.1: Values used for the calculation of the Reynolds number and the capillary number.

symbol	quantity	value	remark
ρ	density	$1000Ns^2/m^4$	density of continuous phase: water (saliva)
v_0	characteristic velocity	$0.0066m/s$	assuming $20\mu L/min$ in the $50\mu m \times 1mm$ inlet channel
L_0	characteristic length	$0.00005m$	inlet channel height
$w_{nano-terrace}$	characteristic width	$0.0005m$	$\frac{1}{2}$ inlet channel width, as suggested by [12]
$h_{nano-terrace}$	inlet channel height	$0.00005m$	
η	viscosity	$0.00166Ns/m^2$	viscosity of continuous phase, measured at low shear rate, see section 2.1.6
γ	interfacial tension	$0.0232N/m$	see section 5.1

4.4.2 Robust Droplet Generation

As already presented in Figure 4.6, we found an absolutely simple and robust method to generate droplets without clogging. At the step we were able to produce droplets of uniform size. The variations of the droplet diameters were found to be smaller than 3%.

The droplet generation method was independent of the microfluidic chip material, but the materials surface energy determined whether oil or water droplets were generated in the two-phase system. Oil-in-water droplet generation, such as the PCE droplet generation in the aqueous saliva, required a hydrophilic chip. Inversely using a hydrophobic chip, water droplets were generated. We verified this phenomenon by producing water droplets in a hydrophobic PDMS chip. As oil-phase, the PDMS compatible [125, 175] organic solvent perfluorodecalin was used.

Furthermore, the orientation of the droplet generation chip and the density of the liquids were not relevant. Figure 4.6 shows downward droplet generation, whereas Figure 7.10 presents upward droplet generation. Our system for PCE droplet generation in saliva showed for the Bond number a small value of 0.066, which also stated that the gravity effects could be ignored (see section 1.1).

4.4.3 Investigations on the Droplet size

The diameter of droplets generated with our method at a step, mainly depended on the height of the inlet channel; the higher the inlet channel, the larger the diameter of the generated

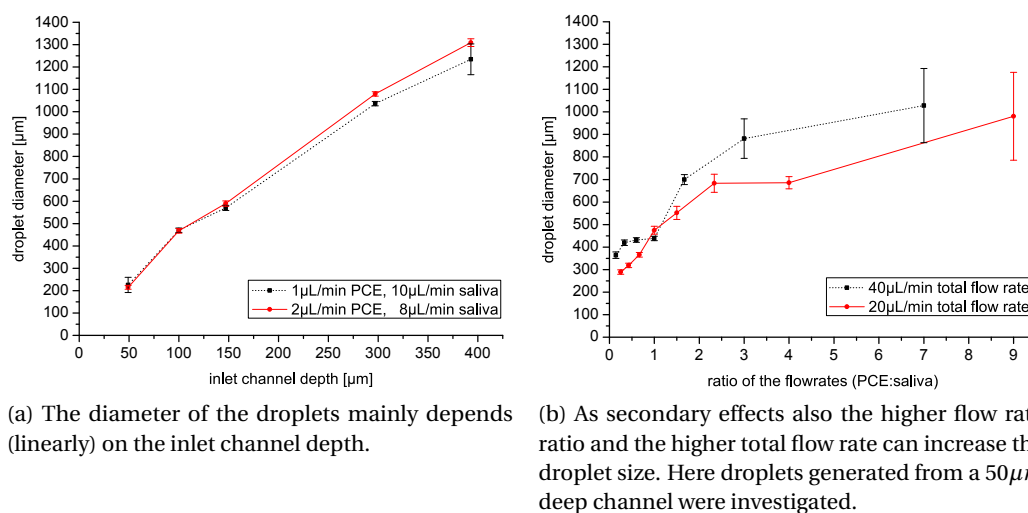


Figure 4.8: Influences on the diameter of the droplets. Error bars indicate the standard deviation for at least 10 measurements.

droplets. We observed the droplet diameter to be 3-5 times larger than the inlet channel height. Figure 4.8a shows the linear dependence of the droplet size on the inlet channel height. Such a linear relation was also observed for the droplets generated by a nano-terrace device [12].

Beside this linear dependence on the inlet channel height, we also found secondary influences such as the ratio of the flow rates of the two immiscible liquids or the total flow rate (see Figure 4.8b). Applying a higher flow rate of the dispersed phase liquid (in our case PCE) resulted in a longer feeding time of the droplet before the snap-off and accordingly to droplets of larger diameter. As mentioned also the higher total flow rate resulted in larger droplet diameter. We assume in this case the higher flow rate stabilized the PCE thread in saliva before the snap-off and thus also allowed a longer feeding time (droplet generation explanation in section 4.2.2).

The dependence of the droplet size on the width of the inlet channel was also investigated. Droplets generated in 50 μm high channels of different widths (800 μm, 1200 μm, 2000 μm) were compared. No tendency was observed, neither by repeating the experiment at different total flow rates.

4.4.4 Flow Field Characteristics during Droplet Generation

The flow field during PCE droplet generation in saliva with our method was explored by using fluorescence microscopy. Fluorescent beads (Polybead Barboxylate Microspheres, diameter 0.452 μm, Polysciences, Germany) were used to visualize the flow during droplet generation. The beads got excited with blue light through a filter (BP 450 – 490 nm). The emitted light of the beads was collected after a color splitting mirror (cut FT 510 nm) excluding the excitation light and another filter (BP 515 – 565 nm). The experiments were performed with a Zeiss Axiovert

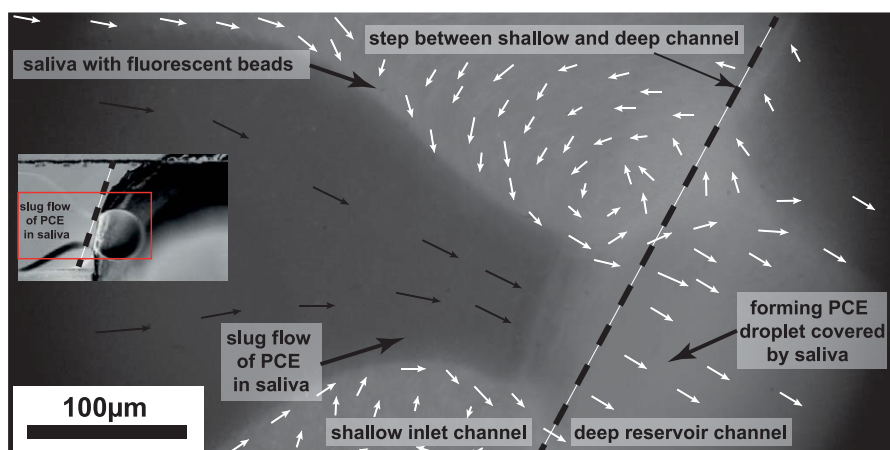


Figure 4.9: Fluorescence microscopy image of the same situation (horizontally mirrored) as shown in step 3 of Figure 4.6: Slug flow of PCE in saliva spiked with fluorescent beads passing over the step down ($100\mu\text{m}$ to $400\mu\text{m}$ deep channel) forming a PCE droplet (main liquid flow rates from the right to the left: $20\mu\text{L}/\text{min}$ saliva, $5\mu\text{L}/\text{min}$ PCE). The directions of the motion of the fluorescent beads are highlighted in the figure with white arrows. Black arrows indicate the PCE flow. While the droplet was formed, small vortexes got established on both sides of the tongue for a few milliseconds.

S100 fluorescence microscope (Carl Zeiss, Germany) equipped with a Xenon 100W power light source and a high-speed camera (Phantom V210, Vision Research, USA). The visualization of the flow using fluorescent beads was only feasible due to the low autofluorescence of the microfluidic chip material NOA81 (see section 3.4).

Our overall system for droplet generation showed laminar flow conditions with a low value of the Reynolds number (see section 4.4.1). During the droplet generation process inertial effects can be observed in certain situations of local high-speed flows as stated by [4]. Figure 4.9 shows the location of the step for droplet generation. The slug flow of PCE (dark no beads) in saliva (spiked with fluorescent beads) passing over the step was forming a PCE droplet. While the droplet was formed, we observed vortexes on both sides of the PCE tongue for a few milliseconds. The directions of the motion of the fluorescent beads are highlighted in the figure by means of white arrows. Black arrows indicate the PCE flow. The PCE droplet generated in the deeper channel does not appear dark, because it is surrounded by saliva containing fluorescent beads.

In the same location, a time dependent series of fluorescence microscopy images is shown in Figure 4.10. Here the main directions of the motion of the fluorescent beads are indicated by white arrows. First saliva was flowing around the tip of the PCE slug (tongue) as a laminar flow. The PCE tongue was growing in the direction of the step (at 37ms). When the tip of the tongue slopped over the step, its shape changed immediately, which induced a first generation of vortexes on both sides of the tongue (at $77 - 86\text{ms}$). These vortexes were able to bring fluorescent beads from locations close to the channel wall in the proximity of the

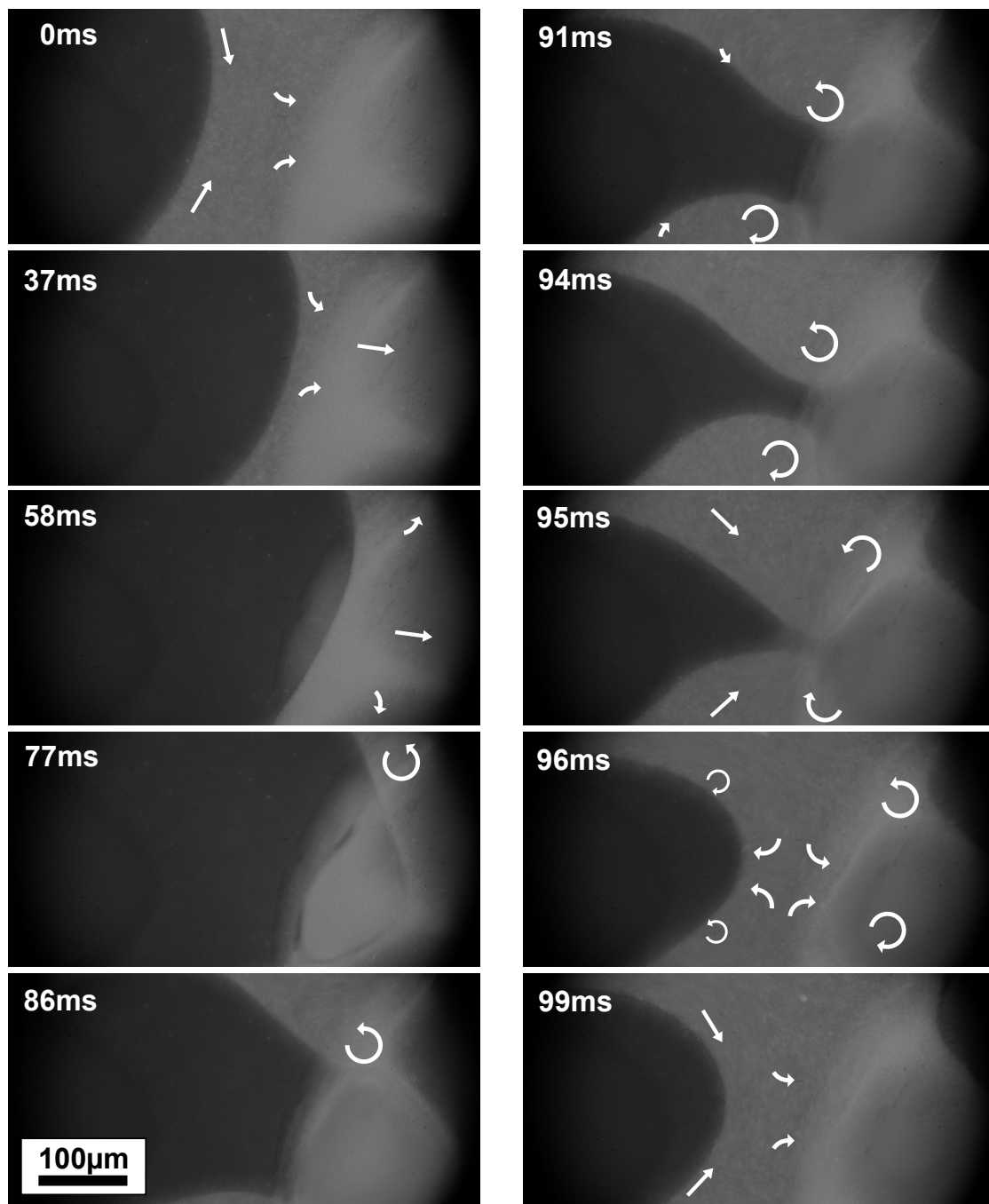


Figure 4.10: Series of fluorescence microscopy images to visualize the flow during the PCE droplet generation (compare with images of the droplet generation process shown in Figure 4.6) in saliva spiked with fluorescent micro beads (diameter of beads $0.452\mu m$). Main flow rates from right to the left: $20\mu L/min$ saliva, $5\mu L/min$ PCE.

PCE tongue ($91 - 95ms$). While the droplet was growing, the PCE feeding tread was shrinking to a sharp tip ($95ms$). The snap-off of the PCE droplet pulled saliva from both sides to the center of the channel where the two saliva streams clashed together and created a second generation of smaller vortexes rotating in the opposite direction as the first generation ($96ms$). Afterwards the flow of saliva was again laminar around the PCE tongue ($99ms$) as observed at the beginning of the cycle ($0ms$).

4.4.5 Parallelization of the Droplet Generation

Our droplet generation method was successfully applied for high-throughput applications. To generate many droplets at once, several input channels were combined for droplet generation into a common outlet. Figure 4.11 shows a chip with the parallelization of four inlet channels. An estimated throughput in the range of $1L/h$ could be reached with our device.

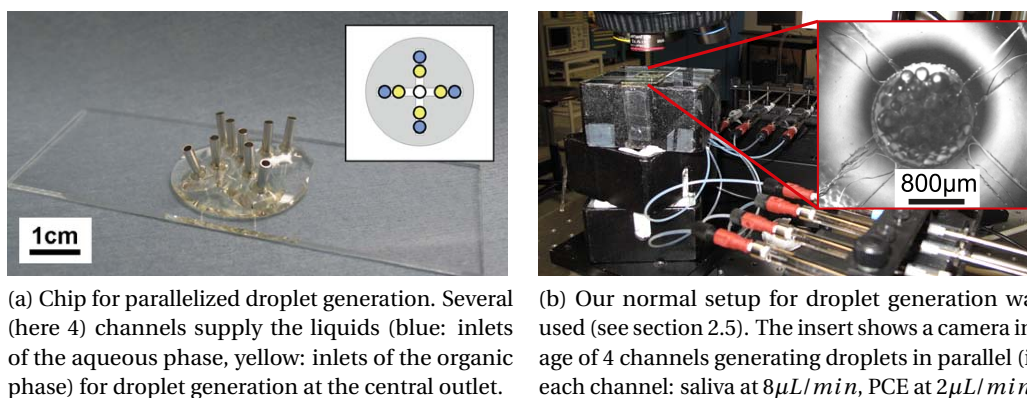


Figure 4.11: Parallelization of the droplet generation allows high throughput.

4.5 Discussion

With our robust droplet generation method we produced monodispersed droplets with a variation of the droplet diameter smaller than 3%, which is comparable to the variation of 1% achieved with the much more expensive and complex nano-terrace devices [12].

Also the liquid supply for our devices was straight forward by using common syringe pumps. Nano-terrace devices ask for an additional integrated flow control system to reduce the flow rates to the nL/min range [173, 176].

The diameter of the droplets generated at the step was linearly related to the inlet channel height like in nano-terrace devices [12]. With our method we also observed secondary influences such as the ratio of the flow rates of the two liquids or the total flow rate. For nano-terrace devices no obvious secondary effects were observed [12, 173].

Thus, under certain conditions, we are able to predict the size of the generated droplets. With

our method we can design a device to create droplets as required, which is not possible or much more challenging for other droplet generation systems such as the flow focusing devices [4, 173].

Applications for microfluidic droplet-generating devices in various fields including food, cosmetic, pharmaceutical, and chemical industry require high-throughput devices. This challenge is approached on microfluidic chips by parallelization of the droplet-generating features (see Figure 4.2). As presented in section 4.4.5, parallelization is also possible with our droplet generation method. The limiting factor, not only for our method, is not the dense packing of microfluidic structures, but the limited space available for connectors and the tubing (connection to the macro world) [170, 177].

Lack of space for fluidic connectors can be avoided by using microchannel emulsification devices, but they are not efficient enough for industrial applications [178].

We observed vortexes during the droplet generation process. Vortexes allow faster mixing on chip, which is normally a challenging task for microfluidic devices with laminar flow conditions [179, 180]. The vortexes generated with our device enable much better mixing (higher extraction efficiency, see chapter 6) than co-flow devices such as microfluidic H-filters, where material transfer is limited to diffusion processes. Vortexes were also observed in other droplet generation devices [4], such as the flow focusing devices, but they tend to clog much faster by using saliva samples (see Figure 2.7).

4.6 Summary

We aimed to develop a new droplet generation method based on the ideas of [12, 173], but which is able to process the complex liquid saliva without clogging. In addition, the device should be easy to fabricate by using our low-cost rapid prototyping technique.

A simple step was found to be the geometry of choice for robust PCE droplet generation in human saliva. No small features were involved which could be clogged by saliva components. Our droplet generation method was even independent of the chip orientation and generated monodispersed droplets (smaller than 3%). Droplets were produced at the microfluidic outlet or at a step in a microfluidic channel to further process the droplets on chip. The developed droplet generation method also allowed high throughput by parallelization of the droplet generation feature. The droplet size was mainly related (linearly) to the geometry of the device (inlet channel height), which allowed to predict the droplet size. Vortexes observed during the droplet generation process enhanced mixing, which is usually difficult to achieve in microfluidic channels due to the laminar flow.

5 Passive Phase Coalescence of Organic Solvent Droplets Dispersed in Saliva

This chapter presents our approach to merge organic solvent droplets dispersed in a continuous aqueous phase, or more specific to merge PCE droplets in human saliva. We had to find a solution not only to merge two droplets, but a device which is merging continuously dispersed droplets to a continuous phase, because only in a continuous phase the optical detection (by means of waveguide spectroscopy) of the cocaine can be performed (see chapter 7).

Parts of the results shown here, were presented at the μ TAS 2012 conference in Japan [158]. Some of the prototypes of physical merging devices were fabricated in the framework of an EPFL student project [181].

5.1 Introduction

Separation of the dispersed and continuous phase of a two phase droplet system is a subject of considerable importance in chemical engineering. To run a droplet merging process on microfluidic chip-level scale is still a challenge, since often macrofluidic methods such as the gravitational or the centrifugational approach cease to hold in applications using continuous flows in microfluidic channels. First, we present here the influence of surfactants and the interfacial tension of the involved liquids on the droplet stability, and afterwards different approaches for microfluidic passive coalescence.

5.1.1 Surfactants and Interfacial Tension

In general (in a system without surfactants), droplets show a higher tendency to merge when the interfacial tension between the involved liquids is lower [182].

Surfactants lower the interfacial tension, but they also have a strong influence on emulsions and are generally used to stabilize droplets against coalescence. Surfactant molecules arrange themselves perpendicular to the interface as a monolayer between the two phases; the polar hydrophilic part facing the aqueous phase and the apolar hydrophobic part facing the organic

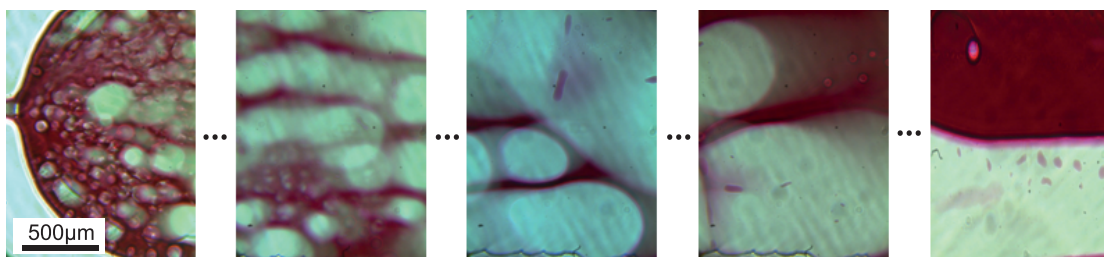


Figure 5.1: The figure on the left shows heptane droplets generated in colored (with amaranth) water by a flow focusing device (see Figure 4.1c) which merge spontaneously further downstream in the microfluidic channel (Figures further to the right are further downstream).

phase. This adsorption at the liquid-liquid interface is the reason for the reduced interfacial tension. Increasing the interfacial tension in a system with surfactants results in separation of the surfactant molecules at the liquid-liquid interface (rupture of the surfactant monolayer) and allows better merging [182].

Droplets of organic solvents, such as PCE or heptane, generated in pure water merge spontaneously in a microfluidic channel as demonstrated in Figure 5.1. However, micro droplets of organic solvents generated in saliva are stable. The reason for this behavior is found in the surfactant proteins SP-A, SP-B, SP-C, and SP-D enclosed in saliva. These surfactants avoiding the coalescence, are responsible in the human body for the immune defense [183].

These facts were confirmed by comparing interfacial tension measurements in the water-PCE system and the saliva-PCE system. The interfacial tension between water and PCE is $\gamma_{water-PCE} = 47.48 mN/m$ [184]. A much smaller value of $\gamma_{saliva-PCE} = 8 \pm 2 mN/m$ was measured for the interfacial tension between saliva and PCE using a Kibron AquaPi (EZ-Pi) surface-tensiometer (Krüss, Germany).

For verification the interfacial tension was calculated alternatively by using Antonov's rule (see equation 1.8 in section 1.1) and the surface tension of the liquids measured against air. A surface tension for PCE of $\gamma_{PCE} = 32.2 \pm 0.1 mN/m$ was measured (reference literature $\gamma_{PCE} = 31.7 mN/m$ [68]) and for the filtered, buffered, and spiked saliva (see section 2.1.4) a value of $\gamma_{saliva} = 55.4 \pm 0.6 mN/m$ was measured (reference literature $\gamma_{puresaliva} = 24.6 - 67.2 mN/m$ [185]). This resulted in a calculated interfacial tension between saliva and PCE of $\gamma_{saliva-PCE} = 23.2 mN/m$ which is more than the initially measured value of $\gamma_{saliva-PCE} = 8 \pm 2 mN/m$, but is still significantly less than the interfacial tension between water and PCE.

5.1.2 Different Approaches for Microfluidic Passive Coalescence

To date most of the microfluidic systems made for droplet coalescence only merge pairs of droplets (batch like process) [186, 187]. Though, in the field of microfluidics a wide variety of microfluidic devices has been employed for merging droplets. They can be divided into two categories: passive and active coalescence devices [188]. Passive devices use specialized

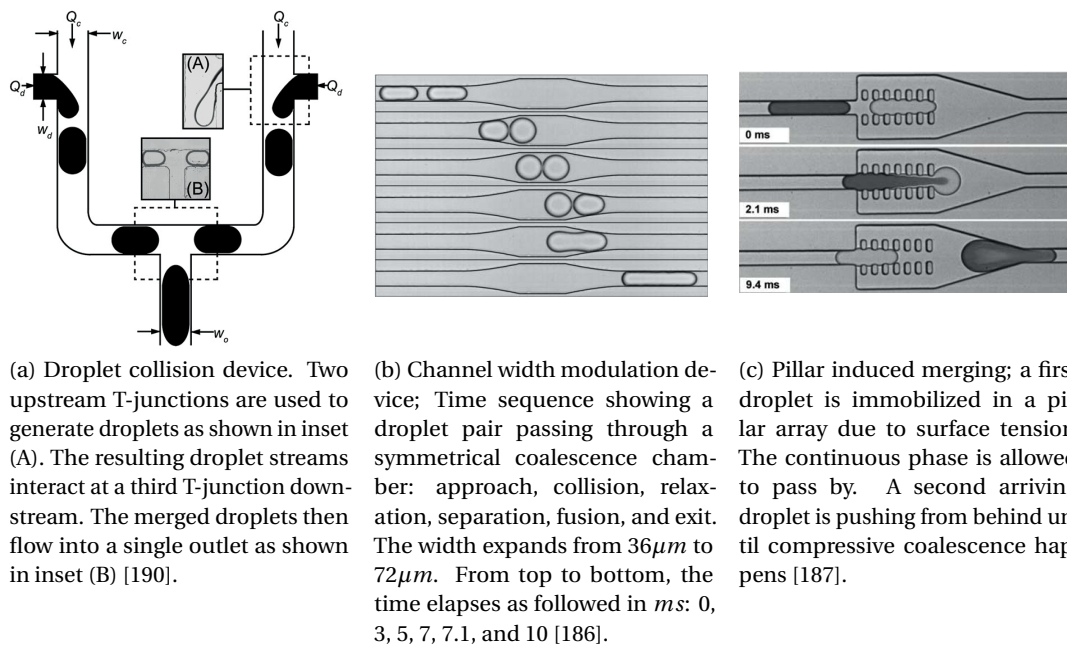


Figure 5.2: State of the art of droplet merging devices.

geometries or surface wetting to cause merging. Active devices employ external forces such as electrical or magnetic fields [189]. Active devices are able to achieve a higher degree of control and flexibility, but this goes along with increased system complexity and higher cost. Here we will focus on the most widely used passive devices with the end goal in mind of fabricating a merging device for a low-cost, disposable, polymer diagnostic chip.

Collision Merging

For collision merging the droplets collide and are pressed together by the liquid flow until coalescence happens. Figure 5.2a shows an example of a collision device, in which droplets to be merged are brought together via two separate channels at a T-junction [190]. This approach requires precise synchronization of the droplets and tuning of flow parameters to ensure merging.

Channel Width Modulation

A popular form of droplet merging is to widen up the channel, either gradually or abruptly, taking advantage of Bernoulli's principle to slow down the front drop and thus bringing the second drop in close proximity. At this point, compressive merging can occur. The channel is then narrowed again which causes decompressive merging due to the acceleration of the first droplet into the narrower part of the channel (Bernoulli effect). A gradual change in the width of the channel allows merging for a wider range of droplet sizes and flow rates [186]. Figure 5.2b presents a channel width modulation device; the time sequence shows a pair of

Chapter 5. Passive Phase Coalescence of Organic Solvent Droplets Dispersed in Saliva

droplets passing through a symmetrical coalescence chamber; approach, collision, relaxation, separation, fusion, and exit.

Pillar Induced Merging

A more complex to fabricate device, uses an array of pillars to immobilize one or more droplets, allowing compressive merging to occur (see Figure 5.2c). Multiple drops may be held in the array of pillars, depending on the number of pillars (length of the pillar array). The final drop size may be tuned by changing the length of the pillar array. When the array is occupied, the pressure at the inlet of the array increases due to the blockage of the channel. This overcomes the force of surface tension holding the merged droplet in the array and pushes the merged droplet out of the array. In case the droplets were not merged due to compressive merging, then decompressive merging can occur, when the first droplet leaves the pillar array. This opportunity for both types of merging (compressive and decompressive) to occur makes this type of device quite robust.

Surface Wettability

Surface modification can be used to induce fusion of several droplets flowing through a microfluidic channel. The effect is based on a surface energy pattern on the walls of the channel. A device to merge aqueous droplets dispersed in an oil by a short hydrophilic part in an intrinsic hydrophobic channel was presented in [191]. This merging approach does not seem to be so robust and depends on many parameters such as the surface energy, droplet size, channel size, and the flow rates.

Phase inversion

While there has been much investigation on merging two droplets (batch process), relatively little literature exists for continuous phase inversion through passive droplet coalescence (continuous process). A so called 'phase inversion' device is shown in Figure 5.3. This design offers insight into how our goal of continuous droplet coalescence may be achieved: the continuous phase is removed by perpendicular drainage channels and the droplets are collected in a chamber downstream. The droplets merge when they get accelerated towards the smaller channel exit by decompressive merging [192].

Based on the examples presented in this introduction, we first tried to merge the PCE droplets dispersed in saliva by chemical approaches. Since this was not successful, we focused on the physical approach - the mechanical deformation of the droplets.

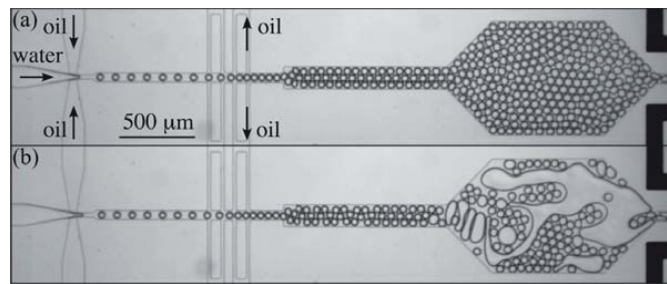


Figure 5.3: Phase inversion device: The continuous phase is removed by perpendicular drainage channels and the droplets are collected in a chamber downstream. The droplets merge when they get accelerated towards the smaller channel exit. [192].

5.2 Theory & Fundamental Principles

5.2.1 Droplet Coalescence Stages

The droplet coalescence process can be broken into four distinct stages: 1) initial approach; 2) drainage of the continuous phase separating the droplets; 3) film rupture and 4) confluence [186]. In certain cases these steps can be closely linked or one or more steps may occur spontaneously.

5.2.2 Compressive Merging

The simplest and best known merging method is called compressive merging, in which droplets are compressed and brought in close proximity. The Van der Waal's forces then pull the droplets in contact and drain the remaining continuous phase between them [186]. Depending on factors such as interfacial tension, availability of surfactants, temperature, etc., the film will rupture more or less spontaneously and the droplets will merge. Examples for the compressive merging principle are the collision merging or pillar induced merging (see section 5.1.2).

5.2.3 Decompressive Merging

This merging method may be more robust than compressive merging due to the active drainage of the fluid between the droplets [186]. However, a more complex mechanism is involved here. Droplets which are close together are pulled apart, reducing the pressure between them. Therefore, the fluid film is drained and the surfaces deformed in locally stressed interfaces. On both droplets a nipple of a small radius and therefore high Laplace pressure occurs (see also section 1.1) [186, 193]. This causes the interface to rupture and to form a bridge between the droplets. Once such a bridge is established, the droplets will confluence. Examples for the decompressive merging principle are the channel width modulation merging or the phase inversion merging (see section 5.1.2).

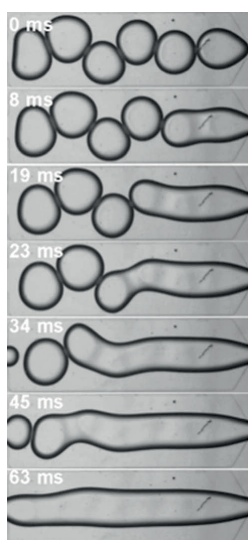


Figure 5.4: Observation of an avalanche of coalescence events. The time corresponding to the successive images (downwards), are indicated in the figure.[194].

5.2.4 Avalanche Coalescence

If the droplets are already in close contact, a single merging event may cause further merging events in an avalanche effect [192, 194]. The shape relaxation of two droplets merging may induce decompressive merging in nearby droplets as shown in Figure 5.4. The probability of merging depends on the angle between the droplets during coalescence, with highest probability of merging, when the droplets are aligned in a row (co-linear) [192].

5.3 Design

Merging droplets of organic solvents in human saliva is a challenging task due to the presence of surfactant proteins as introduced in section 5.1. We designed and tested several chemically assisted merging approaches which are presented in section 5.3.1. Unfortunately these approaches were found not to be successful. More promising was the physically assisted merging method presented here in section 5.3.2. The physically assisted merging method deforms the droplets to allow compressive and decompressive merging (see section 5.2). Furthermore, this section presents the method and the developed layout of our microfluidic chip.

5.3.1 Chemically Assisted Merging Approaches

Increasing pH value The pH value of saliva was increased up to $\sim pH12$ by means of a sodium hydroxide solution (0.1 mol/L). With this approach we tried to make some of the surfactants in saliva completely apolar and consequently inactive. PCE droplets remained stable and did not merge.

Surfactants We added different surfactants (Triton X-100, cetyl trimethylammonium bromide (CTBA), dioctyl sodium sulfosuccinate(DSS) and isopropyl alcohol (IPA)) in different concentrations (0.01%, 1%, and 5%) to saliva. Surfactants align themselves as a monolayer at the interface between the aqueous and organic phase and generally stabilize the droplets which is actually the opposite of what we aimed for. We added surfactants of different size and different structure than the natural surfactant proteins of saliva. Thereby, we tried to destroy the monolayer of the natural saliva surfactant proteins and to allow coalescence. PCE droplets remained stable and did not merge. By adding isopropyl alcohol (acting as surfactant under these conditions) the nucleic acids of saliva precipitated (alcohol) and a sort of veil appeared in saliva.

Anti-foaming agent To cause merging, we tried adding the anti-foaming agent pluronic F-12 (surfactant). We prepared (melting, mixing) a solution of 10 *wt%* pluronic F-12 in water and mixed the solution 1 : 1 with saliva. PCE droplets remained stable and did not merge.

Salting out An organic phase is 'less soluble' in a salty aqueous phase (effect known for isopropyl alcohol). Therefore, we tried to cause coalescence by increasing the NaCl concentration, even a saturated salty solution was not able to merge the PCE droplets in saliva.

Surface Wettability Following the surface wetting coalescence principle presented in section 5.1.2 [191] we also adjusted the wetting behavior of our channel, on one hand chemically (see section 3.3) and on the other hand by changing the surface roughness of the microfluidic channel walls (see section 2.4.1). The effect of different surface wettability was found not to be strong enough to merge the stable PCE droplets in saliva.

Temperature We also tried to cause coalescence by increased temperatures as suggested by [195]. The microfluidic chip containing the PCE droplets dispersed in saliva was mounted on a hotplate which was heated up to 50 °C. No coalescence was observed, but at higher temperatures the microfluidic chip risks to debond.

5.3.2 Physically Assisted Merging Approach

Our physical merging approach can be broken in two stages: First, we drained out the continuous phase saliva to get densely packed droplets. These droplets were then compressed, deformed, and accelerated in a second stage in order to cause merging by compressive and decompressive coalescence (see section 5.2.2 and 5.2.3).

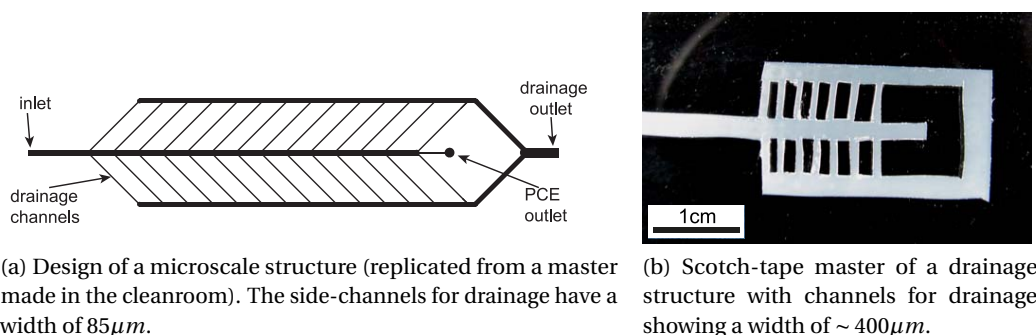


Figure 5.5: Microfluidic structures to drain out the saliva (continuous phase) and to keep the PCE droplets in the central channel for merging.

Drainage of the Continuous Phase

We replicated by rapid prototyping (see section 2.4) a structure on a master made in the cleanroom by photolithography showing small drainage channels ($85\mu\text{m}$ wide, $50\mu\text{m}$ deep, see Figure 5.5a) to drain out saliva (as suggested by [196]). These channels were too small and got clogged by both saliva components and parts of PCE droplets.

A device showing much larger perpendicular drainage channels ($\sim 400\mu\text{m}$ wide, $50\mu\text{m}$ deep, see Figure 5.5b) was replicated from a scotch-tape master. This structure also suffered from clogging by PCE droplets and additionally the flow was unbalanced due to the different channel widths.

The solution for effective saliva draining without clogging was found by replacing the array of perpendicular drainage channels by one extremely wide drainage channel which was shallower ($50\mu\text{m}$) than the main channel ($600\mu\text{m}$) (extraction channel). The droplets preferred to stay in the deep main channel instead of being squeezed into the shallow side-channel as long as the height of the shallow channel was smaller than the droplet size. The height of the drainage channel was set to $50\mu\text{m}$ which represents the minimum feature size in the vertical direction using scotch-tape masters (1 layer of tape). Figure 5.6 shows this saliva drainage channel integrated in the extraction system and also defines the glossary of the different components of the total microfluidic extraction system.

With our method, the shallow drainage channel was not clogged by saliva components and PCE droplets were normally too large to enter the shallow drainage channel. However, in case a PCE droplet became stuck in the drainage channel, it did not completely block the flow, because the drainage channel was wide enough.

Merging Device

The merging geometry we designed was inspired by the phase inversion device (see Figure 5.3). It was based also on the channel width modulation devices, but instead of changing the channel width, we changed the channel depth. The direction of the channel modulation

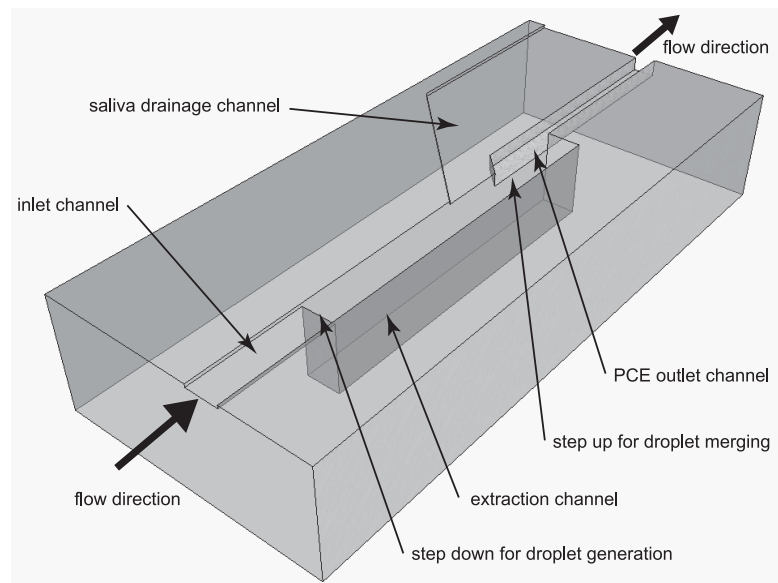


Figure 5.6: Definition of the glossary of different channels on the microfluidic extraction system.

(width or depth) has no influence since our system shows a small Bond number, indicating that gravitational effects can be neglected (see section 1.1).

To merge the densely packed droplets we used a step between a deep and a shallow microfluidic channel. Droplet coalescence in our system was based on two different methods; compressive and decompressive merging. For compressive merging the droplets were brought into close contact and then mechanically pressed against the end of the deep extraction channel (see Figure 5.7). Decompressive merging was observed when a droplet accelerated away from its neighbor into the shallower PCE output channel (constant flow rate, smaller cross-section (Bernoulli effect), see Figure 5.7). This separation resulted in a local pressure drop between the droplets, then the draining of the remaining fluid film of the continuous phase, and finally in the formation of two facing nipples with locally stressed interfaces (high Laplace pressure) and droplet coalescence as explained in section 5.2.3. Since the droplets were densely packed, sometimes also avalanche coalescence took place.

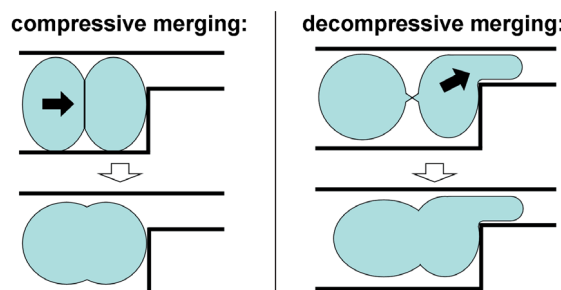


Figure 5.7: Schematic (cross-section view) of the two different modes of droplet merging at the step between a deep and shallow microfluidic channel.

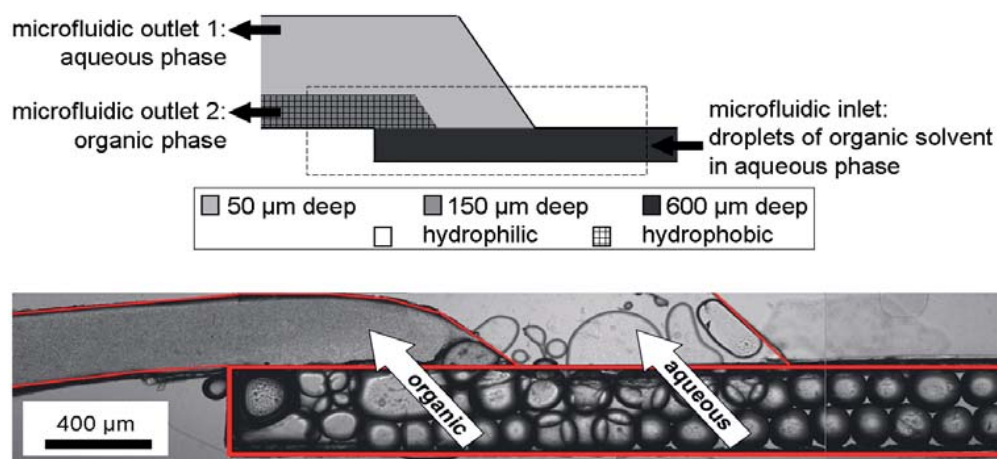


Figure 5.8: Scheme of the merging chip with different channel depths and surface properties together with a microscopy image of the zone within the dashed frame showing the drainage of the aqueous phase and the merging of the organic phase.

The PCE droplets were merged and the PCE left the device as continuous organic phase through the PCE output channel. An initially designed separation wall between the PCE outlet channel (150 μm deep) and the saliva drainage channel (50 μm deep) was removed in order to allow the remaining saliva in the PCE outlet, to change to the saliva side. Separation of the two liquids is supported on one hand by the different channel depth and on the other hand by different wettability of the channel walls (adjustable channel wettability by using scotch-tape masters, see section 2.4.1). The saliva drainage channel showed a smooth hydrophilic channel surface, whereas the PCE outlet channel was rough and more hydrophobic.

5.4 Results

For characterization, our devices were tested with our measurement setup presented in section 2.5. The coalescence of the PCE droplets was verified optically. Figure 5.8 presents a schematic of the merging part of the chip with different channel depths and surface properties, together with a microscopy image of the drainage and merging process. PCE droplets arrive in the deep extraction channel. First, the continuous aqueous saliva is drained out via a shallow side-channel. Also some PCE droplets might escape unintentionally through the drainage channel. The droplets are pushed together against the end of the extraction channel and they merge by entering the PCE outlet channel. The PCE leaves as a continuous phase.

The merging system was working best by using droplets with a diameter of $\sim 600 \mu\text{m}$ diameter produced by a step of 150 μm . These droplets were too large to enter the 50 μm deep saliva drainage channel. The droplets merged well at the step between the 600 μm deep extraction channel and the 150 μm deep PCE outlet channel, when they were squeezed into the channel of a depth of roughly $\frac{1}{4}$ of the droplet diameter. Smaller droplets produced at a step from a 50 μm or 100 μm deep inlet channel (1 or 2 scotch-tape layers) did not merge.

5.5 Discussion

The developed method, continuously merging organic solvent droplets (stabilized by surfactants), is a passive droplet merging method and thus it does not come along with added system complexity and fabrication cost.

The literature describes mainly merging of two droplets (batch processing) which is of interest, if example given, the droplets are considered as a reaction chamber, but there were only a few ideas presented how to merge successively many individual droplets to a continuous phase. Furthermore, mainly systems with aqueous droplets dispersed in an organic solvent were studied. To the best of our knowledge we present here the first system which merges continuously organic solvent droplets in aqueous solution (amongst other things predetermined by our hydrophilic chip material), whereas the aqueous solvent is a non standardized human body fluid already containing some surfactants. Our method does not include small drainage channels which tend to clog by processing saliva, but a shallow and wide clogging-resistant drainage channel.

We combined the drainage and the simple step in the microfluidic channel resulting in droplet coalescence. The system has shown to merge successfully PCE droplets in human saliva, but still the system shows some restrictions such as the droplet size or the flow rate.

If the droplets were too small (diameter smaller than twice the depth of the PCE outlet channel), they were not squeezed, accelerated, and separated enough to merge (by decompressive coalescence) when entering the shallower channel.

If the flow rates were too high, coalescence failed, because the continuous phase between the droplets could not be drained fast enough. For our design coalescence became critical at flow rates higher than $\sim 40\mu L/min$.

In the design shown in Figure 5.6 and 5.8 the PCE outlet channel leaves the main extraction channel at the side. In the opposite corner a dead zone of stagnant flow was observed. The design was then improved by arranging the PCE outlet channel co-linearly to the extraction channel.

5.6 Summary

We aimed to merge PCE droplets dispersed in human saliva. The droplets were stable due to the surfactant proteins already present in saliva, unlike PCE droplets dissolved in water which merge spontaneously.

The surface tension between both liquids needed to be increased which induced stressed interfaces and resulted in easier coalescence. Several chemically assisted merging approaches were tested and failed, such as increasing the pH value, the salting out method, elevated temperatures, adjusted surface wettability, or the addition of anti-foaming agents and different surfactants.

We developed a physical, passive method to merge continuously the PCE droplets dispersed

Chapter 5. Passive Phase Coalescence of Organic Solvent Droplets Dispersed in Saliva

in saliva. First, the continuous phase was drained out by a shallow side-channel (low risk of clogging) and then the droplets were physically deformed by the microfluidic chip geometry (step in the main channel from a deep to a shallow channel) resulting in coalescence based on the compressive and decompressive merging principle.

6 Liquid-Liquid Extraction of Cocaine from Human Saliva

We aimed to transfer cocaine from a saliva sample to an IR-transparent, organic phase in order to allow detection by waveguide based IR-spectroscopy. Here we present a new and promising droplet-based liquid-liquid extraction method as well as a compact microfluidic extraction system (ES) including on the same chip droplet generation (see chapter 4), liquid-liquid extraction, and droplet merging (see chapter 5). Here we present the optimization of the extraction efficiency of our extraction system within a certain given range which allows stable operation of the overall system.

The results shown here, were presented at the μ TAS 2012 conference in Japan [158].

6.1 Introduction

Liquid-liquid extraction methods are currently used in several fields, mostly analytical chemistry, chemical engineering, and biology. Liquid-liquid extraction is a passive diffusion-based technique to extract solutes from a specified phase. No chemical reaction takes place. The transfer of matter from one liquid to another is driven by unbalanced chemical potentials between the two liquid phases.

It is a promising approach to use liquid-liquid extraction in microfluidic systems, since there the extraction process is orders of magnitude faster than in non-miniaturized systems [197]. This comes from the fact that the diffusion time scales as the square of the system size (see equation 1.6 in section 1.1), and obviously the distances of travel are much shorter.

Liquid phase microextraction through a porous hollow fiber membrane was presented to extract drugs from human biological samples [198]. The extraction times were long (15 – 60 *min*) and such a membrane risks to be blocked.

Another microfluidic extraction system was using a fluid film instead of a solid membrane [199]. A stable three-layer flow system, water / organic solvent / water, was established in a microfluidic channel. In the continuous laminar flow, the solute (methyl red) was extracted across the microchannel from the donor (water) to the acceptor phase (water) through the

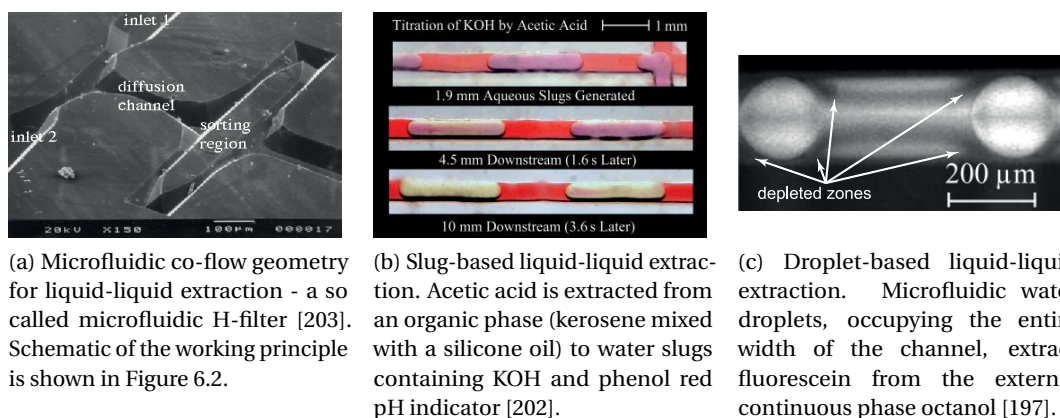


Figure 6.1: State of the art of microfluidic liquid-liquid extraction devices.

organic solvent phase (cyclohexane).

Simpler were the microfluidic extractions of solutes from an aqueous to an organic solvent in a parallel laminar flow as presented by [200, 201].

Besides these co-flow approaches (H-filters) for liquid-liquid extraction, also slugs in a capillary were studied [202] or the droplet-based liquid-liquid extraction method [197] was investigated (see Figure 6.1).

6.1.1 Microfluidic H-filter

The microfluidic H-filter (see Figure 6.1a) was developed at the University of Washington in the late 90's [204–206]. An H-filter is a co-flow geometry, which can be used for filtration purposes or liquid-liquid extraction. Two liquids are brought together in one channel (diffusion channel) as a parallel flow. Based on the laminar flow conditions, the liquids do not mix and can be separated again after the continuous filtration/extraction process. Only driven by diffusion, particles or molecules change from one liquid to the other. The traveled distance of a solute depends on its diffusion coefficient. The diffusion coefficient scales roughly with the inverse of the size of the molecule (the hydrodynamic radius) [3]. Therefore, solutes with high diffusion coefficients can be separated from components of the sample with lower diffusion coefficients (see Figure 6.2). In a two-phase system, the solutes are extracted by diffusion to the liquid showing better solubility of the solute.

We investigated the extraction potential of a microfluidic H-filter for our application (cocaine extraction from saliva to the organic solvent PCE) by studying the equation for a traveled distance of a molecule and by a comsol simulation (chemical reaction engineering module) of cocaine diffusion in a co-flow device.

The time-dependend root-mean-square distance traveled by a molecule in solution is given by equation 1.6 in section 1.1. The diffusion coefficient of cocaine in water is as small as $2.7 \cdot 10^{-9} \frac{m^2}{s}$ (lower in saliva due to obstruction by proteins) as determined by [207]. Assuming

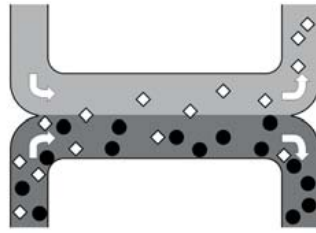


Figure 6.2: Working principle of a microfluidic H-filter. Square particles show a larger diffusion coefficient than the round ones and therefore, they travel faster to the other liquid and can be filtered out.

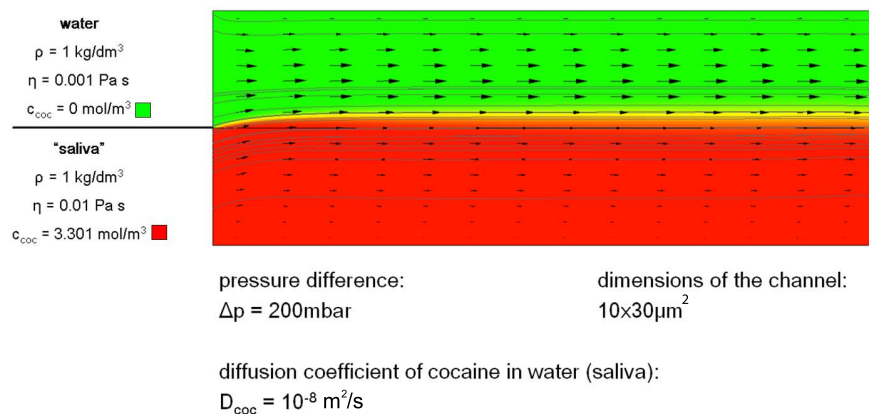


Figure 6.3: Comsol simulation of the cocaine concentration distribution when water and non-Newtonian saliva are flowing side by side in a microfluidic channel.

a retention time in the microfluidic system of 1 s for a molecule, the diffused distance is at most $50 \mu\text{m}$. This is a reasonable distance for really small microfluidic channels (H-filters with channel widths smaller than $100 \mu\text{m}$ [205]). But by far, this is not enough for our saliva system which asks for larger channels, because of the high risk of channel clogging by saliva components (see Figure 2.7a).

Even smaller diffusion distances perpendicular to the flow were determined by a numerical simulation of a parallel flow of water and saliva with cocaine ($300 \mu\text{g/mL}$) in co-flow in a microfluidic channel (see Figure 6.3).

6.1.2 Slugs in a Capillary

In this liquid-liquid extraction method, slugs of immiscible liquids flow through a capillary or a microfluidic channel (see Figure 6.1b). Mass transfer takes place at their interface, based on diffusion. Liquid circulations within the slugs get established, which are stimulated by the shear between the stationary fluid at the wall and the slug axis (see Figure 6.4). These internal circulations are responsible for an enhancement in the interfacial mass transfer due to the induced additional mixing.

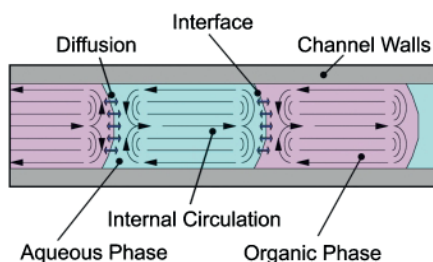


Figure 6.4: Schematic of the internal circulations generated within an immiscible slug flow [202].

6.1.3 Droplet-Based Liquid-Liquid Extraction

Droplet-based liquid-liquid extraction was suggested by [197] (see Figure 6.1c). They provided theoretical calculations of the extraction time (defined by the equilibrium conditions) and presented an experiment extracting fluorescent markers. Using this droplet-based extraction technique, droplets of a diameter equal to the channel width flow through a channel and a solute is extracted from the continuous phase to the droplet phase. The theoretical maximum of transferred mass is defined by the volume of the continuous phase between two droplets. Larger distances between the droplets provide more solute to be extracted. They observed a saturation level several times lower than the expected theoretical equilibrium value (partition coefficient), because of the inhomogeneity of the concentration field inside and outside the droplet at all times. Close to the droplet surface, depleted zones in the external continuous phase were observed (see Figure 6.1c).

Liquid-liquid extraction with a co-flow device is a continuous process, which allows easier separation of the two phases for further processing after the extraction. However, the slug- and droplet-based extraction methods are more efficient due to the induced liquid circulations and a relatively larger interface between both phases for the mass transfer. Assuming two liquid phases of the same volume, a droplet in cube shows an interface around 3 times larger compared to a configuration, in which the two liquids are arranged besides each other (larger surface-to-volume ratio, see Figure 6.5).

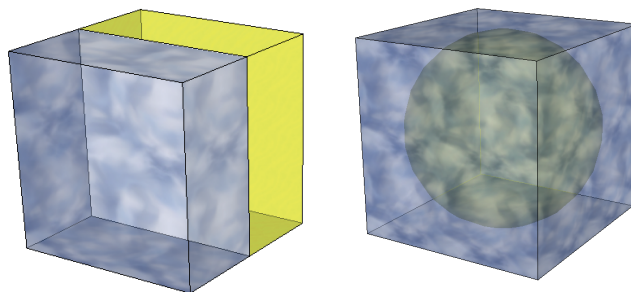


Figure 6.5: A droplet in cube shows an interface around 3 times larger compared to two liquids of the same volume arranged besides each other. This larger surface-to-volume ratio favors the liquid-liquid extraction.

6.2 Theory & Fundamental Principles

Liquid-liquid extraction is a diffusion-based, passive process, which is driven by an unbalanced chemical potential (concentration differences). Solutes also migrate to the phase in which they are more soluble until the equilibrium conditions are reached. The equilibrium can be manipulated by adapting the conditions such as the pH value.

Cocaine dissolved in water is negatively charged (ionized) at a pH value of 7 (acidic behavior). In this polar form, cocaine is supposed to show better solubility in polar water than in a apolar organic solvent [198].

pKa is the acid dissociation constant, a measure of the strength of an acid in solution. It is the equilibrium constant of the acid-base reaction. Cocaine has a pKa value of 8.6 [68]. For pH values higher than 8.6 most of the cocaine is found in the unionized, apolar form. Under such conditions, cocaine prefers to be dissolved in the apolar organic solvent, rather than in the polar water.

Consider the equilibrium of an acid in a two-phase system (here aqueous saliva and the organic solvent PCE) at an aqueous phase pH value, such that the acid is partially ionized. The distribution of a solute between the aqueous and organic phase is defined as the partition coefficient (PC) or distribution coefficient (DC) and depends on the pH and the pKa value.

The distribution coefficient is defined as the ratio of the concentration of the solute in the organic phase to the concentration of all species in the aqueous phase at a given pH, whereas the organic phase is assumed to contain only unionized species [208]:

$$DC = \frac{[solute]_{PCE}}{[solute]_{saliva}^{ionized} + [solute]_{saliva}^{unionized}}. \quad (6.1)$$

The partition coefficient is defined as the ratio of the unionized solute in each phase, such as [208]

$$PC = \frac{[solute]_{PCE}}{[solute]_{saliva}^{unionized}}. \quad (6.2)$$

The partition coefficient can also be estimated from the distribution coefficient, knowing the pKa and pH value of the system as described by [208, 209]:

$$\log(PC) = \log(DC) - \log\left(\frac{1}{1 + 10^{pKa-pH}}\right). \quad (6.3)$$

For pH values above the pKa value, the distribution coefficient and the partition coefficient are the same.

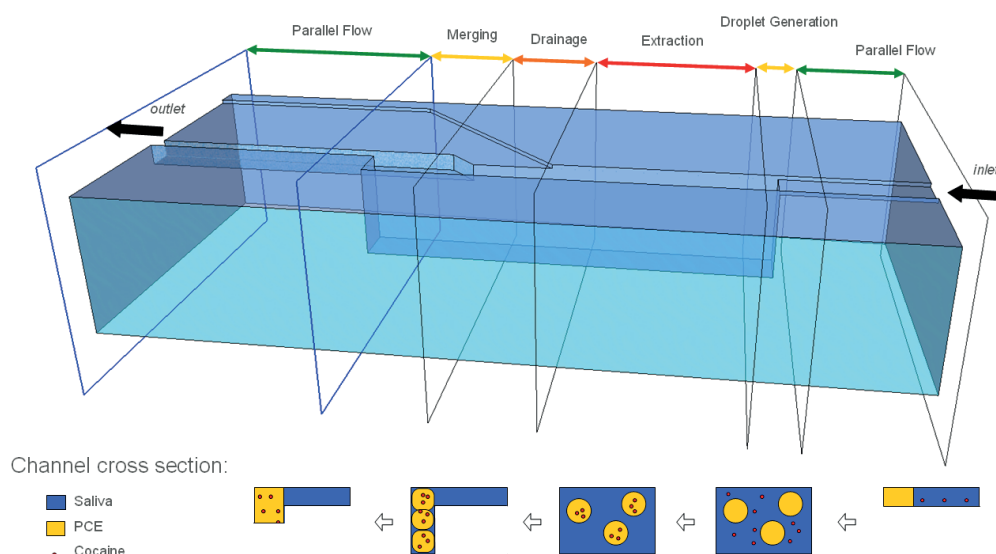


Figure 6.6: Schema of the extraction system explaining the different steps of the liquid-liquid extraction: After the inlet, saliva with cocaine flows in parallel with PCE. Droplets are generated at the step to increase the surface-to-volume ratio which allows faster liquid-liquid extraction. After the extraction, saliva is drained out and the PCE droplets merged to a continuous phase. Towards the outlet, the two phases flow in parallel, but now cocaine is dissolved in the PCE.

6.3 Design

6.3.1 Principle of the Microfluidic System for Droplet-Based Liquid-Liquid Extraction

The aim of our microfluidic droplet-based liquid-liquid extraction system is to bring cocaine from saliva to the IR-transparent PCE, in which it will be detected by IR-spectroscopy.

As presented in section 6.1, it has been suggested to replace co-flow devices by droplet-based extraction systems showing higher extraction efficiencies, mainly due to the better surface-to-volume ratio and internal circulations.

We designed the microfluidic system shown schematically in Figure 6.6, which produces droplets for enhanced liquid-liquid extraction. After the cocaine extraction to PCE, the system merges the organic solvent droplets again to a continuous phase for the cocaine detection by IR-spectroscopy.

Via inlets, saliva containing cocaine was brought in a shallow microfluidic channel together with PCE. Both phases were flowing in parallel towards a step in the microfluidic channel. There, PCE droplets were generated in saliva as explained in chapter 4. In the extraction channel, cocaine was transferred from saliva into the PCE droplets driven by the chemical potential. After the performed liquid-liquid extraction, the PCE droplets were merged again to a continuous phase as presented in chapter 5. To allow coalescence of the PCE droplets, first the continuous phase saliva was drained out by a shallow side-channel and then the droplets

were merged at the end of the extraction channel. Towards the outlet, a continuous phase of PCE was flowing besides the saliva, like in the inlet channel, but now with most of the cocaine dissolved in the organic phase (PCE).

6.3.2 Design Variations

We used two different designs. The liquid-liquid extraction method was developed with a first extraction system (ES 1) shown in Figure 6.7a. For the integration with the optical detection waveguide chip, the design was adapted and called second extraction system (ES 2) (see Figure 6.7b). The footprint of the ES 2 was reduced compared to ES 1 by folding the design twice. Furthermore, the outlet channel was arranged collinear with the extraction channel. This way a dead zone of stagnant flow in the extraction channel (on the opposite side of the outlet channel) could be avoided.

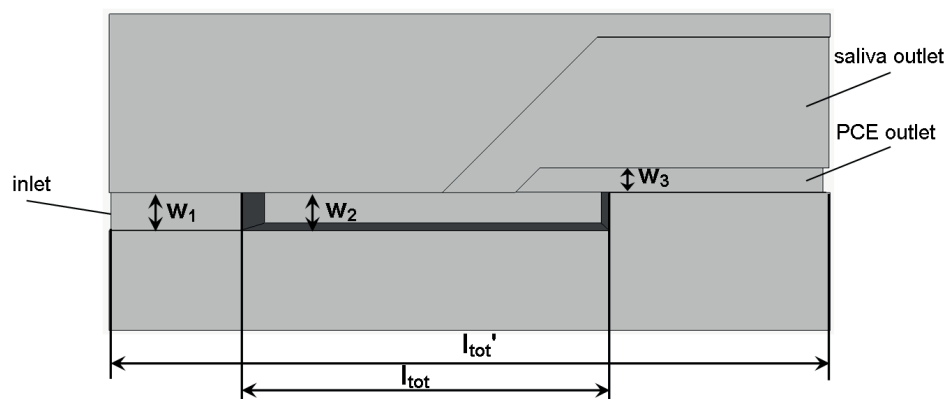
The vertical dimensions of the microfluidic channels were given by a multiple of the thickness of the scotch-tape used for the scotch-tape masters (see section 2.4.1). The depth of the inlet channel was $50\mu\text{m}$ (ES 1) and $200\mu\text{m}$ (ES 2), the depth of the extraction channel always $600\mu\text{m}$, of the saliva drainage channel $50\mu\text{m}$ and of the PCE outlet channel $150\mu\text{m}$ (see Figure 5.6 and 5.8).

The lateral dimensions denoted in Figure 6.7 were varied according to Table 6.1. Versions A, B, and C of the ES 2 showed similar total length, measured from the PCE inlet to the PCE outlet. ES 2A featured a 6mm long and $100\mu\text{m}$ deep shallow channel part in the extraction channel. ES 2B showed a shorter extraction channel and ES 2C wider extraction channels than the other two designs.

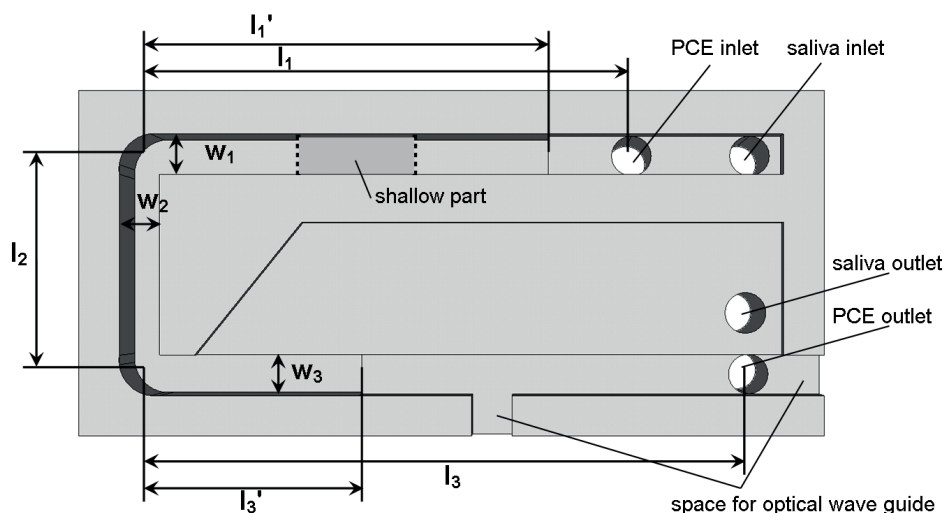
6.4 Results

The goal was to maximize the extraction efficiency of the developed system. Our droplet-based approach for liquid-liquid extraction showed fabulous extraction efficiencies and even allowed cocaine preconcentration. But to successfully operate the whole extraction system, the parameters could only be varied within a certain range, which does not allow to tap the full potential of this droplet-based extraction method.

In this section we present the optimization of the extraction efficiency of the extraction system by pointing out the influences of several parameters. First, the pH value is adjusted and then the extraction efficiency is evaluated for varying geometrical dimensions. The extraction efficiency was always determined by comparing the concentration of cocaine extracted to PCE with the one of cocaine in saliva. The cocaine concentration was measured by an appropriate mass spectrometry method (UPLC-MS) which is described in section 2.2.



(a) First extraction system ES 1 used for system development.



(b) Second extraction system ES 2 which was more compact for the integration with the optical waveguide for detection. Some of the chips showed an additional shallow part in the extraction channel as indicated. Spaces were designed for the integration of the optical waveguide which were sealed after bonding by PE.

Figure 6.7: Design of the microfluidic extraction systems with dimensions of the microfluidic channels (width w , length l from the PCE inlet to the outlet, length l' of the extraction channel, see Table 6.1).

6.4.1 pH Value Optimized Extraction Conditions

To measure the distribution coefficient, we mixed $1\mu\text{g}/\text{mL}$ cocaine in saliva together with the same volume of PCE. After 24 hours, at equilibrium conditions, the cocaine concentrations in saliva and PCE were determined by mass spectrometry (section 2.2). At pH 7 already 94% of the cocaine was found in PCE. At pH 8 more than 99% of the cocaine was transferred to

Table 6.1: Dimensions of the microfluidic channels on the extraction systems (ES) (see also Figure 6.7). The depth of the inlet channel was $50\mu m$ (ES 1) and $200\mu m$ (ES 2), the extraction channel always $600\mu m$, the saliva drainage channel $50\mu m$ and the PCE outlet channel $150\mu m$ (see Figure 5.6 and 5.8).

device	ES 1A	ES 1B	ES 2A	ES 2B	ES 2C
length of the first part $l_1 [mm]$	n.a.	n.a.	23.5	21.0	25.0
length of the first part (extraction channel only) $l'_1 [mm]$	n.a.	n.a.	14.5 ¹⁾	12.0	18.0
length of the second part $l_2 [mm]$	n.a.	n.a.	11.5	11.5	12.0
length of the third part $l_3 [mm]$	n.a.	n.a.	33.0	30.5	30.0
length of the third part (extraction channel only) $l'_3 [mm]$	n.a.	n.a.	15.0	12.5	13.0
width of the first part $w_1 [mm]$	1.5	0.7	0.5	0.5	0.9
width of the second part $w_2 [mm]$	1.5	0.7	0.9	1.0	1.1
width of the third part $w_3 [mm]$	1.5	0.7	1.0	1.1	1.3
total length $l_{tot} [mm]$	41.0	25.0	68.0	63.0	67.0
total length of the extraction channel $l'_{tot} [mm]$	36.0	18.0	41.0	36.0	43.0
footprint of the extraction channel $A [mm^2]$	54.0	12.6	32.6	31.3	46.3

¹⁾ contains a $6mm$ long and $100\mu m$ deep shallow channel part

PCE. From these data, the distribution and partition coefficient for cocaine in the saliva-PCE system were calculated (see Figure 6.8). For pH values higher than 9 most of the cocaine was unionized ($pK_a = 8.6$) and the distribution and partition coefficient showed the same values.

As explained in section 6.2, more cocaine is extracted by PCE when the cocaine is unionized. Therefore, the pH value has to be at least higher than the pK_a of 8.6. It was chosen always to adjust the pH value to 9 for saliva samples as a sample pretreatment step (see section 2.1.4). This way more than 99% of the cocaine was dissolved in PCE and we could avoid the risk of etching our silicon substrate of the optical waveguide by components of buffers for higher pH values (hydroxide).

6.4.2 Influence of the Flow Rates on the Extraction Efficiency

The extraction efficiency grew with the total flow rate (saliva flow rate + PCE flow rate) of the system (see Figure 6.9). The extraction efficiency also benefited from unbalanced flow rates (higher saliva than PCE flow rate). More cocaine was available for the same amount of PCE. Saliva was flowing through a bead of packed PCE droplets in the extraction channel where the cocaine was absorbed by the PCE droplets. This unbalance of the flow rates even allowed preconcentration of cocaine in PCE and thus, an extraction efficiency higher than 100% (see Figure 6.9). The design ES 1A had a wider and longer extraction channel than design ES 1B and showed higher extraction efficiency.

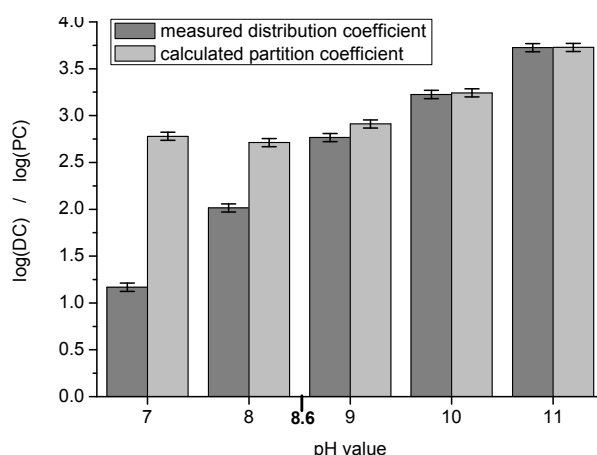


Figure 6.8: Distribution coefficient of cocaine in PCE and human saliva measured by UPLC-MS and calculated partition coefficient (see equation 6.3 in section 6.2) [209]. The higher the pH value, the more cocaine is uncharged and preferably found in the apolar PCE. Error bars indicate the propagated measurement error of the UPLC-MS measurement.

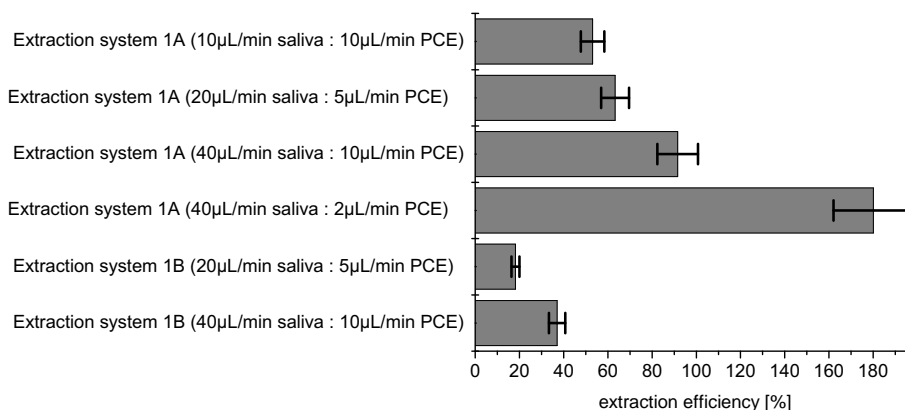
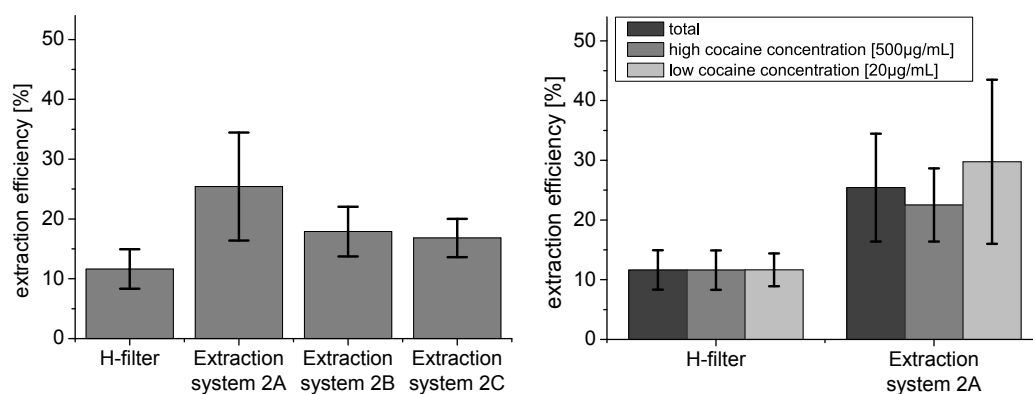


Figure 6.9: Effect of different flow rates and flow rate ratios on the extraction efficiency. The unbalanced flow rates (more saliva than PCE) allowed preconcentration of cocaine in PCE and therefore an extraction efficiency higher than 100%. The extraction efficiency was determined measuring the cocaine concentrations in PCE and saliva by mass spectrometry (UPLC-MS) (error bars indicate the propagated measurement error).

6.4.3 Influence of the Geometrical Dimensions on the Extraction Efficiency

Flow rate parameters were chosen so that the extraction systems were working robustly (20 $\mu\text{L}/\text{min}$ saliva spiked with cocaine, 5 $\mu\text{L}/\text{min}$ PCE). Compared to microfluidic H-filters (flow rates 20 $\mu\text{L}/\text{min}$) with the same total length (PCE in contact with saliva) and a channel width of 1.5 mm, our extraction system (ES 2) showed a 2-3 times better extraction efficiency, but also a higher standard deviation (see Figure 6.10). The measurement uncertainty was calculated using the standard deviation of measurements performed on several chips with the



(a) Comparison of the extraction efficiency of different dimensions of the channels. In addition the design 2A contains a shallow part in the extraction channel acting like the droplet generation step (see Table 6.1) which increases notably the extraction efficiency and the deviation.

(b) Extraction system 2A compared with H-filter of exact the same length for two different cocaine concentrations in saliva.

Figure 6.10: Comparison of the extraction efficiency of microfluidic H-filters and our extraction systems. Our extraction systems show a better extraction efficiency. The extraction efficiency was determined measuring the cocaine concentrations in PCE and saliva by mass spectrometry (UPLC-MS). Error bars indicate the standard deviation for measurements performed with 5 to 10 devices.

same geometry (same master used for molding, see section 2.4). The standard deviation was larger than the propagated error of the mass spectrometry measurements ($\sim 10\%$). The large deviation of the measurements was most likely due to the turbulent flow conditions (vortexes) in our system causing it to be larger than the deviation measured with the microfluidic H-filter which provides stable laminar flow conditions. Five to ten devices were measured per data point. A larger data set would provide more information about how to improve the accuracy of the measurements.

Comparing the values of ES 2 (averaged design B&C) with the ones of ES 1 (averaged design A&B) which were achieved under the same conditions ($20\mu\text{L}/\text{min}$ saliva with $500\mu\text{g}/\text{mL}$ cocaine, $5\mu\text{L}/\text{min}$ PCE), the extraction efficiencies of ES 2 are a little bit lower, probably because of the different surface to volume ratio. For the ES 2, 4 times larger droplets (based on a $200\mu\text{m}$ deep inlet channel instead of $50\mu\text{m}$ for ES 1) were required for a better and more stable merging capability.

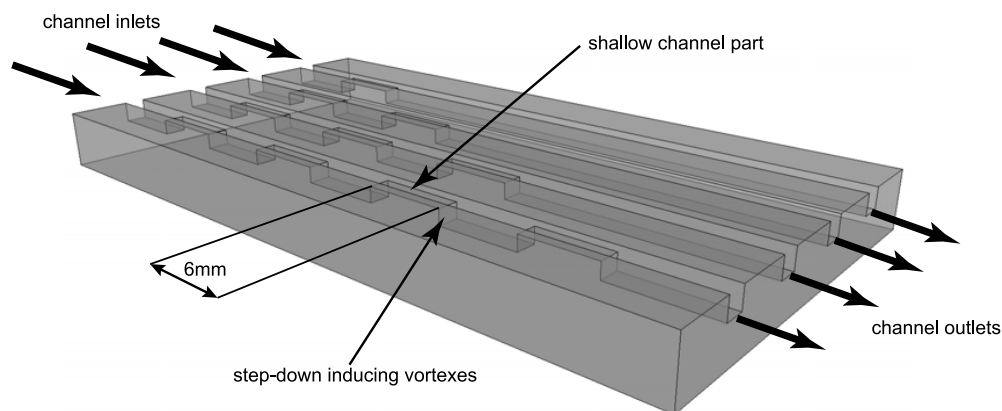
The lateral geometrical dimensions of the channels (length, width) were varied, but no significant influence on the extraction efficiency was observed. However, microfluidic extraction systems with the design ES 2A showed significant better extraction efficiencies than the other two (ES 2B&C). As mentioned in Table 6.1, this design contains in addition a 6mm long, $100\mu\text{m}$ deep shallow part in the extraction channel, which squeezed the passing droplets. This influence will be further investigated and verified in section 6.4.5.

6.4.4 Extraction Efficiency at Different Concentrations

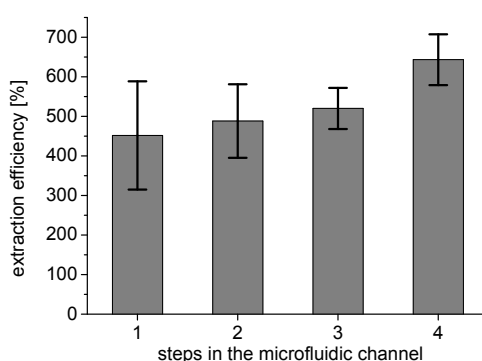
The extraction systems showed better extraction efficiency at low cocaine concentrations ($20\mu\text{g}/\text{mL}$) than at high concentrations ($500\mu\text{g}/\text{mL}$), whereas for microfluidic H-filters no dependence was observed (see Figure 6.10b).

6.4.5 Influence of the Induced Turbulences on the Extraction Efficiency

The effect of induced vortexes on the extraction efficiency was investigated with a microfluidic chip (see Figure 6.11a) consisting of straight channels of uniform length (55mm), depth ($600\mu\text{m}$), and width (1.5mm), but containing a different number of shallow channel parts



(a) Microfluidic structure to evaluate the influence of shallow channel parts (steps-down) on the extraction efficiency. This chip contains four parallel channels with different number of shallow channel parts (6mm long, $50\mu\text{m}$ deep).



(b) Steps induce vortex mixing. The more steps included in the channel, the larger the extraction efficiency. Error bars indicate the larger value of either the standard deviation or the propagated measurement error of the mass spectrometry measurement (UPLC-MS).

Figure 6.11: The extraction efficiency depends on the number of steps-down (after shallow channel parts) in the microfluidic channel.

(6mm long and 50 μ m deep). Applying the same conditions as for the extraction systems (20 μ L/min saliva with 500 μ g/mL cocaine, 5 μ L/min PCE) droplets were produced at the first step. The following shallow parts did not merge the droplets (no drainage). The droplets were squeezed and during the shape relaxation at the step after a shallow part, the same vortex phenomenon (inducing mixing) occurred as it was observed at the droplet generation step (see section 4.4.4). In these test channels no merging geometry was integrated. The droplets were collected at the outlet and merged by a centrifuge prior the determination of the cocaine concentration by mass spectrometry (see section 2.2).

An obvious trend was observed: The more steps-down integrated in the microfluidic channel, the higher the extraction efficiency (see Figure 6.11).

6.5 Discussion

In this section we discuss the improvements of the extraction efficiency of our system and the modifications from the first to the second extraction system. Then we also compare our system with the state-of-the-art microfluidic H-filter.

6.5.1 Improvements of the extraction efficiency

We improved the extraction conditions of cocaine to PCE by increasing the pH value above the cocaine pKa value of 8.6. Already at pH 9, more than 99% of the cocaine was transferred to PCE. Therefore, we adjusted the pH only to 9 avoiding the risk of etching our silicon substrate of the optical waveguides by components of the buffers for higher pH values (see section 2.1.4).

Our microfluidic liquid-liquid extraction approach using small (smaller than the microfluidic channel width) droplets showed fabulous efficiencies and even allowed preconcentration of the solute in the organic solvent unlike other droplet-based approaches which even failed to reach the theoretical equilibrium value given by the distribution coefficient [197]. Within the integrated extraction system the extraction efficiency was limited (to 20 – 30%) by parameters, which were fixed to enable successful and stable operation of the extraction system. We had to find a tradeoff between maximized extraction efficiency (up to 180%, using flow rates of 40 μ L/min (saliva) and 2 μ L/min (PCE)) and successful operation of the system (droplet coalescence for detection in a continuous organic phase). To optimize the extraction efficiency, small droplets with large surface-to-volume ratio should be produced with highly unbalanced flow rate ratios at high flow rates to induce vortex mixing; however, in these conditions our system was not able to merge the droplets for the following detection.

A much higher saliva than PCE flow rate (such as 40 μ L/min (saliva) and 2 μ L/min (PCE), see Figure 6.9) would provide more cocaine for a certain amount of PCE and would result in preconcentration. However, the drainage channel we designed was not large enough to drain all saliva from a highly unbalanced flow rate ratio, which inhibited coalescence of the

PCE droplets. For the ES 2 the flow rate ratio of saliva to PCE was found to be optimal for coalescence at a ratio of 4 : 1.

The lateral dimensions of the microfluidic channels had no significant influence on the extraction efficiency. Much more obvious was the effect of shallow parts integrated in the extraction channel, which squeezed the droplets and during their shape relaxation, turbulences were induced in the laminar flow. The higher the number of shallow parts (more vortex mixing), the larger the extraction efficiency. Increasing the number of shallow channel parts from one to four, a 45% higher extraction efficiency was observed in a test device (see Figure 6.11b). In order to proof the increased extraction efficiency in system ES 2A was caused by the explained vortex mixing, the additional shallow channel part (see Figure 6.7b) was removed. Indeed this resulted in a 10 – 20% lower extraction efficiency (comparable with the other extraction systems without additional shallow part, see Figure 6.10a).

6.5.2 Changes from the First to the Second Extraction System

The main geometrical improvement was the collinear arrangement of the PCE outlet channel with the extraction channel to avoid a region of stagnant flow in the extraction channel. Furthermore, to reduce the footprint of the microfluidic device, the channel was bended twice in the second extraction system, which was then more convenient for the integration with the optical waveguide.

On the second extraction system, larger droplets were produced to avoid them to enter and clog the saliva drainage channel.

As explained above (section 6.5.1) in order to obtain the optimum extraction conditions, droplets should be generated with highly unbalanced flows and at high flow rates (to induce vortex mixing); however, in these conditions the designed system was no more able to merge the droplets (not enough saliva drainage). For the ES 2 the flow rate ratio of saliva to PCE was found to be optimal at a ratio of 4 : 1. Therewith, the designed drainage channel managed to drain out enough saliva to cause merging of the PCE droplets at the step-up at the end of the extraction channel. The stable operation of the system was observed up to $20\mu\text{L}/\text{min}$ saliva flow rate and $5\mu\text{L}/\text{min}$ PCE flow rate. PCE droplet coalescence could not always be ensured for larger saliva to PCE flow rates such as $24\mu\text{L}/\text{min}:6\mu\text{L}/\text{min}$, $32\mu\text{L}/\text{min}:8\mu\text{L}/\text{min}$ or $40\mu\text{L}/\text{min}:10\mu\text{L}/\text{min}$.

6.5.3 Comparison with the State of the Art

We developed a microfluidic liquid-liquid extraction system to transfer cocaine from human saliva to the IR-transparent organic solvent PCE under continuous flow conditions. The state-of-the-art microfluidic H-filter also would allow continuous extraction and in addition easy separation of the liquids after extraction [204, 205], but our system showed a 2-3 times better extraction efficiency. To perform best, the H-filter would require microfluidic channels smaller than $50\mu\text{m}$ (diffusion length of cocaine), but they would be clogged immediately by saliva.

Compared to H-filters, slug-based extraction systems not only depend on diffusion, but also on induced liquid circulations which allow additional mixing in the laminar flow [202]. Also in our system mixing is supported by vortexes created during the droplet generation step as explained in section 4.4.4.

The droplet based approach suggested by [197], shows a better surface-to-volume ratio for higher extraction efficiency than the slug-based approach (see Figure 6.5). Furthermore, the smaller the PCE droplets in the same amount of saliva are, the better this ratio. The suggestion of a droplet-based approach is a promising idea, but ends up with an emulsion after the extraction process instead of two separated phases, which does not allow further processing or detection. Droplets as large as the channel width were proposed, which resulted in a limited volume of the continuous phase between the droplets and also depleted regions were observed (see Figure 6.1c). To overcome the diffusion limited problem (see section 6.1.1) in our system, vortexes generated by shallow channel parts induced mixing and so they provided a more homogeneous solute distribution and a higher extraction efficiency (see Figure 6.11). Furthermore, our droplets were smaller than the channel width. The continuous phase could flow around the droplets. If the continuous phase was flowing at higher flow rate (compared to the dispersed phase), even cocaine preconcentration up to 180% in PCE droplets was achieved (see Figure 6.9). Our droplet-based approach therefore provides an attractive method of microfluidic liquid-liquid extraction.

6.6 Summary

The set goal was to transfer cocaine from the saliva sample to an IR-transparent organic phase in order to be detected by waveguide IR-spectroscopy in the continuous organic phase.

Here we presented a liquid-liquid extraction system which transferred continuously cocaine from human saliva to the organic solvent PCE. We followed and improved the idea of droplet-based liquid-liquid extraction. Our approach of producing droplets smaller than the width of the microfluidic channel achieved promising results based on vortex mixing in the laminar system (up to 40% higher extraction efficiency in a test device) and on unbalanced flow rates allowing cocaine preconcentration in PCE (extraction efficiencies up to 180% measured).

We presented a compact microfluidic system including on the same chip: droplet generation (see chapter 4), liquid-liquid extraction, and droplet merging (see chapter 5). This integrated, serial arrangement of the components fixed some parameters within a certain range, which did not allow to tap the full potential of this droplet-based extraction method.

However, our system developed for droplet-based liquid-liquid extraction showed a 2-3 times larger extraction efficiency than the state-of-the-art microfluidic H-filter. Optimized conditions for most efficient extraction at robust system performance (for ES 2) were found at the flow rate ratio of 4 : 1 with the following flow rates; $20\mu L/min$ saliva spiked with cocaine, $5\mu L/min$ PCE.

7 Integrated Cocaine Sensor for Saliva Samples based on IR-Spectroscopy

The results shown in this chapter are based on the knowledge developed and presented in the previous chapters. Here we present an integrated optofluidic device which is the output of a close collaboration together with the micro-optics group of Prof. Hans Peter Herzig at EPFL. Germanium strip waveguides on silicon substrates were integrated with microfluidic systems to detect cocaine as a pilot demonstration in the framework of the project IrSens. In the evanescent field of the waveguide, cocaine absorbed the light of a wavelength near $5.8\mu\text{m}$ which was emitted from a quantum cascade laser.

Some of the information presented in this chapter was both published in the journal *Lab on a Chip* [210] and at the μTAS 2012 conference [158].

7.1 Introduction

Integrated optofluidic systems including microfluidics and laser detection of chemical analytes were first demonstrated in 2006 [14] (see section 1.2).

Chemical detection and identification based on mid-infrared (mid-IR) spectroscopy have been widely used for samples in gases, liquids, or solids. In the condensed phase, attenuated total reflection Fourier transform infrared spectroscopy (ATR-FTIR) conveniently probes the analyte in the evanescent field. Such tabletop setups are limited to laboratories due to their large footprint [211, 212]. During the last few decades, the progress of mid-IR spectroscopy with mid-IR fiber probes or planar waveguides largely reduced the device size and the required sample volume [213]. Such waveguides were based on silver halides, chalcogenide glasses, GaAs or hollow waveguides [214–218]. In addition, mid-IR quantum cascade lasers (QCLs) provide light sources with high power, high tunability, and compact sizes which can further reduce the size of sensor systems [219].

Microfluidic systems have been used in combination with IR-detection as presented in section 1.2.3. The most commonly used techniques are chromatography and electrophoresis on a separate microfluidic chip for sample preparation and preconcentration prior to the conventional IR-detection.

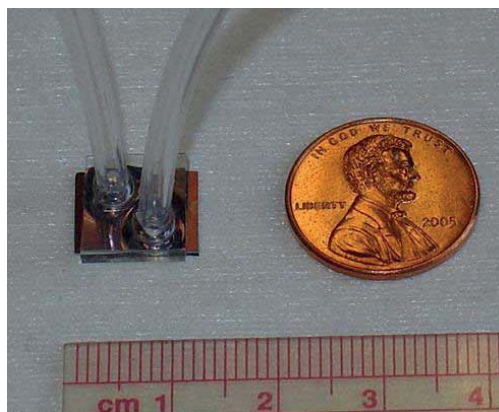


Figure 7.1: Planar chalcogenide waveguide integrated with microfluidic sensor [216].

Recently, optical waveguide-based detection techniques were presented in combination with microfluidic systems. A SU-8/PDMS microfluidic device integrated with a planar chalcogenide glass waveguide on a silicon substrate was presented in 2007 for detection of N-methylaniline at the wavelength of $1.55\mu\text{m}$ (see Figure 7.1) [216]. A limit of detection of 0.7 vol. % ($7\mu\text{g}/\text{mL}$) was achieved for N-methylaniline in a non-absorbing solvent (carbon tetrachloride). Ultra-sensitive mid-infrared evanescent field sensors combining thin-film strip waveguides with quantum cascade lasers were published in 2011 [220]. Acetic anhydride was detected with a wavelength of $10.3\mu\text{m}$ with a limit of detection of 19.4 ng (= 18 pL droplets deposited on the waveguide surface).

Beside, commercial products combining QCLs and flow cells for the detection of oil in water are available [221].

7.2 Theory & Fundamental Principles

An optical waveguide is a physical structure that guides electromagnetic waves in the optical spectrum. The most common types of optical waveguides are the optical fibers and rectangular waveguides. The latter can be split in strip waveguides and the flatter slab waveguides, also called planar waveguides. Compared to a slab waveguide, a strip waveguide has higher fraction of energy in the evanescent field and hence shows increased limits of detection [220].

For the optical detection, we used a single-mode total reflection strip waveguide, in which the light bounced several times forming a surrounding evanescent field. An evanescent wave is a near-field standing wave with an intensity that decays exponentially with distance from the boundary at which the wave was formed. Evanescent waves are a general property of wave-equations and occur in all phenomena to which a wave-equation applies. They are formed at the boundary between two materials with different wave propagation properties. Their highest intensity is within one third of a wavelength from the surface (interface between two materials) of formation. The evanescent field waves can be excited very efficiently with light near the visible range. [222]

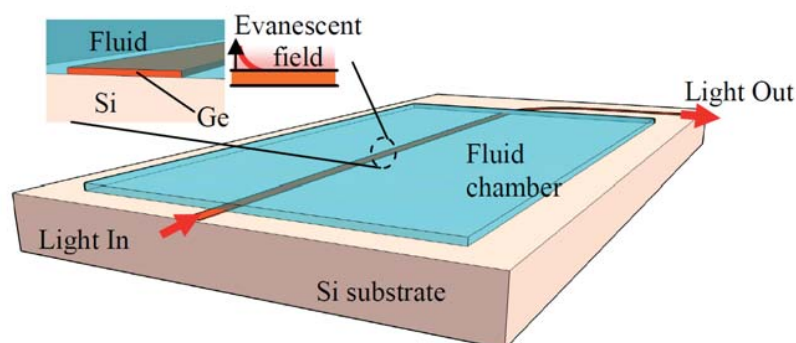


Figure 7.2: Scheme of the waveguide spectroscopy sensor concept in liquid. The light emitted from the QCL is coupled into a Si/Ge single-mode waveguide. The evanescent field of the mode (about 5% of the injected light) is then interacting with the analyte within the liquid. After analyte interaction, the light is collected and focused onto a quantum cascade detector.

The analyte (cocaine) in the liquid phase was detectable because it absorbs energy of the evanescent field surrounding this waveguide (see schematic in Figure 7.2). The information about the analyte concentration can be determined by measuring the intensity of the light at the waveguide output. The wavelength of the laser light was chosen to accord with the characteristic absorption peaks of cocaine [223].

7.3 Design

This section presents the design of both parts of the optofluidic system. First we describe the optical waveguide and then we present the two different integrated microfluidic systems. The first optofluidic system is called 'detection-evaluation system' and detects different cocaine concentrations in PCE. The second device is called 'extraction-detection system' and integrates the liquid-liquid extraction and the waveguide detection.

In this section also the optical and microfluidic experimental setup for the characterization of the optofluidic systems is introduced.

7.3.1 Optical Waveguide

The mid-IR waveguide is made from a mono-crystalline Ge layer grown on a Si substrate, by means of standard photolithography and reactive ion etching using CF_4 . Intrinsic Ge and Si have low absorption in a wide range of mid-IR. This material combination is Si-process compatible and can be integrated with the current Si technology. Figure 7.3 shows the cross section view of the fabricated strip waveguide. The waveguide is designed for single mode, transverse magnetic polarization at the wavelength of $5.8\mu m$, while the thickness is $2\mu m$ and the width $2.9\mu m$ [224].

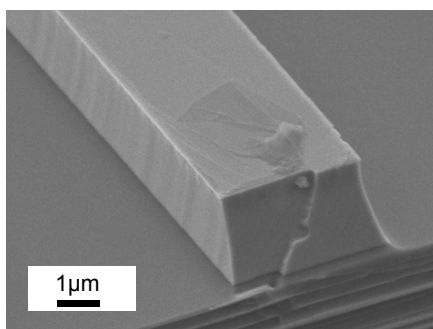


Figure 7.3: Image of the cross section of a Ge waveguide on silicon, taken with a scanning electron microscope. The waveguide was designed for the wavelength of $5.8\mu m$ (thickness $2\mu m$, width $2.9\mu m$).

7.3.2 Integration with the Microfluidic System

The single-mode strip waveguides were integrated with a microfluidic system made by rapid prototyping of NOA81 as explained in section 2.4.2. After usage, the low-cost, disposable, polymer microfluidic system can be detached from the optical substrate by soaking everything in acetone and the waveguide can be recycled.

In the microfluidic system, small openings were fabricated to let the waveguides enter the microfluidic channel. These gaps were sealed afterwards by melted polyethylene or by epoxy glue (2 tone epoxy, Devcon) which absorb less IR-light than the material of the microfluidic system [123].

Two different integrated systems were fabricated and tested. On the one hand, the simplified 'detection-evaluation system', where the microfluidic part consists only of simple straight channels ($1mm$ wide, $7mm$ long, and $50\mu m$ deep), showing one microfluidic inlet and one microfluidic outlet per channel (see Figure 7.4). The microfluidic channel sits over an optical waveguide of $\sim 8mm$ length. This system was built to verify the detection method and to determine the limit of detection in PCE.

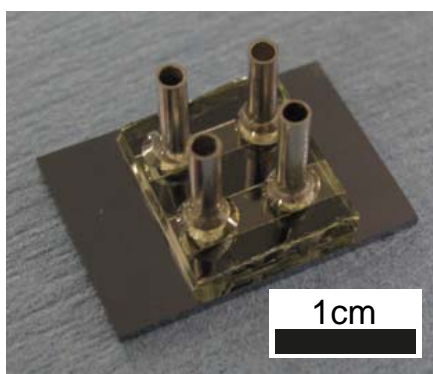


Figure 7.4: Integrated 'detection-evaluation system' with two waveguides covered by simple straight microfluidic channels showing one inlet and one outlet per channel.

On the other hand, a more complex integrated optofluidic system, the so called 'extraction-detection system', was built. The 'extraction-detection system' combines the droplet-based microfluidic liquid-liquid extraction of cocaine from human saliva and the strip waveguide detection in PCE. Compared to the 'detection-evaluation system' this device shows an around 4 times longer optical waveguides ($\sim 23.8\text{mm}$). Figure 7.5 shows the microfluidic system, the design of the waveguides as well as a photograph of the complete integrated 'extraction-detection system'.

7.3.3 Optical Experimental Setup

The integrated sensing devices, consisting of an optical waveguide and a microfluidic system, were evaluated by a QCL light source emitting light at a wavelength of $5.71 \pm 0.01\mu\text{m}$ (wave number $1750 \pm 5\text{cm}^{-1}$). The laser was provided by our collaborators of the group of Prof. Jérôme Faist at ETHZ and was fabricated as described in [225].

The measurement setup consisted of a tabletop optical system measuring the waveguide output. The light emitted from the QCL was coupled into the strip waveguide with a 1/f ZnSe doublet. After interaction with the sample in the liquid chamber, the light went through a waveguide bend and was redirected to a liquid nitrogen cooled MCT (mercury cadmium telluride) detector by two parabolic mirrors. The use of a bended waveguide avoided the QCL stray light of the emission axis from being detected, which increased the signal to noise ratio. The setup is presented in Figure 7.6.

7.3.4 Microfluidic Experimental Setup

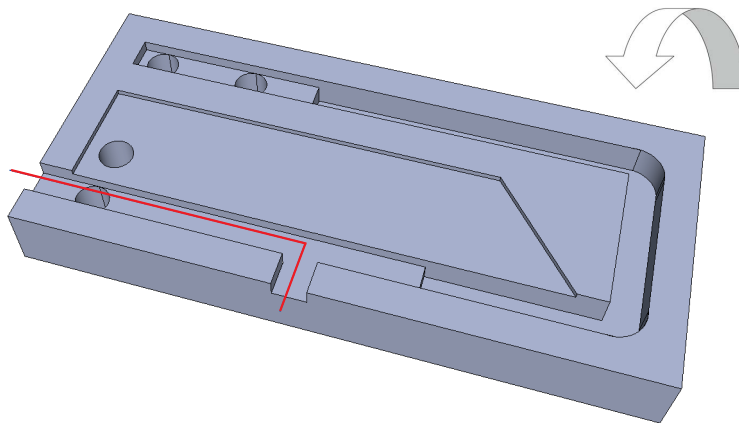
Here the fluidic setups for the simple 'evaluation-detection system' and the more complex 'extraction-detection system' are explained.

Detection-Evaluation System

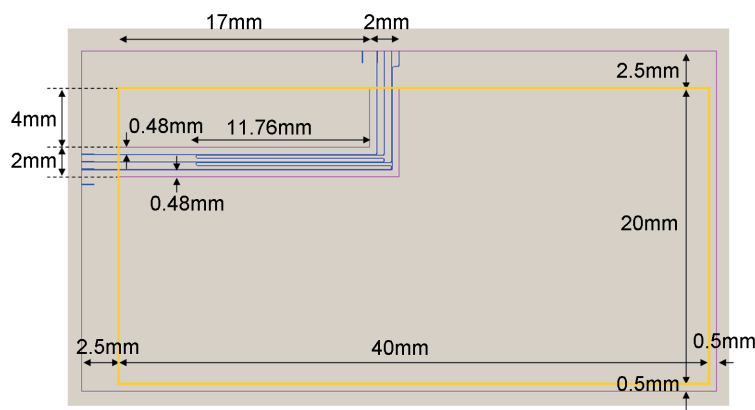
For the 'detection-evaluation system' no saliva was involved but different concentrations of cocaine in PCE. The PCE solutions were pumped with a syringe pump at a constant flow rate. Different concentrations were selected continuously while pumping by using a six-way valve. For easy characterization of the 'detection-evaluation system' pure PCE was alternated with PCE solutions with cocaine. Step by step the concentrations were changed between $100\mu\text{g}/\text{mL}$, $300\mu\text{g}/\text{mL}$, and $1000\mu\text{g}/\text{mL}$.

Extraction-Detection System

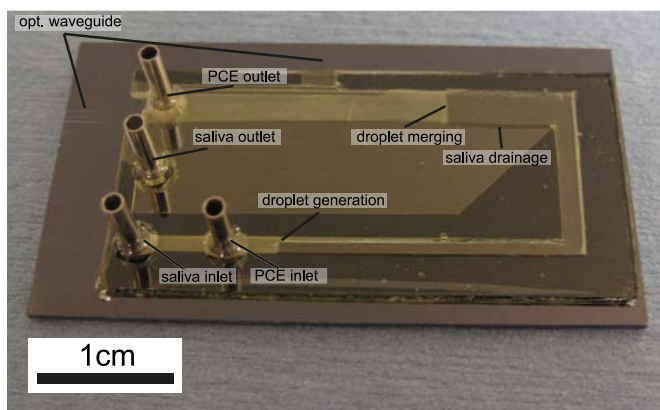
The flow rate in the fluidic system of the 'extraction-detection system' was also controlled by a syringe pump (see Figure 7.7). PCE was provided in parallel with either pure saliva or saliva spiked with cocaine (chosen by a fluidic valve). First pure saliva was injected into the system,



(a) This 3D schematic shows the microfluidic part upside down with the surface bonded to the substrate (with waveguides) on top. In red the position of the integrated waveguides is indicated.



(b) Design of the optical waveguides in blue. The yellow square represents the footprint of the microfluidic system.



(c) Image of the NOA81 microfluidic system integrated with the optical waveguides on a silicon substrate.

Figure 7.5: Integrated optofluidic 'extraction-detection system'.

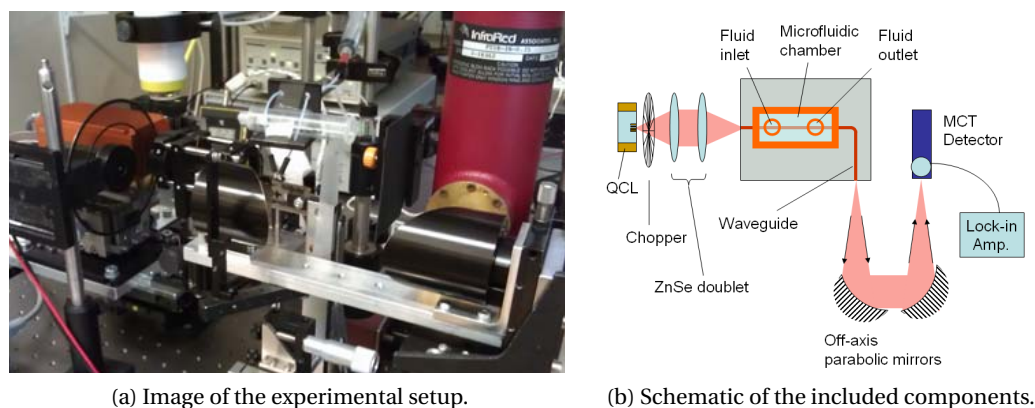


Figure 7.6: Optical components of the measurement setup for both integrated systems: QCL light source, light beam shaping components, optofluidic sensing device and the MCT detector.

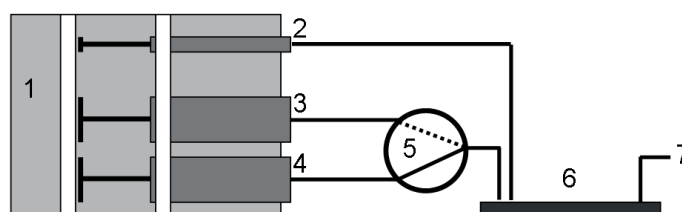


Figure 7.7: Tubing for the integrated setup using only one syringe pump: 1) syringe pump, 2) syringe with PCE (small diameter), 3) syringe with saliva, 4) syringe with cocaine spiked saliva, 5) selection valve, 6) optofluidic chip, 7) microfluidic waste.

then saliva experienced the same pretreatment (see section 2.1.4) but spiked with cocaine ($500\mu\text{g}/\text{mL}$), followed again by the pure saliva. By selecting different syringe diameters also the flow rate ratio between PCE and saliva was adjustable.

7.4 Results

Different cocaine concentrations dissolved in PCE were measured with the 'detection-evaluation system' (see Figure 7.5) by pumping the liquids through the microfluidic device at a flow rate of $50\mu\text{L}/\text{min}$. The waveguide output light intensity was detected promptly when we switched between different concentrations of cocaine as shown in Figure 7.8. Between each concentration, we added 5-7 minutes of pure PCE solvent. The signal always reached again the baseline while pure PCE was flowing in the channel. The device responded well to each change of the concentration. The transmission drop (energy absorption of the cocaine molecules) was linearly proportional to the cocaine concentration, while the lowest detected concentration was $100\mu\text{g}/\text{mL}$.

Chapter 7. Integrated Cocaine Sensor for Saliva Samples based on IR-Spectroscopy

The 'extraction-detection system' first extracted cocaine from saliva to PCE, then detected cocaine further downstream in the microfluidic channel with the optical waveguide. Figure 7.9 shows the detection of $500\mu\text{g}/\text{mL}$ cocaine by switching between pure and spiked saliva at constant flow rates of $20\mu\text{L}/\text{min}$ for saliva and of $5.4\mu\text{L}/\text{min}$ for PCE.

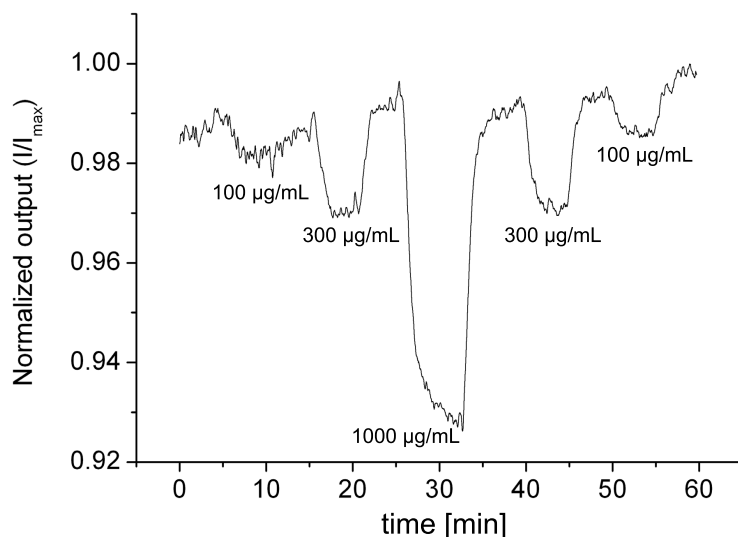


Figure 7.8: Waveguide output intensity with different cocaine concentrations in the organic solvent PCE using the short waveguides on the 'detection-evaluation system': in the dynamic measurement, the smallest detected concentration was $100\mu\text{g}/\text{ml}$.

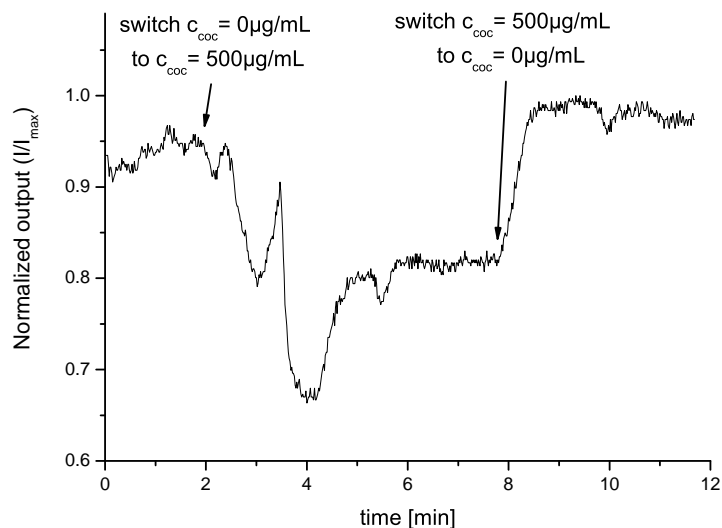


Figure 7.9: Optical detection of cocaine extracted from saliva to PCE on chip during the measurement using the integrated optofluidic 'extraction-detection system'. The concentration of cocaine in saliva was switched between zero and $500\mu\text{g}/\text{mL}$.

Table 7.1: LOD of different systems detecting cocaine in saliva or systems using integrated optical waveguides.

System	Analyte	Matrix	LOD	Time to result	Reference
our 'detection-evaluation system'	cocaine	PCE	100 $\mu\text{g}/\text{mL}$	real time	[158, 210]
our 'extraction-detection system'	cocaine	saliva	500 $\mu\text{g}/\text{mL}$	real time	[158, 210]
tabletop ATR-IR spectrometer	cocaine	saliva (evaporated)	10 $\mu\text{g}/\text{mL}$	~ 10min	[223]
different immunoassay systems	cocaine	saliva	ng/mL-range	~ 20min	see Table 2.4
mass spectrometry	cocaine	saliva	ng/mL-range	several hours	[228]
integrated chalcogenide waveguide	N-methylaniline	carbon tetrachloride	7 $\mu\text{g}/\text{mL}$ (0.7 vol.%)	n.a.	[216]
integrated GaAs waveguide	acetic anhydride	air (droplets on waveguide)	18pL/19.4ng	n.a.	[220]

7.5 Discussion

The lowest detected cocaine concentration in PCE of our integrated 'detection-evaluation system' was 100 $\mu\text{g}/\text{mL}$. This simple device featured a really fast response time compared to less reliable and portable systems based on immunoassay (where the time-to-results can exceed 20min, see section 1.2.2) or compared to the reliable state-of-the-art cocaine detection by mass spectrometry (time to result: several hours) which makes it applicable for trustable real-time measurements. Even a faster response than the one shown in Figure 7.8 can be achieved by shortening the supply tubing as presented in [210] or by directly integrating the pumping on the microfluidic system by micro pumps [226, 227].

Using the more complex 'extraction-detection system' a cocaine concentration of 500 $\mu\text{g}/\text{mL}$ in saliva was extracted to PCE and detected. Concentrations in real saliva samples can exceed 1000ng/mL for 2-4 hours after consumption [45]. By detecting a cocaine concentration of 500 $\mu\text{g}/\text{mL}$ we are far from this concentration as well as from the detection limit of 20ng/mL proposed by the SAMHSA (see section 2.1.2). Table 7.1 compares the limit of detection (LOD) of different systems detecting cocaine in saliva or systems using integrated optical waveguides. Furthermore, the device developed here not only lacks of a fairly high LOD, but the system needs also to be calibrated before application in the field.

The integrated optofluidic system, the so called 'extraction-detection system', showed much higher relative sensitivity compared to measurements in PCE with the simple 'detection-evaluation system' (compare Figure 7.9 to Figure 7.8). This increase resulted from the usage of a longer optical waveguide.

The relative sensitivity was better, but the detected intensity of the signal was at a really low level (less than 0.1 mV), because when the optical waveguides were in contact with the highly light absorbing aqueous liquid once, the output signal dropped and stayed low.

The microfluidic system is working well, continuously extracting cocaine from saliva to PCE and then merging PCE droplets towards the waveguide area as shown in Figure 7.10. However, our system suffered from a basic fluidic design flaw occurring during the initialization phase of the microfluidic system: as explained in Figure 7.11, the initialization phase started from an empty microfluidic channel. PCE droplets were produced in saliva. Since the PCE droplets

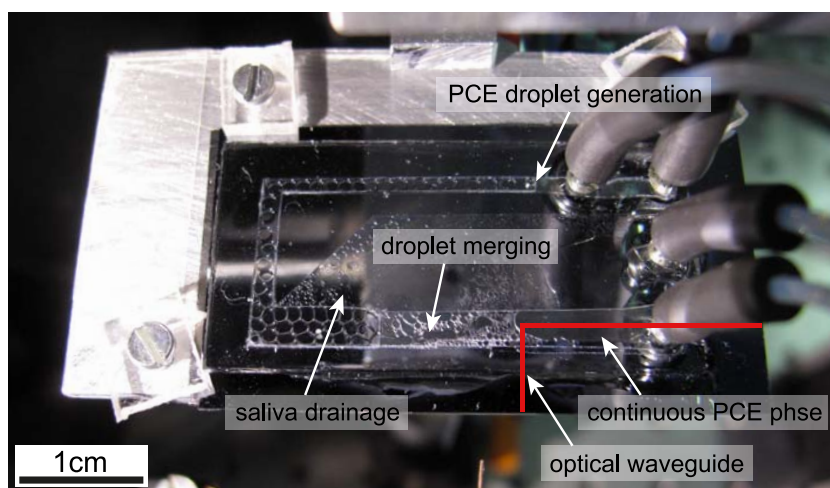
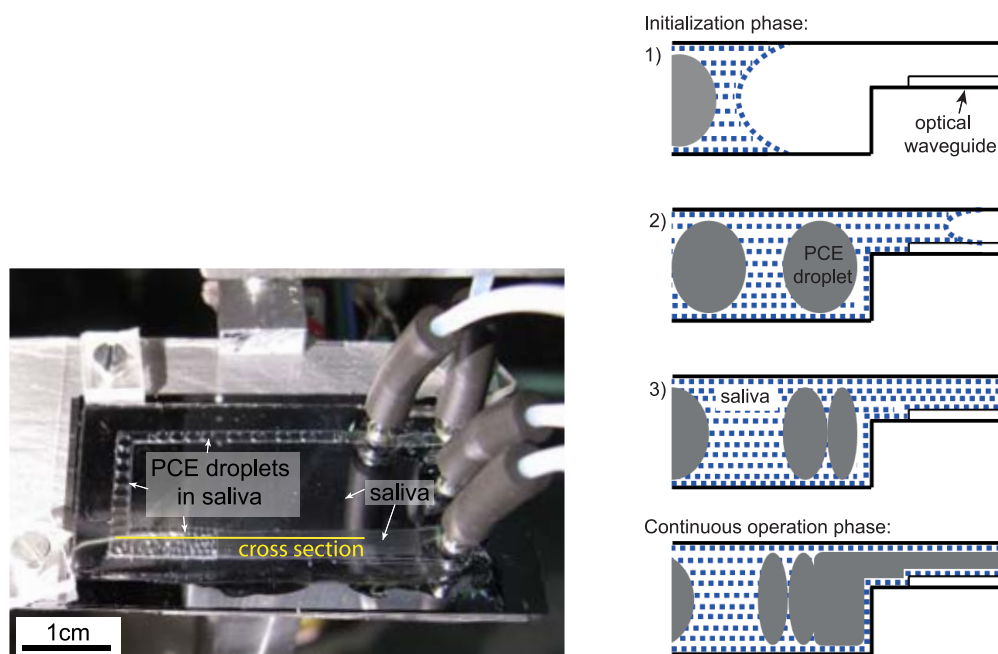


Figure 7.10: Integrated 'extraction-detection system' on the chip holder performing the microfluidic droplet-based liquid-liquid extraction (continuous operation) while real time optical detection.

were embedded in the aqueous continuous phase saliva, the channel walls always got wetted first by saliva (step 1, Figure 7.11b). The same applied for the hydrophilic optical waveguide channel (step 2, Figure 7.11b). The PCE droplets arriving first at the step were stopped, squeezed, and then merged together (step 3, Figure 7.11b). Meanwhile the saliva continued to flow over the optical waveguide instead of separating out via the shallow drainage side-channel. As soon as the pressure on the droplets was high enough, they merged and a continuous phase of PCE left through the shallower channel containing the optical waveguide (continuous operation phase). Since saliva was in contact with the hydrophilic surface of the optical waveguide first, a very thin lubrication film of saliva was remaining on the waveguide in the continuous operation phase (PCE surrounded by a thin film of saliva, slug-like flow) [4, 229, 230]. Assuming the slug-like flow is comparable to the phenomenon of a large inviscid bubble moving at small capillary number in a microfluidic channel, the thickness of the lubrication film e can be estimated by the nonlinear law $\frac{e}{h} \propto Ca^{\frac{2}{3}}$ [231], where h is the height of the microfluidic channel. The capillary number of 0.00715 in our system would result in an estimated thickness of this lubrication film of $\sim 5\mu m$.

We tried to prevent the saliva-waveguide contact by initializing the microfluidic system with channels filled with PCE - with and without blocking the PCE outlet by a valve during the initialization phase. It could not be avoided that saliva touched the optical waveguide and remained as a thin layer on the surface of the waveguide. To overcome this issue, it could be tried to make the optical waveguide completely hydrophobic by a surface treatment which should force the saliva to leave only through the hydrophilic saliva outlet channel. Another approach could be to design an additional PCE outlet channel in parallel to the detection channel. This way, one channel would be closed after the initialization phase and another channel (pre-filled with PCE) then opened for the detection only.



(a) Image of the microfluidic system during the initialization phase (step 3): The PCE droplets were stopped at the step and saliva fills both the drainage and the detection channel. The yellow line indicates the location of the series of cross section views shown in Figure 7.11b.

(b) This schema shows the initialization and the continuous operation phase of the microfluidic system. The initialization phase is presented in three steps: 1) Continuous phase saliva with embedded PCE droplets were filling the empty hydrophilic channel, 2) Saliva reached the step first and started to wet the channel with the waveguide, 3) PCE droplets were stopped at the step and were squeezed together while saliva flowed over the waveguide. In the continuously operating state, PCE droplets were merged and continuous organic phase left through the channel, but a very thin saliva film was remaining on the waveguide (slug flow).

Figure 7.11: Initialization of the microfluidic droplet-based extraction system.

The mentioned saliva layer ($\sim 5\mu\text{m}$) covering the optical waveguide after the initialization phase absorbed most likely the largest amount of energy of the evanescent field which shows its highest intensity at about one third of the used wavelength measured from the waveguide ($5.7\mu\text{m}/3 = 1.9\mu\text{m}$) (see section 7.2). The evanescent field technique is of advantage for the detection of analytes in a highly absorbing matrix, because the field only interacts within a thin layer of the liquid. In the case of a large volume of a transparent matrix (PCE) surrounded by a thin highly light absorbing saliva layer, a transmission measurement (light shining through the sample) in combination with an IR-transparent chip material, would probably be better suitable, since the liquid-liquid extraction of cocaine from saliva to PCE was shown to be efficient (see chapter 6).

Regarding the waveguide detection system, the limit of detection of our device could be improved by using longer waveguides and an integrated splitter with a reference waveguide. The noise needs to be reduced by stabilizing the temperature and by avoiding mechanical vibrations. Furthermore, there is a shift of the average output-power observed based on the fluctuation of alignment between the laser and the waveguide. This could be avoided by integration of the waveguide and the light source on the same substrate.

The QCL light source and the optical waveguide are already portable, but the additional components of the optical system are still based on a tabletop setup and not applicable for a POC device.

To handle the liquids in the microfluidic system a bulky syringe pump was used. This driving system is not handy for a portable POC system. The syringe pump SPS01 from LabSmith is much smaller and portable [232]. There are also portable, battery powered pumps available on the market with a footprint of a coin e.g. Bartels Micropumps [226] or pumps from Osmotex [227]. The pumps mp6 from Bartels (Bartels Mikrotechnik, Dortmund, Germany) were tested, but not applied in the research project, because they show lower accuracy in terms of the flow rate and need to be calibrated before use.

However, to the best of our knowledge we showed in this chapter for the first time the successful integration of a low-cost microfluidic system for sample preparation together with optical detection by IR spectroscopy. Thanks to the microfluidic liquid-liquid extraction of cocaine from the highly absorbing saliva to an IR-transparent solvent, cocaine detection by IR-spectroscopy was feasible (see absorption spectra in Figure 1.6).

7.6 Summary

In this chapter we presented with two systems the successful integration of a low-cost microfluidic part with the IR-waveguide spectrometry chip. The first 'detection-evaluation system' measured quantitatively different cocaine concentrations in PCE with a LOD of $100\mu\text{g}/\text{mL}$. The second 'extraction-detection system' performed the liquid-extraction of cocaine from saliva to PCE together with the detection on the same device with a LOD of $500\mu\text{g}/\text{mL}$ in saliva. The low limit of detection of the 'extraction-detection system' suffered from an issue occurring during the initialization of the microfluidic system which reduced the detectable signal intensity. The microfluidic system performed well, but the combination with an evanescent field detection was not the most suitable one. Nevertheless, for the first time cocaine detection in human saliva succeeded on a compact, integrated optofluidic system, even if the LOD of our systems did not reach our expectations.

8 Summary & Outlook

The goal of this research was to develop a compact, portable microfluidic system for cocaine detection in human saliva by IR-spectroscopy. We also wanted to develop a low-cost, disposable chip which is easy to fabricate by a low-cost rapid prototyping method. Therefore, we chose polymer as the chip material which satisfied the above requirements, but asked for further specific material characterization. Furthermore, the microfluidic system itself had to be integrable with the optical waveguide for detection purpose. The task of the microfluidic device was to transfer cocaine from the IR-light absorbing saliva to an IR-transparent organic solvent enabling its detection.

Saliva is a good matrix for road side testing, but also a complex, non-Newtonian fluid which tends to clog microfluidic channels. Hence, it required specific description and sample pretreatment. We characterized the UV-polymer NOA81 for microfluidic applications and developed a simple rapid prototyping method using scotch-tape masters. Equipped with these tools we designed a new microfluidic droplet-based liquid-liquid extraction method to transfer cocaine from saliva to the IR-transparent organic solvent PCE. Our system included a simple and robust droplet generation method as well as a merging geometry. Then, this microfluidic system was successfully integrated with a waveguide chip for the optical detection of cocaine.

8.1 Summary

First, for our application we emphasized the nature of saliva and its usage as an easily accessible sample matrix for the detection of cocaine in the human body. We explained the saliva sample pretreatment, which had to be applied prior to its processing on microfluidic chips in order not to clog the microfluidic channels and to allow reproducible measurements. We focused on the influence of these pretreatments on the rheological behavior of this body fluid.

Second, the advantages of polymers as chip material for microfluidic systems were highlighted and we presented a low-cost, time-efficient, and highly flexible microfluidic chip fabrication method for the UV-curable polymer NOA81 (chapter 2).

Chapter 8. Summary & Outlook

A new suitable polymer chip material was found which met the relevant material requirements of the project IrSens. The **third** aspect involved the investigation of microfluidic and IrSens project relevant material properties, including the compatibility to IR-transparent solvents, the low cocaine adsorption, the adjustable wetting behavior as well as the suitability for low cost prototyping. The material characterization was presented, and the mentioned material properties were illustrated by different applications (chapter 3).

We developed a droplet-based microfluidic liquid-liquid extraction method to transfer cocaine from saliva to the IR-transparent organic solvent PCE including droplet generation and droplet merging. Therefore, we aimed to develop a new, simple, and robust droplet generation method, which can process the complex liquid saliva without clogging. The **fourth** aspect concerned the droplet generation geometry (chapter 4). This geometry did not involve small features, which could be clogged by saliva components. Our droplet generation method was independent of the chip orientation and produced monodispersed droplets (smaller than 3%). Micro droplets could be produced at the microfluidic outlet or at a step in a microfluidic channel (for further processing of the droplets on chip). The method also enabled high throughput by parallelization of the droplet generation feature. The size of the generated droplets mainly depended (linearly) on the inlet channel height of the device which allowed to predict the droplet size. In the flow field, vortexes were observed, occurring during the droplet generation process and enhancing the mixing in the normally laminar flow of such a microfluidic channel.

In the **fifth** endeavor, after extracting cocaine, we aimed to merge PCE droplets, which were dissolved in the human saliva, so that the cocaine could be detected by the optical waveguide (chapter 5). Droplets in saliva were stabilized by surfactant proteins already present in saliva, avoiding spontaneous droplet coalescence.

Several chemically assisted merging approaches were tested and failed, such as the increase in the pH value, the salting out method, elevated temperatures, adjusted surface wettability, or the addition of anti-foaming agents and different other surfactants.

Therefore, a physical, passive method was developed to continuously merge the droplets. The continuous saliva phase was drained out by a shallow side-channel and then the PCE droplets were physically deformed by the microfluidic chip geometry resulting in coalescence based on the physical compressive and decompressive merging principles.

The **sixth** aspect of the project addressed the efficiency of transferring cocaine from saliva to the organic PCE solvent using our compact droplet-based extraction system (chapter 6). Our approach of producing droplets smaller than the width of the microfluidic channel, achieved promising results (extraction efficiencies up to 180%) based on generated vortexes inducing mixing in the laminar system and also based on unbalanced applied flow rates enabling cocaine preconcentration in PCE.

The integrated, serial arrangement of the system components (droplet generation, liquid-liquid extraction, droplet merging, detection) only permitted to set some parameters within certain ranges, which did not allow us to tap the full potential of the presented droplet-

based extraction method. However, our system showed at least 2-3 times higher extraction efficiencies than the state-of-the-art microfluidic H-filter.

The **seventh** aspect of this work involved the successful integration of the low-cost microfluidic parts with the IR-waveguide spectrometer chips (chapter 7). The first 'detection-evaluation design' measured quantitatively different cocaine concentrations in PCE with a LOD of $100\mu\text{g}/\text{mL}$. The second 'extraction-detection design' involved the liquid-liquid extraction of cocaine from saliva to PCE together with the detection on the same device with a LOD of $500\mu\text{g}/\text{mL}$ in saliva. The second 'extraction-detection design' suffered from an issue occurring during the initialization of the microfluidic system, which reduced dramatically the detectable signal intensity. The microfluidic system performed well, but the combination with an evanescent field detection method was not the most suitable one. Nevertheless, for the first time cocaine detection in human saliva succeeded on a compact, integrated optofluidic system, even if the LOD of our systems did not reach our expectations.

8.2 Outlook

Future work aiming at the improvement and industrialization of the droplet based liquid-liquid extraction system developed in this thesis should focus on five main aspects.

First, we developed a low-cost, highly flexible, and time-efficient rapid prototyping method for NOA81 using scotch-tape masters. If higher accuracy is needed, the scotch-tape could be structured by laser cutting. However, this method was designed for flexible lab work and is not suited for mass production.

Second, the geometry of the extraction system has to be improved, so that we can tap the full potential of the presented droplet-based liquid-liquid extraction method. Additional shallow parts with steps in the microfluidic channels would enhance the mixing by vortices for better extraction efficiency. Further, a particular improvement of the merging part is required to merge small droplets with a huge surface-to-volume ratio, which are produced at high flow rates inducing turbulences for mixing purposes and at highly unbalanced flow rates (requiring larger drainage channels).

Third, the detection limit of the integrated system of the microfluidic part and the optical waveguide could be improved greatly by avoiding water (saliva) contact with the optical waveguide during the initialization phase, because a thin, but highly absorbing aqueous lubrication layer remains on the optical waveguide.

Fourth, the portability of the device needs to be enabled by replacing the tabletop syringe pumps. Compact, portable, and battery-powered micropumps can be integrated with the microfluidic system.

Fifth, the integrated 'extraction-detection system' needs to be calibrated and the accuracy

Chapter 8. Summary & Outlook

of the extraction system to be verified. In this thesis only saliva samples spiked with cocaine were used. The high inter- and intra-subject variations of saliva samples might also influence the accuracy of our liquid-liquid extraction system.

A Appendix:

UPLC-MS Cocaine Calibration Curve

For the the cocaine measurements at the Swiss Laboratory for Doping Analyses (LAD) a calibration curve for the ultra performance liquid chromatography - mass spectrometer (Xevo TQ-S from Waters) was recorded using well defined cocaine concentration standards. The calibration curve (Figure A.1) showed linearity for the concentration range 5-2500ng/mL. Higher concentrations had to be diluted before measuring.

Compound name: Cocaine
Correlation coefficient: $r = 0.999901$, $r^2 = 0.999803$
Calibration curve: $0.0361883 * x + -0.036243$
Response type: Internal Std (Ref 2), Area * (IS Conc. / IS Area)
Curve type: Linear, Origin: Exclude, Weighting: 1/x, Axis trans: None

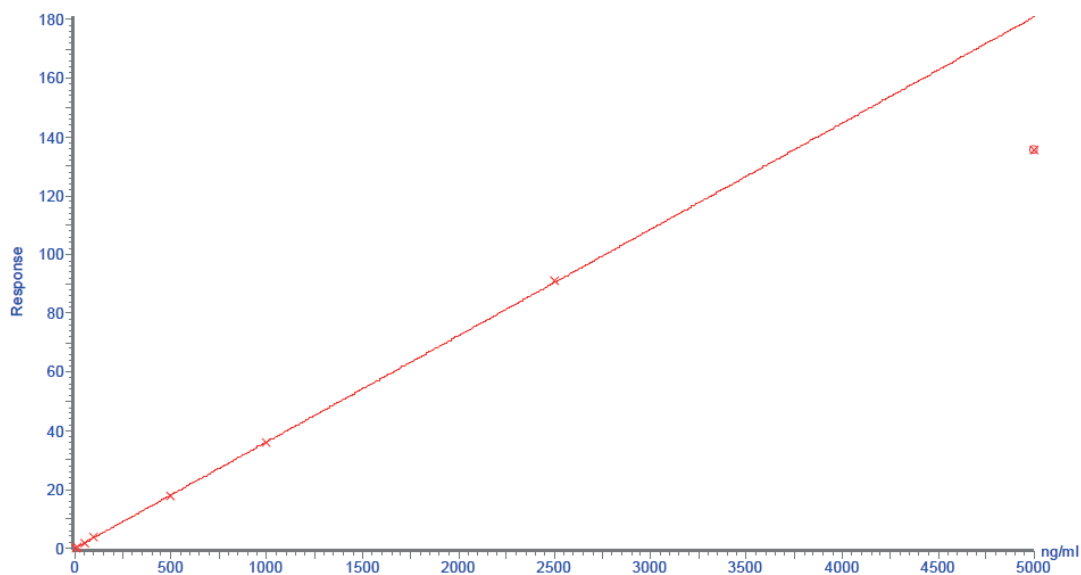


Figure A.1: Cocaine calibration curve for the UPLC-MS, Xevo TQ-S from Waters.

Bibliography

- [1] H. Bruus. *Theoretical Microfluidics*. Oxford University Press, 2008.
- [2] C.D. Chin, V. Linder, and S.K. Sia. Commercialization of microfluidic point-of-care diagnostic devices. *Lab on a Chip*, 12(12):2118–2134, 2012.
- [3] E.L. Cussler. *Diffusion, Mass Transfer in Fluid Systems*. Cambridge University Press, Cambridge UK, 2nd edition, 1997.
- [4] C.N. Baroud, F. Gallaire, and R. Dangla. Dynamics of microfluidic droplets. *Lab on a Chip*, 10(16):2032–2045, 2010.
- [5] G.N. Antonov. *Journal of Chemical Physics*, 5:372, 1907.
- [6] P. Yager, T. Edwards, E. Fu, K. Helton, K. Nelson, M.R. Tam, and B.H. Weigl. Microfluidic diagnostic technologies for global public health. *Nature*, 442(7101):412–418, 2006.
- [7] V.R. Horowitz, D.D. Awschalom, and S. Pennathur. Optofluidics: field or technique? *Lab on a Chip*, 8(11):1856–1863, 2008.
- [8] D. Psaltis, S.R. Quake, and C.H. Yang. Developing optofluidic technology through the fusion of microfluidics and optics. *Nature*, 442(7101):381–386, 2006.
- [9] D.B. Wolfe, R.S. Conroy, P. Garstecki, B.T. Mayers, M.A. Fischbach, K.E. Paul, M. Prentiss, and G.M. Whitesides. Dynamic control of liquid-core/liquid-cladding optical waveguides. *Proceedings of the National Academy of Sciences of the United States of America*, 101(34):12434–12438, 2004.
- [10] W. Buchegger, C. Wagner, B. Lendl, M. Kraft, and M. Vellekoop. A highly uniform lamination micromixer with wedge shaped inlet channels for time resolved infrared spectroscopy. *Microfluidics and Nanofluidics*, 10(4):889–897, 2010.
- [11] T.M. Floyd, M.A. Schmidt, and K.F. Jensen. Silicon micromixers with infrared detection for studies of liquid-phase reactions. *Industrial & Engineering Chemistry Research*, 44(8):2351–2358, 2005.
- [12] F. Malloggi, N. Pannacci, R. Attia, F. Monti, P. Mary, H. Willaime, P. Tabeling, B. Cabane, and P. Poncet. Monodisperse colloids synthesized with nanofluidic technology. *Langmuir*, 26(4):2369–2373, 2009.

Bibliography

- [13] A. Manz, N. Graber, and H.M. Widmer. Miniaturized total chemical analysis systems: A novel concept for chemical sensing. *Sensors and Actuators B: Chemical*, 1(1–6):244–248, 1990.
- [14] S. Balslev, A.M. Jorgensen, B. Bilenberg, K.B. Mogensen, D. Snakenborg, O. Geschke, J.P. Kutter, and A. Kristensen. Lab–on–a–chip with integrated optical transducers. *Lab on a Chip*, 6(2):213–217, 2006.
- [15] Caliper Life Sciences
www.caliperlifesciences.com, accessed June 16th 2012.
- [16] BioTrove
www.biotrove.com, accessed June 16th 2012.
- [17] Cellix Inc.
www.cellixltd.com, accessed June 16th 2012.
- [18] N. Blow. Microfluidics: in search of a killer application. *Nature Methods*, 4:665 – 670, 2007.
- [19] Micronics Inc.
www.micronics.net, accessed June 16th 2012.
- [20] Micronit Microfluidics
www.micronit.com, accessed June 16th 2012.
- [21] Diagnostics For All
www.dfa.org, accessed June 16th 2012.
- [22] N. Peled. Design and implementation of a microchemistry analyzer. *Pure & Applied Chemistry*, 68(10):1837–1841, 1996.
- [23] Abaxis Inc.
www.abaxis.com, accessed June 16th 2012.
- [24] J.O. Tenovuo. *Human Saliva: Clinical Chemistry and Microbiology*, volume 2. CRC Press, Boca Raton, Florida, 1989.
- [25] E. Fu, T. Chinowsky, K. Nelson, K. Johnston, T. Edwards, K. Helton, M. Grow, J.W. Miller, and P. Yager. SPR imaging-based salivary diagnostics system for the detection of small molecule analytes. *Annals of the New York Academy of Sciences*, 1098(Oral-Based Diagnostics):335–344, 2007.
- [26] K.L. Helton, K.E. Nelson, E. Fu, and P. Yager. Conditioning saliva for use in a microfluidic biosensor. *Lab on a Chip*, 8(11):1847–1851, 2008.
- [27] C.-Y. Yang, E. Brooks, Y. Li, P. Denny, C.-M. Ho, F. Qi, W. Shi, L. Wolinsky, B. Wu, D.T. Wong, and C.D. Montemagno. Detection of picomolar levels of interleukin-8 in human saliva by SPR. *Lab on a Chip*, 5(10):1017–1023, 2005.

- [28] A.E. Herr, A.V. Hatch, W.V. Giannobile, D.J. Throckmorton, H.M. Tran, J.S. Brennan, and A.K. Singh. Integrated microfluidic platform for oral diagnostics. *Annals of the New York Academy of Sciences*, 1098(Oral-Based Diagnostics):362–374, 2007.
- [29] A.E. Herr, A.V. Hatch, D.J. Throckmorton, H.M. Tran, J.S. Brennan, W.V. Giannobile, and A.K. Singh. Microfluidic immunoassays as rapid saliva-based clinical diagnostics. *Proceedings of the National Academy of Sciences*, 104(13):5268–5273, 2007.
- [30] T. Miyado, Y. Tanaka, H. Nagai, S. Takeda, K. Saito, K. Fukushi, Y. Yoshida, S. Wakida, and E. Niki. High-throughput microfluidic devices for no assay based on electrophoretic separation. In *Microtechnology in Medicine and Biology*, pages 66–68, 2005.
- [31] D.J. Marchiarullo, J.Y. Lim, Z. Vaksman, J.P. Ferrance, L. Putcha, and J.P. Landers. Towards an integrated microfluidic device for spaceflight clinical diagnostics: Microchip-based solid-phase extraction of hydroxyl radical markers. *Chromatography A*, 1200(2):198–203, 2008.
- [32] Z. Chen, M.G. Mauk, J. Wang, W.R. Abrams, P.L.A.M. Cortjens, R.S. Niedbala, D. Malamud, and H.H. Bau. A microfluidic system for saliva-based detection of infectious diseases. *Annals of the New York Academy of Sciences*, 1098(Oral-Based Diagnostics):429–436, 2007.
- [33] W.R. Abrams, C.A. Barber, K. Mccann, G. Tong, Z. Chen, M.G. Mauk, J. Wang, A. Volkov, P. Bourdelle, P.L.A.M. Corstjens, M. Zuiderwijk, K. Kardos, S. Li, H.J. Tanke, R.S. Niedbala, D. Malamud, and H. Bau. Development of a microfluidic device for detection of pathogens in oral samples using upconverting phosphor technology (UPT). *Annals of the New York Academy of Sciences*, 1098(Oral-Based Diagnostics):375–388, 2007.
- [34] X. Qiu, J. Thompson, Z. Chen, C. Liu, D. Chen, S. Ramprasad, M. Mauk, S. Ongagna, C. Barber, W. Abrams, D. Malamud, P. Corstjens, and H. Bau. Finger-actuated, self-contained immunoassay cassettes. *Biomedical Microdevices*, 6:1175–86, 2009.
- [35] C. Teller, J. Halamek, J. Zeravik, W.F.M. Stöcklein, and F.W. Scheller. Development of a bifunctional sensor using haptized acetylcholinesterase and application for the detection of cocaine and organophosphates. *Biosensors and Bioelectronics*, 24(1):111–117, 2008.
- [36] T. Frisk, D. Ronnholm, W.V.D. Wijngaart, and G. Stemme. A micromachined interface for airborne sample-to-liquid transfer and its application in a biosensor system. *Lab on a Chip*, 6(12):1504–1509, 2006.
- [37] Y. Du, C. Chen, J. Yin, B. Li, M. Zhou, S. Dong, and E. Wang. Solid-state probe based electrochemical aptasensor for cocaine: A potentially convenient, sensitive, repeatable, and integrated sensing platform for drugs. *Analytical Chemistry*, 82(4):1556–1563, 2010.

Bibliography

- [38] K.-Y. Lien, C.-J. Liu, P.-L. Kuo, and G.-B. Lee. Bead-based microfluidic platform integrated with optical detection devices for rapid detection of genetic deletion from saliva. In *MEMS Conference*, pages 340–343, Sorrento, Italy, 2009.
- [39] T.M. Blicharz, W.L. Siqueira, E.J. Helmerhorst, F.G. Oppenheim, P.J. Wexler, F.F. Little, and D.R. Walt. Fiber-optic microsphere-based antibody array for the analysis of inflammatory cytokines in saliva. *Analytical Chemistry*, 81(6):2106–2114, 2009.
- [40] K. Sun, N. Ramgir, and S. Bhansali. An immunoelectrochemical sensor for salivary cortisol measurement. *Sensors and Actuators B: Chemical*, 133(2):533–537, 2008.
- [41] B.E. Collins and E.V. Anslyn. Pattern-based peptide recognition. *Chemistry – A, European Journal*, 13(17):4700–4708, 2007.
- [42] D.R. Walt, T.M. Blicharz, R.B. Hayman, D.M. Rissin, M. Bowden, W.L. Siqueira, E.J. Helmerhorst, N. Grand-Pierre, F.G. Oppenheim, J.S. Bhatia, F.F. Little, and J.S. Brody. Microsensor arrays for saliva diagnostics. *Annals of the New York Academy of Sciences*, 1098(Oral-Based Diagnostics):389–400, 2007.
- [43] E.M. Starke, J.C. Smoot, J.-H. Wu, W.-T. Liu, D. Chandler, and D.A. Stahl. Saliva-based diagnostics using 16S rRNA microarrays and microfluidics. *Annals of the New York Academy of Sciences*, 1098(Oral-Based Diagnostics):345–361, 2007.
- [44] J.V. Jokerst, A. Raamanathan, N. Christodoulides, P.N. Floriano, A.A. Pollard, G.W. Simmons, J. Wong, C. Gage, W.B. Furmaga, S.W. Redding, and J.T. Mcdevitt. Nano-biochips for high performance multiplexed protein detection: Determinations of cancer biomarkers in serum and saliva using quantum dot bioconjugate labels. *Biosensors and Bioelectronics*, 24(12):3622–3629, 2009.
- [45] N. Samyn and C. Van Haeren. On-site testing of saliva and sweat with drugwipe and determination of concentrations of drugs of abuse in saliva, plasma and urine of suspected users. *Legal Medicine*, 113(3):150–154, 2000.
- [46] J.M. Walsh, R. Flegel, D.J. Crouch, L. Cangianelli, and J. Baudys. An evaluation of rapid point-of-collection oral fluid drug-testing devices. *Analytical Toxicology*, 27(7):429–439, 2003.
- [47] G. Cooper, L. Wilson, C. Reid, D. Baldwin, C. Hand, and V. Spieher. Validation of the cozart microplate EIA for cocaine and metabolites in oral fluid. *Analytical Toxicology*, 28(6):498–503, 2004.
- [48] D.A. Kidwell, J.D. Kidwell, F. Shinohara, C. Harper, K. Roarty, K. Bernadt, R.A. Mccauley, and F.P. Smith. Comparison of daily urine, sweat, and skin swabs among cocaine users. *Forensic Science International*, 133(1–2):63–78, 2003.
- [49] P.J. Viskari and J.P. Landers. Unconventional detection methods for microfluidic devices. *Electrophoresis*, 27(9):1797–1810, 2006.

- [50] T.D. Nguyen Hong, M. Jouan, N. Quy Dao, M. Bouraly, and F. Mantsi. Coupling of high-performance liquid chromatography with raman spectrometry. *Chromatography A*, 743(2):323–327, 1996.
- [51] B. Saegmueller, G. Brehm, and S. Schneider. In situ generated photolytic silver in a gelatin matrix: an approach for high-throughput sers spectroscopy applying microtiter plates. *Applied Spectroscopy*, 54(12):1849–1856, 2000.
- [52] M.A. De Jesus, K.S. Giesfeldt, and M.J. Sepaniak. Factors affecting the sorption of model environmental pollutants onto silver polydimethylsiloxane nanocomposite raman substrates. *Applied Spectroscopy*, 58(10):1157–1164, 2004.
- [53] J. Kuligowski, G. Quintas, M. De La Guardia, and B. Lendl. Analytical potential of mid-infrared detection in capillary electrophoresis and liquid chromatography: A review. *Analytica Chimica Acta*, 679(1–2):31–42, 2010.
- [54] S. Kulka, G. Quintas, and B. Lendl. On-line capillary electrophoresis FTIR detection for the separation and characterization of proteins. *Vibrational Spectroscopy*, 42(2):392–396, 2006.
- [55] S. Kulka, G. Quintas, and B. Lendl. Automated sample preparation and analysis using a sequential-injection-capillary electrophoresis (SI-CE) interface. *Analyst*, 131(6):739–744, 2006.
- [56] S. Kulka, N. Kaun, J.R. Baena, J. Frank, P. Svasek, D. Moss, M.J. Vellekoop, and B. Lendl. Mid-ir synchrotron radiation for molecular specific detection in microchip-based analysis systems. *Analytical and Bioanalytical Chemistry*, 378(7):1735–1740, 2004.
- [57] T. Pan, R.T. Kelly, M.C. Asplund, and A.T. Woolley. Fabrication of calcium fluoride capillary electrophoresis microdevices for on-chip infrared detection. *Chromatography A*, 1027(1–2):231–235, 2004.
- [58] R.M. Connatser, L.A. Riddle, and M.J. Sepaniak. Metal-polymer nanocomposites for integrated microfluidic separations and surface enhanced raman spectroscopic detection. *Separation Science*, 27(17–18):1545–1550, 2004.
- [59] M. Haberkorn, J. Frank, M. Harasek, J. Nilsson, T. Laurell, and B. Lendl. Flow-through picoliter dispenser: A new approach for solvent elimination in FT-IR spectroscopy. *Applied Spectroscopy*, 56(7):902–908, 2002.
- [60] H.A. Waterman, C. Blom, H.J. Holterman, E.J. s’Gravenmade, and J. Mellema. Rheological properties of human saliva. *Archives of Oral Biology*, 33(8):589–596, 1988.
- [61] B.K.B. Berkovitz, G.R. Holland, and B.J. Moxham. *Oral anatomy, histology and embryology*, volume 3. Mosby, New York, 2002.
- [62] S.S. Davis. The rheological properties of saliva. *Rheologica Acta*, 10(1):28–35, 1971.

Bibliography

- [63] P.H. Gann, S. Giovanazzi, L. Van Horn, A. Branning, and R.T. Chatterton. Saliva as a medium for investigating intra- and interindividual differences in sex hormone levels in premenopausal women. *Cancer Epidemiol Biomarkers Prev*, 10(1):59–64, 2001.
- [64] K.R. Atkinson, K.R. Lo, S.R. Payne, J.S. Mitchell, and J.R. Ingram. Rapid saliva processing techniques for near real-time analysis of salivary steroids and protein. *Clinical Laboratory Analysis*, 22(6):395–402, 2008.
- [65] P.D.V. de Almeida, A.M.T. Gregio, and M.A.N. Machando. Saliva composition and functions: A comprehensive review. *Contemporary Dental Practice*, 9(3):72–80, 2008.
- [66] S.P. Humphrey and R.T. Williamson. A review of saliva: Normal composition, flow, and function. *Prosthetic Dentistry*, 85(2):162–169, 2001.
- [67] C. Dawes. Rhythms in salivary flow rate and composition. *Chronobiology*, 2:253–279, 1974.
- [68] S. Budavari, M.J. O’Neil, A. Smith, P.E. Heckelman, and J.F. Kinneary. *The Merck Index*. Merck & Co., Inc., 12th edition, 1996.
- [69] D.R. Lide. *Handbook of Chemistry and Physics*, volume 89. CRC Press, London, 2009.
- [70] L.C.P.M. Schenkels, E.C.I. Veerman, and A.V. Nieuw Amerongen. Biochemical composition of human saliva in relation to other mucosal fluids. *Critical Reviews in Oral Biology and Medicine*, 6(2):161–175, 1995.
- [71] H. Berg, I.C. Cecilia, L. Lindh, and T. Arnebrant. Intraoral lubrication of PRP-1, statherin and mucin as studied by AFM. *Biofouling*, 20(1):65–70, 2003.
- [72] P.H. Wiernik, J.M. Goldman, J.P. Dutcher, and R.A. Kyle. *Neoplastic diseases of the blood*. Cambridge University Press, 4th edition, 2003.
- [73] K.L. Helton and P. Yager. Interfacial instabilities affect microfluidic extraction of small molecules from non-Newtonian fluids. *Lab on a Chip*, 7(11):1581–1588, 2007.
- [74] C. Dawes and G.H. Dibdin. Salivary concentrations of urea released from a chewing gum containing urea and how these affect the urea content of gel-stabilized plaques and their pH after exposure to sucrose. *Caries Research*, 35:344–353, 2001.
- [75] G.C. Battistone and G.W. Burnett. The free amino acid composition of human saliva. *Archives of Oral Biology*, 3(3):161–170, 1961.
- [76] P. Praeve, U. Faust, W. Sittig, and D.A. Sukatsch. *Handbuch der Biotechnologie*. Oldenbourg, 4th edition, 1994.
- [77] J.V. Houte and D.B. Green. Relationship between the concentration of bacteria in saliva and the colonization of teeth in humans. *Infection and Immunity*, 9(4):624–630, 1974.

- [78] E.G.C. Clarke. *Clarke's isolation and identification of drugs in pharmaceuticals, body fluids, and post-mortem materials*. The Pharmaceutical Press, London, 2nd edition, 1986.
- [79] A.J. Jenkins, J.M. Opler, and E.J. Cone. Comparison of heroin and cocaine concentrations in saliva with concentrations in blood and plasma. *Journal of Analytical Toxicology*, 19(6):359–374, 1995.
- [80] E. Reynolds. *Martindale the Extra Pharmacopoeia*. The Pharmaceutical Press, London, 29th edition, 1989.
- [81] N.A. Larsen, B. Zhou, A. Heine, P. Wirsching, K.D. Janda, and I.A. Wilson. Crystal structure of a cocaine-binding antibody. *Molecular Biology*, 311(1):9–15, 2001.
- [82] W.-L. Wang, W.D. Darwin, and E.J. Cone. Simultaneous assay of cocaine, heroin and metabolites in hair, plasma, saliva and urine by gas chromatography-mass spectrometry. *Chromatography B*, 660:279–290, 1994.
- [83] Verkehrsregelverordnung Schweiz (VRV)
www.admin.ch/ch/d/sr/741_11/a2.html, accessed June 16th 2012.
- [84] I. Kim, A.J. Barnes, R. Schepers, E.T. Moolchan, L. Wilson, G. Cooper, C. Reid, C. Hand, and M.A. Huestis. Sensitivity and specificity of the cozart microplate eia cocaine oral fluid at proposed screening and confirmation cutoffs. *Clinical Chemistry*, 49(9):1498–1503, 2003.
- [85] E.M. Munoz, S. Lorenzo-Abalde, A. Gonzaez-Fernandez, O. Quintela, M. Lopez-Rivadulla, and R. Riguera. Direct surface plasmon resonance immunosensor for in situ detection of benzoylecgonine, the major cocaine metabolite. *Biosensors and Bioelectronics*, 26(11):4423–4428, 2011.
- [86] E.J. Cone, M. Hillsgrove, and W.D. Darwin. Simultaneous measurement of cocaine, cocaethylene, their metabolites, and "crack" pyrolysis products by gas chromatography-mass spectrometry. *Clinical Chemistry*, 40(7):1299–1305, 1994.
- [87] E.J. Cone, K. Kumor, L.K. Thompson, and M. Scherer. Correlation of saliva cocaine levels with plasma levels and with pharmacologic effects after intravenous cocaine administration in human subjects. *Analytical Toxicology*, 12:200–206, 1988.
- [88] W. Schramm, R.H. Smith, P.A. Craig, and D.A. Kidwell. Drugs of abuse in saliva: a review. *Analytical Toxicology*, 16(1):1–9, 1992.
- [89] European research project ROadSide Testing Assessment
www.rosita.org, accessed June 16th 2012.
- [90] D.T. Wong. Salivary diagnostics. *American Scientist*, 96(1), 2008.

Bibliography

- [91] R. Lennox, M.L. Dennis, C.K. Scott, and R. Funk. Combining psychometric and biometric measures of substance use. *Drug and Alcohol Dependence*, 83(2):95–103, 2006.
- [92] D.T. Wong. Salivary diagnostics powered by nanotechnologies, proteomics and genomics. *American Dental Association*, 137(3):313–321, 2006.
- [93] I.D. Mandel. SALIVARY DIAGNOSIS – More than a lick and a promise. *Journal of the American Dental Association*, 124(1):85–87, 1993.
- [94] M. Navazesh and C.M. Christensen. A comparison of whole mouth resting and stimulated salivary measurement procedures. *Dental Research*, 61(10):1158–1162, 1982.
- [95] W.H. Rowe and I.L. Shannon. *The biochemistry of human saliva in: Health and disease in Salivary glands and their secretion*. University of Michigan Press, 1972.
- [96] K. Kato, M. Hillsgrove, L. Winhold, D.A. Gorelick, W.D. Darwin, and E.J. Cone. Cocaine and metabolite excretion in saliva under stimulated and nonstimulated conditions. *Analytical Toxicology*, 17:338–341, 1993.
- [97] Saliva Drug Test Center
www.salivadrug.com, accessed June 16th 2012.
- [98] SciMart
www.scimart.com/product/detail/salivette-synthetic-swab-for-cortisol-determination-100pack/, accessed June 16th 2012.
- [99] C. Holm-Hansen, G. Tong, C. Davis, W.R. Abrams, and D. Malamud. Comparison of oral fluid collectors for use in a rapid point-of-care diagnostic device. *Clinical and Vaccine Immunology*, 11(5):909–912, 2004.
- [100] O.H. Drummer. Drug testing in oral fluid. *Chinical Biochemical Review*, 27:147–159, 2006.
- [101] A. Burnett, W. Fan, P. Upadhya, J. Cunningham, E. Linfield, G. Davies, H. Edwards, T. Munshi, and A. O’neil. Analysis of drugs-of-abuse and explosives using terahertz time-domain and Raman spectroscopy. volume 6120, page 61200M. SPIE, 2006.
- [102] D.J. Crouch, J.M. Walsh, R. Flegel, L. Cangianelli, J. Baudys, and R. Atkins. An evaluation of selected oral fluid point-of-collection drug-testing devices. *Analytical Toxicology*, 29(4):244–248, 2005.
- [103] G. Cooper, L. Wilson, C. Reid, L. Main, and C. Hand. Evaluation of the cozart rapiscan drug test system for opiates and cocaine in oral fluid. *Forensic Science International*, 150(2–3):239–243, 2005.
- [104] Craig Medical Distribution Inc.
www.craigmedical.com/saliva_drug_osr.htm, accessed June 16th 2012.

- [105] Biomar Diagnostic Systems GmbH
www.biomar.de/schnellteste/drogen/toxiquick%20allgemein.pdf, accessed June 16th 2012.
- [106] M. Concheiro, A. De Castro, O. Quintela, A. Cruz, and M. Lopez-Rivadulla. Confirmation by lc-ms of drugs in oral fluid obtained from roadside testing. *Forensic Science International*, 170(2-3):156-162, 2007.
- [107] G. Cooper, L. Wilson, C. Reid, L. Main, and C. Hand. Evaluation of the cozart rapiscan drug test system for opiates and cocaine in oral fluid. *Forensic Science International*, 150(2-3):239-243, 2005.
- [108] Drug Testing World
www.drugtestingworld.com/drug-test-kits-cocaine-drug-tests-c-38_10.html, accessed June 16th 2012.
- [109] S.M. Wille, N. Samyn, M.M. Ramirez-Fernandez, and G. De Boeck. Evaluation of on-site oral fluid screening using drugwipe-5(+), rapidstat and drug test 5000 for the detection of drugs of abuse in drivers. *Forensic Science International*, 198(1-3):2-6, 2010.
- [110] P.J.F. Rantonen and J.H. Meurman. Viscosity of whole saliva. *Acta Odontologica Scandinavica*, 56(4):210 - 214, 1998.
- [111] M. Levy, B. Koeppen, and B. Stanton. *Berne & Levy Principles of Physiology*. Mosby, 4th edition, 2005.
- [112] S.S. Davis. Saliva is viscoelastic. *Cellular and Molecular Life Sciences*, 26(12):1298-1300, 1970.
- [113] Waters Inc.
www.waters.com, accessed June 16th 2012.
- [114] A. Manz and J.C.T. Eijkel. Miniaturization and chip technology. what can we expect? *Pure and Applied Chemistry*, 73(10):1555-1561, 2001.
- [115] B.H. Weigl, R. Bardell, T. Schulte, F. Battrell, and J. Hayenga. Design and rapid prototyping of thin-film laminate-based microfluidic devices. *Biomedical Microdevices*, 3(4):267-274, 2001.
- [116] C.E. White. *Advanced methods, materials, and devices for microfluidics*. PhD thesis, 2003.
- [117] U. Attia, S. Marson, and J. Alcock. Micro-injection moulding of polymer microfluidic devices. *Microfluidics and Nanofluidics*, 7(1):1-28, 2009.
- [118] A. De Mello. Plastic fantastic? *Lab on a Chip*, 2(2):31N-36N, 2002.

Bibliography

- [119] H. Becker and L.E. Locascio. Polymer microfluidic devices. *Talanta*, 56(2):267–287, 2002.
- [120] B.-S. Chiou, R.J. English, and S.A. Khan. Rheology and photo-cross-linking of thiol-ene polymers. *Macromolecules*, 29(16):5368–5374, 1996.
- [121] L.H. Hung, R. Lin, and A.P. Lee. Rapid microfabrication of solvent-resistant biocompatible microfluidic devices. *Lab on a Chip*, 8(6):983–987, 2008.
- [122] D. Bartolo, G. Degre, P. Nghe, and V. Studer. Microfluidic stickers. *Lab on a Chip*, 8(2):274–279, 2008.
- [123] MSDS NOA81, Norland Products Inc.
www.norlandprod.com/adhesives/noa%2081.html, accessed June 16th 2012.
- [124] O. Frey, T. Holtzman, R.M. Mcnamara, D.E.H. Theobald, P.D. van der Wal, N.F. de Rooij, J.W. Dalley, and M. Koudelka-Hep. Simultaneous neurochemical stimulation and recording using an assembly of biosensor silicon microprobes and su-8 microinjectors. *Sensors and Actuators B: Chemical*, 154(2):96–105, 2010.
- [125] J.N. Lee, C. Park, and G.M. Whitesides. Solvent compatibility of poly(dimethylsiloxane)-based microfluidic devices. *Analytical Chemistry*, 75(23):6544–6554, 2003.
- [126] A. Waldbaur, H. Rapp, K. Länge, and B.E. Rapp. Let there be chip - towards rapid prototyping of microfluidic devices: one-step manufacturing processes. *Analytical Methods*, 3:2681–2716, 2011.
- [127] D.C. Duffy, J.C. McDonald, O.J.A. Schueller, and G.M. Whitesides. Rapid prototyping of microfluidic systems in poly(dimethylsiloxane). *Analytical Chemistry*, 70(23):4974–4984, 1998.
- [128] J.P. Rolland, E.C. Hagberg, G.M. Denison, K.R. Carter, and J.M. De Simone. High-resolution soft lithography: Enabling materials for nanotechnologies. *Angewandte Chemie*, 43:5796–5799, 2004.
- [129] B.K. Lee, L.-Y. Hong, H.Y. Lee, D.-P. Kim, and T. Kawai. Replica mold for nanoimprint lithography from a novel hybrid resin. *Langmuir*, 25(19):11768–11776, 2009.
- [130] L.M. Campos, T.T. Truong, D.E. Shim, M.D. Dimitriou, D. Shir, I. Meinel, J.A. Gerbec, H.T. Hahn, J.A. Rogers, and C.J. Hawker. Applications of photocurable pmms thiol-ene stamps in soft lithography. *Chemistry of Materials*, 21(21):5319–5326, 2009.
- [131] P. Wägli, A. Homsy, and N.F. de Rooij. Norland optical adhesive (NOA81) microchannels with adjustable surface properties and high chemical resistance against IR-transparent organic solvents. *Procedia Engineering*, 5:460–463, 2010.

- [132] A.B. Shrirao and R. Perez-Castillejos. Simple fabrication of microfluidic devices by replicating scotch-tape masters (<http://blogs.rsc.org/chipsandtips/>, accessed May 20th 2010). *Chips & Tips*, May 17th 2010.
- [133] P. Wägli, A. Homsy, and N.F. de Rooij. Norland optical adhesive (NOA81) microchannels with adjustable wetting behavior and high chemical resistance against a range of mid-infrared-transparent organic solvents. *Sensors and Actuators B: Chemical*, 156(2):994–1001, 2011.
- [134] B.T. Ginn and O. Steinbock. Polymer surface modification using microwave-oven-generated plasma. *Langmuir*, 19(19):8117–8118, 2003.
- [135] J. Bibette, F. Leal-Calderon, V. Schmitt, and P. Poulin. *Emulsion Science*. Springer, New York, 2007.
- [136] S.H. Kim, Y. Yang, M. Kim, S.-W. Nam, K.-M. Lee, N.Y. Lee, Y.S. Kim, and S. Park. Simple route to hydrophilic microfluidic chip fabrication using an ultraviolet (UV)-cured polymer. *Advanced Functional Materials*, 17(17):3493–3498, 2007.
- [137] P. Wägli, A. Homsy, and N.F. de Rooij. Norland optical adhesive (NOA81) microchannels with adjustable wetting behavior and high chemical resistance against a range of mid-infrared-transparent organic solvents. *Sensors and Actuators B: Chemical*, 156(2):994–1001, 2011.
- [138] P. Wägli, B. Guélat, A. Homsy, and N.F. de Rooij. Microfluidic devices made of UV-curable glue (NOA81) for fluorescence detection based applications. In *International Conference on Miniaturized Systems for Chemistry and Life Sciences (MicroTAS)*, Groningen, Netherlands, 2010.
- [139] P. Wägli, P.D. van der Wal, A. Homsy, and N.F. de Rooij. UV-curable adhesive as the low-cost material of choice for microfluidic forensic applications. In *International Meeting on Chemical Sensors (IMCS)*, Nürnberg, Germany, 2012.
- [140] E.W. Washburn. *Physical Review*, 17:273–283, 1921.
- [141] A. Han, G. Mondin, N.G. Hegelbach, N.F. de Rooij, and U. Staufer. Filling kinetics of liquids in nanochannels as narrow as 27 nm by capillary force. *Colloid and Interface Science*, 293(1):151–157, 2006.
- [142] T.-H. Yoon, S.-H. Park, K.-I. Min, X. Zhang, S.J. Haswell, and D.-P. Kim. Novel inorganic polymer derived microreactors for organic microchemistry applications. *Lab on a Chip*, 8:1454–1459, 2008.
- [143] H. Lai, I. Corbin, and J.R. Almirall. Headspace sampling and detection of cocaine, mdma, and marijuana via volatile markers in the presence of potential interferences by solid phase microextraction-ion mobility spectrometry (spme-ims). *Analytical and Bioanalytical Chemistry*, 392(1–2):105–113, 2008.

Bibliography

- [144] J. Pawliszyn. *Handbook of solid phase microextraction*. Chemical Industry Press of China, 2009.
- [145] A. Homsy, P. van der Wal, W. Doll, R. Schaller, S. Korsatko, M. Ratzner, M. Ellmerer, T.R. Pieber, A. Nicol, and N.F. de Rooij. Development and validation of a low cost blood filtration element separating plasma from undiluted whole blood. *Biomicrofluidics*, 6(1):012804, 2012.
- [146] A.B. Lowe. Thiol-ene "click" reactions and recent applications in polymer and materials synthesis. *Polymer Chemistry*, 1(1):17–36, 2009.
- [147] S. Silvestrini, D. Ferraro, T. Toth, M. Pierno, T. Carofiglio, G. Mistura, and M. Maggini. Tailoring the wetting properties of thiolene microfluidic materials. *Lab on a Chip*, 12(20):4041–4043, 2012.
- [148] R. Tadmor. Line energy and the relation between advancing, receding, and young contact angles. *Langmuir*, 20(18):7659–7664, 2004.
- [149] R. Bongiovanni, M. Sangermano, G. Malucelli, and A. Priola. Uv curing of photoinitiator-free systems containing bismaleimides and diacrylate resins: bulk and surface properties. *Progress in Organic Coatings*, 53(1):46–49, 2005.
- [150] J.A. Muck, M.P. Chatrathi, G. Chen, N. Mittal, S.D. Spillman, and S. Obeidat. Bulk modification of polymeric microfluidic devices. *Lab on a Chip*, 5(2):226–230, 2005.
- [151] B. Bhushan, D. Hansford, and K.K. Lee. Surface modification of silicon and polydimethylsiloxane surfaces with vapor-phase-deposited ultrathin fluorosilane films for biomedical nanodevices. *Vacuum Science & Technology A: Vacuum Surfaces and Films*, 24(4):1197–1202, 2006.
- [152] H. Maeda, N. Ishida, H. Kawauchi, and K. Tuzimura. Reaction of fluorescein-isothiocyanate with proteins and amino acids. *Biochemistry*, 65(5):777–783, 1969.
- [153] B. Zhao, J.S. Moore, and D.J. Beebe. Surface-directed liquid flow inside microchannels. *Science*, 291(5506):1023–1026, 2001.
- [154] E.P. Dupont, R. Luisier, and M.A.M. Gijss. Noa 63 as a UV-curable material for fabrication of microfluidic channels with native hydrophilicity. *Microelectronic Engineering*, 87(5–8):1253–1255, 2010.
- [155] R. Bharadwaj, J.G. Santiago, and B. Mohammadi. Design and optimization of on-chip capillary electrophoresis. *Electrophoresis*, 23:2729–2744, 2002.
- [156] Budget Sensors, Bulgaria
www.budgetsensors.com, accessed June 16th 2012.

- [157] S. Bhattacharya, A. Datta, J.M. Berg, and S. Gangopadhyay. Studies on surface wettability of poly(dimethyl) siloxane (PDMS) and glass under oxygen-plasma treatment and correlation with bond strength. *Microelectromechanical Systems*, 14(3):590–597, 2005.
- [158] P. Wägli, Y.-C. Chang, P.D. van der Wal, L Hovzdara, A. Homsy, H.P. Herzig, and N.F. de Rooij. Droplet based liquid-liquid extraction and on-chip IR-waveguide-spectroscopy detection of cocaine in human saliva. In *International Conference on Miniaturized Systems for Chemistry and Life Sciences (MicroTAS)*, Okinawa, Japan, 2012.
- [159] J. Xu and D. Attinger. Drop on demand in a microfluidic chip. *Micromechanics and Microengineering*, 18(6):065020–065030, 2008.
- [160] C. Cramer, P. Fischer, and E.J. Windhab. Drop formation in a co-flowing ambient fluid. *Chemical Engineering Science*, 59(15):3045–3058, 2004.
- [161] T. Thorsen, R.W. Roberts, E.H. Arnold, and S.R. Quake. Dynamic pattern formation in a vesicle-generating microfluidic device. *Physical Review Letters*, 86(18):4163–4166, 2001.
- [162] P. Garstecki, M.J. Fuerstman, H.A. Stone, and G.M. Whitesides. Formation of droplets and bubbles in a microfluidic T-junction-scaling and mechanism of break-up. *Lab on a Chip*, 6(3):437–446, 2006.
- [163] S. Sugiura, M. Nakajima, H. Ushijima, K. Yamamoto, and M. Seki. Preparation characteristics of monodispersed water-in-oil emulsions using microchannel emulsification. *Chemical Engineering of Japan*, 34(6):757–765, 2001.
- [164] I. Kobayashi, K. Uemura, and M. Nakajima. Formulation of monodisperse emulsions using submicron-channel arrays. *Colloids and Surfaces A: Physicochemical and Engineering Aspects*, 296:285–289, 2007.
- [165] I. Kobayashi, Y. Wada, K. Uemura, and M. Nakajima. Microchannel emulsification for mass production of uniform fine droplets: integration of microchannel arrays on a chip. *Microfluidics and Nanofluidics*, 8(2):255–262, 2010.
- [166] E. van der Zwan, K. Schroen, and R. Boom. A geometric model for the dynamics of microchannel emulsification. *Langmuir*, 25(13):7320–7327, 2009.
- [167] I. Kobayashi, S. Mukataka, and M. Nakajima. Production of monodisperse oil-in-water emulsions using a large silicon straight-through microchannel plate. *Industrial and Engineering Chemistry Research*, 44(15):5852–5856, 2005.
- [168] I. Kobayashi, T. Takano, R. Maeda, Y. Wada, K. Uemura, and M. Nakajima. Straight-through microchannel devices for generating monodisperse emulsion droplets several microns in size. *Microfluidics and Nanofluidics*, 4(3):167–177, 2008.
- [169] K. Wang, Y. Lu, J. Xu, and G. Luo. Droplet generation in micro-sieve dispersion device. *Microfluidics and Nanofluidics*, 10(5):1087–1095, 2011.

Bibliography

- [170] T. Nisisako and T. Torii. Microfluidic large-scale integration on a chip for mass production of monodisperse droplets and particles. *Lab on a Chip*, 8(2):287–293, 2008.
- [171] S.L. Anna, N. Bontoux, and H.A. Stone. Formation of dispersions using 'flow focusing' in microchannels. *Applied Physics Letters*, 82(3):364–366, 2003.
- [172] R. Dreyfus, P. Tabeling, and H. Willaime. Ordered and disordered patterns in two-phase flows in microchannels. *Physical Review Letters*, 90(14):1445051–1445054, 2003.
- [173] L. Shui, A. Van Den Berg, and J. Eijkel. Scalable attoliter monodisperse droplet formation using multiphase nano-microfluidics. *Microfluidics and Nanofluidics*, 11(1):87–92, 2011.
- [174] S. Darvishi and T. Cubaud. Lubrication of highly viscous core-annular flows in microfluidic chambers. *Fluids Engineering*, 133(3):0312031–0312037, 2011.
- [175] R. Dangla, F. Gallaire, and C.N. Baroud. Microchannel deformations due to solvent-induced PDMS swelling. *Lab on a Chip*, 10(21):2972–2978, 2010.
- [176] E. Tamaki, A. Hibara, H.-B. Kim, M. Tokeshi, and T. Kitamori. Pressure-driven flow control system for nanofluidic chemical process. *Chromatography A*, 1137(2):256–262, 2006.
- [177] C. Neumann, A. Voigt, L. Pires, and B.E. Rapp. Design and characterization of a platform for thermal actuation of up to 588 microfluidic valves. *Microfluidics and Nanofluidics*, in press.:1–10, 2012.
- [178] K.C. van Dijke, K. Schroen, A. van der Padt, and R. Boom. Edge emulsification for food-grade dispersions. *Food Engineering*, 97(3):348–354, 2010.
- [179] A.D. Stroock, S.K.W. Dertinger, A. Ajdari, I. Mezic, H.A. Stone, and G.M. Whitesides. Chaotic mixer for microchannels. *Science*, 295(5555):647–651, 2002.
- [180] W. Buchegger, C. Wagner, P. Svasek, B. Lendl, M. Kraft, and M.J. Vellekoop. Fabrication and characterization of a vertical lamination micromixer for mid-ir spectroscopy. *Sensors and Actuators B: Chemical*, 159(1):336–341, 2011.
- [181] A. Peters. Passive discrete phase coalescence and extraction in droplet based microfluidic devices. *Semester thesis EPF Lausanne*, 2012.
- [182] H. Gu, M.H.G. Duits, and F. Mugele. Droplets formation and merging in two-phase flow microfluidics. *Molecular Sciences*, 12(4):2572–2597, 2011.
- [183] L. Bräuer, S. Möschter, S. Beileke, K. Jäger, F. Garreis, and F. Paulsen. Human parotid and submandibular glands express and secrete surfactant proteins A, B, C and D. *Histochemistry and Cell Biology*, 132(3):331–338, 2009.
- [184] A.H. Demond and A.S. Lindner. Estimation of interfacial tension between organic liquids and water. *Environmental Science & Technology*, 27(12):2318–2331, 1993.

- [185] A. Preetha and R. Banerjee. Comparison of artificial saliva substitutes. *Trends in Biomaterials & Artificial Organs*, 18(2):178–186, 2005.
- [186] N. Bremond, A.R. Thiam, and J. Bibette. Decompressing emulsion droplets favors coalescence. *Physical Review Letters*, 100(2):0245011–0245014, 2008.
- [187] X. Niu, S. Gulati, J.B. Edel, and A.J. Demello. Pillar-induced droplet merging in microfluidic circuits. *Lab on a Chip*, 8(11):1837–1841, 2008.
- [188] C.-X. Zhao and A.P.J. Middelberg. Two-phase microfluidic flows. *Chemical Engineering Science*, 66(7):1394–1411, 2011.
- [189] C. Priest, S. Herminghaus, and R. Seemann. Controlled electrocoalescence in microfluidics: Targeting a single lamella. *Applied Physics Letters*, 89(13):134101–134103, 2006.
- [190] G.F. Christopher, J. Bergstein, N.B. End, M. Poon, C. Nguyen, and S.L. Anna. Coalescence and splitting of confined droplets at microfluidic junctions. *Lab on a Chip*, 9(8):1102–1109, 2009.
- [191] L.M. Fidalgo, C. Abell, and W.T.S. Huck. Surface-induced droplet fusion in microfluidic devices. *Lab on a Chip*, 7(8):984–986, 2007.
- [192] N. Bremond, H. Domejean, and J. Bibette. Propagation of drop coalescence in a two-dimensional emulsion: A route towards phase inversion. *Physical Review Letters*, 106(21):214502, 2011.
- [193] A. Lai, N. Bremond, and H.A. Stone. Separation-driven coalescence of droplets: an analytical criterion for the approach to contact. *Fluid Mechanics*, 632:97–107, 2009.
- [194] D.Z. Gunes, X. Clain, O. Breton, G. Mayor, and A.S. Burbidge. Avalanches of coalescence events and local extensional flows - stabilisation or destabilisation due to surfactant. *Colloid and Interface Science*, 343(1):79–86, 2010.
- [195] B. Xu, N.-T. Nguyen, and T.N. Wong. Temperature-induced droplet coalescence in microchannels. *Biomicrofluidics*, 6(1):012811–012818, 2012.
- [196] D.E. Angelescu and D. Siess. Microfluidic phase separation. In *IEEE Sensors*, Irvine, CA, USA, 2005.
- [197] P. Mary, V. Studer, and P. Tabeling. Microfluidic droplet-based liquid-liquid extraction. *Analytical Chemistry*, 80(8):2680–2687, 2008.
- [198] S. Pedersen-Bjergaard and K.E. Rasmussen. Bioanalysis of drugs by liquid-phase microextraction coupled to separation techniques. *Journal of Chromatography B*, 817(1):3–12, 2005.
- [199] M. Surmeian, M.N. Slyadnev, H. Hisamoto, A. Hibara, K. Uchiyama, and T. Kitamori. Three-layer flow membrane system on a microchip for investigation of molecular transport. *Analytical Chemistry*, 74(9):2014–2020, 2002.

Bibliography

- [200] A. Smirnova, K. Mawatari, A. Hibara, M.A. Proskurnin, and T. Kitamori. Multiphase laminar flows for the extraction and detection of carbaryl derivative. *Analytica Chimica Acta*, 558(1–2):69–74, 2006.
- [201] M. Tokeshi, T. Minagawa, and T. Kitamori. Integration of a microextraction system: Solvent extraction of a co-2-nitroso-5-dimethylaminophenol complex on a microchip. *Journal of Chromatography A*, 894(1–2):19–23, 2000.
- [202] J.R. Burns and C. Ramshaw. The intensification of rapid reactions in multiphase systems using slug flow in capillaries. *Lab on a Chip*, 1(1):10–15, 2001.
- [203] Microfluidics tutorial University of Washington
www.faculty.washington.edu/yagerp/microfluidicstutorial/hfilter/hfilterhome.htm, accessed June 16th 2012.
- [204] J.P. Brody, T.D. Osborn, F.K. Forster, and P. Yager. A planar microfabricated fluid filter. *Sensors and Actuators A: Physical*, 54(1–3):704–708, 1996.
- [205] M.R. Holl, P. Galambos, F.K. Forster, J.P. Brody, M.A. Afromowitz, and P. Yager. Optimal design of a microfabricated diffusion-based extraction device. *ASME Meeting, DSC59*:189–195, 1996.
- [206] J.P. Brody and P. Yager. Diffusion-based extraction in a microfabricated device. *Sensors and Actuators A: Physical*, 58(1):13–18, 1997.
- [207] M.T.F. Abedul, J.R.B. Rodriguez, A.C. Garcia, and P.T. Blanco. Voltammetric determination of cocaine in confiscated samples. *Electroanalysis*, 3(4-5):409–412, 1991.
- [208] R.A. Scherrer and S.M. Howard. Use of distribution coefficients in quantitative structure-activity relations. *Medicinal Chemistry*, 20(1):53–58, 1977.
- [209] D.C. Scott and J.W. Clymer. Estimation of distribution coefficients from the partition coefficient and pKa. *Pharmaceutical Technology*, 11:30–40, 2002.
- [210] Y.-C. Chang, P. Wägli, V. Paeder, A. Homsy, L. Hvozdar, P.D. van der Wal, J. Di Francesco, N.F. de Rooij, and H.P. Herzig. Cocaine detection by a mid-infrared waveguide integrated with a microfluidic chip. *Lab on a Chip*, 3:3020–3023, 2012.
- [211] N.J. Harrick. Study of physics and chemistry of surfaces from frustrated total internal reflections. *Physical Review Letters*, 4(5):224–226, 1960.
- [212] J. Fahrenfort. Attenuated total reflection: A new principle for the production of useful infra-red reflection spectra of organic compounds. *Spectrochimica Acta*, 17(7):698–709, 1961.
- [213] A.C. McIntyre, M.L. Bilyk, A. Nordon, G. Colquhoun, and D. Littlejohn. Detection of counterfeit scotch whisky samples using mid-infrared spectrometry with an attenuated total reflectance probe incorporating polycrystalline silver halide fibres. *Analytica Chimica Acta*, 690(2):228–233, 2011.

- [214] L. Hvozdar, S. Gianordoli, G. Strasser, W. Schrenk, K. Unterrainer, E. Gornik, C.S.S.S. Murthy, M. Kraft, V. Pustogow, B. Mizaikoff, A. Inberg, and N. Croitoru. Spectroscopy in the gas phase with gaas/algaas quantum-cascade lasers. *Applied Optics*, 39(36):6926–6930, 2000.
- [215] O. Eyal, V. Scharf, S. Shalem, and A. Katzir. Single-mode mid-infrared silver halide planar waveguides. *Optics Letters*, 21(15):1147–1149, 1996.
- [216] J. Hu, V. Tarasov, A. Agarwal, L. Kimerling, N. Carlie, L. Petit, and K. Richardson. Fabrication and testing of planar chalcogenide waveguide integrated microfluidic sensor. *Optical Express*, 15(5):2307–2314, 2007.
- [217] C. Charlton, M. Giovannini, J. Faist, and B. Mizaikoff. Fabrication and characterization of molecular beam epitaxy grown thin-film gaas waveguides for mid-infrared evanescent field chemical sensing. *Analytical Chemistry*, 78(12):4224–4227, 2006.
- [218] K. Seong-Soo, C. Young, and B. Mizaikoff. Miniaturized mid-infrared sensor technologies. *Analytical and Bioanalytical Chemistry*, 390:231–237, 2008.
- [219] J. Faist, F. Capasso, D.L. Sivco, C. Sirtori, A.L. Hutchinson, and A.Y. Cho. Quantum cascade laser. *Science*, 264(5158):553–556, 1994.
- [220] X. Wang, S.-S. Kim, R. Rossbach, M. Jetter, P. Michler, and B. Mizaikoff. Ultra-sensitive mid-infrared evanescent field sensors combining thin-film strip waveguides with quantum cascade lasers. *Analyst*, 137(10):2322–2327, 2012.
- [221] Quantared Technologies, Vienna, Austria
www.quantared.com, accessed June 16th 2012.
- [222] A. Karalis, J.D. Joannopoulos, and M. Soljacic. Efficient wireless non-radiative mid-range energy transfer. *Annals of Physics*, 323(1):34–48, 2008.
- [223] M.-C. Hans, M. Gianella, and M.W. Sigrist. Sensing cocaine in saliva with attenuated total reflection infrared (atr-ir) spectroscopy combined with a one-step extraction method. In *SPIE*, volume 8229, pages 822919 1–822919 7, San Francisco, California, USA, 2012.
- [224] Y.-C. Chang, V. Paeder, L. Hvozdar, J.-M. Hartmann, and H.P. Herzig. Low loss germanium strip waveguides on silicon for the mid-infrared. *Optics Letters*, ID 167799, in press., 2012.
- [225] B. Hinkov, A. Bismuto, Y. Bonetti, M. Beck, S. Blaser, and J. Faist. Single-mode quantum cascade lasers with power dissipation below 1w. *Electronics Letters*, 48(11), 2012.
- [226] Bartels Mikrotechnik, Dortmund, Germany
www.bartels-mikrotechnik.de, accessed June 16th 2012.
- [227] Osmotex, Alpnach, Switzerland
www.osmotex.ch, accessed June 16th 2012.

Bibliography

- [228] L. Perrenoud. Swiss laboratory for doping analyses (LAD). Lausanne, Switzerland, 2012.
- [229] F. Fairbrother and A.E. Stubbs. Studies in electroendosmosis. part vi the bubble-tube methods of measurement. *Chemical Society*, 1935.
- [230] G.I. Taylor. Deposition of a viscous fluid on the wall of a tube. *Fluid Mechanics*, 10:161–165, 1961.
- [231] F.P. Bretherton. The motion of long bubbles in tubes. *Fluid Mechanics*, 10:166–188, 1961.
- [232] LabSmith, Livermore, CA, USA
www.labsmith.com/microfluidicssyringepump.html, accessed June 16th 2012.

Glossary

List of Symbols

A	area
Bo	Bond number
Ca	Capillary number
CF_4	tetrafluoromethane
D	diffusion coefficient
DC	distribution coefficient
e	thickness of lubrication film
ES	extraction system
g	gravitational acceleration
G'	elastic storage modulus
G''	viscous loss modulus
$GaAs$	gallium arsenide
Ge	germanium
h	height
j	flux of matter per surface area
L_0	characteristic length
l	length
m	flow consistency index
n	flow behavior index
p	pressure
PC	partition coefficient
pH	measure of the activity of the (solved) hydrogen ion
pKa	equilibrium constant for a chemical reaction
R	droplet radius
Re	Reynolds number
Si	silicon
t	time
v_0	characteristic velocity
w	width
x	distance in x-direction

z	distance in z -direction
$ZnSe$	zinc selenide
γ	interfacial tension
ξ	shear rate
η	dynamic viscosity
λ	wavelength
Θ	contact angle
ρ	density
τ	shear stress

List of Abbreviations

<i>AFM</i>	atomic force microscopy
<i>APTES</i>	((3-aminopropyl)triethoxysilane)
<i>ATR – IR</i>	attenuated total reflection infrared spectroscopy
<i>CE</i>	capillary electrophoresis
<i>CHUV</i>	Centre Hospitalier Universitaire Vaudois
<i>CTBA</i>	cetyl trimethylammonium bromide
<i>CV</i>	coefficient of variation
<i>DMF</i>	dimethylformamide
<i>DNA</i>	deoxyribonucleic acid
<i>DSS</i>	dioctyl sodium sulfosuccinate
<i>EMPA</i>	Eidgenössische Materialprüfungsanstalt Dübendorf
<i>EPFL</i>	Ecole Polytechnique Fédérale de Lausanne
<i>ES</i>	extraction system
<i>ESPCI</i>	Ecole Supérieure de Physique et de Chimie Industrielles de la ville de Paris
<i>ETHZ</i>	Eidgenössische Technische Hochschule Zürich
<i>FHNW</i>	Fachhochschule Nordwestschweiz
<i>FOTS</i>	((tridecafluoro-1,1,2,2-tetrahydrooctyl)trichlorosilane)
<i>FT – IR</i>	Fourier transformed infrared spectroscopy
<i>IPA</i>	isopropyl alcohol
<i>IR</i>	infrared
<i>IrSens</i>	integrated sensing platform for gases and liquids in the near and mid-infrared range (Nano-Tera project)
<i>ISFET</i>	ion-sensitive field-effect transistor
<i>LAD</i>	Swiss Laboratory for Doping Analyses
<i>LMTS</i>	Microsystems for Space Technologies Laboratory
<i>LOC</i>	lab-on-a-chip
<i>LOD</i>	limit of detection
<i>MCE</i>	microchannel emulsification
<i>MCT</i>	mercury cadmium telluride

<i>MEMS</i>	micro electro-mechanical system
<i>MFFD</i>	microfluidic flow-focusing device
<i>MS</i>	mass spectrometry
<i>μTAS</i>	micro total analysis system
<i>NOA81</i>	Norland Optical Adhesive 81
<i>PC</i>	polycarbonate
<i>PCE</i>	perchloroethylene / tetrachloroethylene
<i>PCR</i>	polymerase chain reaction
<i>PDMS</i>	polydimethylsiloxane
<i>PES</i>	polyethersulfone
<i>PMMA</i>	polymethylmethacrylate
<i>POC</i>	point-of-care
<i>QCD</i>	quantum cascade detector
<i>QCL</i>	quantum cascade laser
<i>QCM</i>	quartz crystal microbalance
<i>SAMLAB</i>	Sensors, Actuators, and Microsystems Laboratory
<i>SAMHSA</i>	Substance Abuse and Mental Health Services Administration, USA
<i>SD</i>	standard deviation
<i>SI – CE</i>	sequential-injection capillary electrophoresis
<i>SMCE</i>	straight-trough microchannel emulsification
<i>SP</i>	surfactant protein
<i>SPME</i>	solid-phase micro-extraction
<i>SPRI</i>	surface plasmon resonance imaging
<i>SU – 8</i>	high aspect ratio epoxy based photoresist
<i>THF</i>	tetrahydrofuran
<i>UniNe</i>	Université Neuchâtel
<i>UPLC – MS</i>	ultra performance liquid chromatography - mass spectrometer
<i>UV</i>	ultra violet
<i>VCSEL</i>	vertical-cavity surface-emitting laser
<i>XPS</i>	X-ray photoelectron spectroscopy

Acknowledgements

In 2009 I hesitated to accept the PhD position in the Swiss French part, but in retrospect this was definitely one of the best decisions in my life and I would not miss a single day! In SAMLAB I found a very inspiring environment where high level research meets the atmosphere of the Mediterranean way of life, what made me rich in scientific and social experiences.

First of all, I like to thank my thesis director Prof. Nico de Rooij for giving me the opportunity to work in the stimulating environment of SAMLAB, for providing a lab with excellent infrastructure, and for giving me the chance to interact with specialists in the field of microtechnology and to present my research at many international conferences all around the world.

My gratitude goes to my co-director and supervisor Alexandra Homsy. I thank her for the introduction to the interesting field of microfluidics, for her careful supervision and guidance, her trust, and the time and efforts she devoted to our project IrSens. I also highly appreciated the flexibility and personal responsibility I had during the last years.

I also gratefully acknowledge Prof. Jürgen Brugger, Dr. Bastian E. Rapp, Dr. Pierre Jouy, and Prof. Herbert Shea for kindly accepting to be the co-examiners in my PhD exam.

Special thanks also go to the rest of SAMLAB's microfluidic team, Luca Ribetto and Blaise Guélat for the great collaboration, for sharing know-how, experiences, and resources.

Another important personality in SAMLAB is Peter van der Wal. Especially during the last year he did a great job as my first-point-of-contact. I like to thank him for his essential support for chemical issues, all the scientific and non-scientific suggestions, the long discussions, and the thousands of nasty but finally fruitful questions.

I also should express my gratitude to Karine Frossard for the incredible efficient support with administrative issues and to my office mate Claudio Novelli for the IT support and the great time we had together sharing the office.

In SAMLAB I met colleagues with valuable advice and at the same time wonderful open-minded friends from all around the world. I am grateful for all the time we spent together studying, experimenting, sharing ideas and experiences, but also for the leisure time at aperitifs, at festivals, at BBQs, at concerts as well as at sport or excursions. Furthermore, SAMLAB people were a great and rich source of saliva samples for my experiments. I would like to thank Terunobu Akyiama, Dara Bayat, Roland Bitterli, Danick Briand, Michael Canonica, El Hadji Malick Camara, Jérôme Courbat, David de Koninck, Cécile Fattebert, Olivier Frey, Franz

Acknowledgements

Friedrich, Sebastian Gautsch, Nicolas Golay, Rokhaya Gueye, Don Isarakorn, Pattanaphong Janphuang, Fabio Jutzi, Sébastien Lani, Robert Lockhart, Frédéric Loizeau, Olivier Lässer, Francisco Molina Lopez, Jonathan Masson, Giorgio Mattana, Wilfried Noell, Yves Pétremand, Sotiria Psoma, Jason Ruan, Rahel Strässle, Sara Talaei, Andres Vasquez Quintero, Peter Vettiger, Stefan Weber, and Yexian Wu.

Moreover, I also like to mention people from LMTS sharing labs with us: Prof. Herbert Shea, Samin Akbari, Seun Araromi, Caglar Ataman, Subha Chakraborty, Simon Dandavino, Kaustav Ghose, Luc Maffli, Muhamad Niklaus, Myriam Poliero, Andres Punning, Pille Rinne, Samuel Rosset, Jun Shintake, and Vinu Venkatraman.

I also got the opportunity to supervise the EPFL master students Loïc Hans and Allen Peters and like to thank them for their work and contribution to our project.

Thank also goes to people of CSEM; to division C for fabrication support, to the Microscopy Service of Massoud Daddras and Mireille Leboeuf for the AFM images and special thanks go to Nicolas Blondiaux of division N for the inputs and discussions about surface chemistry and wetting behavior.

The frame of my thesis was given by the Nano-Tera project IrSens of the Swiss National Science Foundation, which is acknowledged here for the financial support. We also acknowledge the SNF R'Equip program for the funding of the high speed data acquisition test bench.

It was a pleasure to work with many motivated collaborators on this Nano-Tera project towards the same goal. I like to thank especially a couple of institutes we had close collaboration with: I sincerely thank Kerstin Hans, Michele Gianella, and Prof. Markus Sigrist of ETHZ/D-PHYS/IQE/LSSL for the preliminary studies for cocaine detection and the system integration, Yu-Chi Chang, Joab Di Francesco, Lubos Hvozدارa, and Prof. Hans Peter Herzig of EPFL/STI/IMT/OPT for the fabrication of optical wave guides and Pierre Jouy, Yargo Bonetti, and Prof. Jérôme Faist of ETHZ/D-PHYS/IQE/QOG mainly for the project coordination.

I also appreciate the inputs and the discussions with the polymer specialist Bastian Rapp of the Institute of Microstructure Technology at the Karlsruhe Institute of Technology in Germany, and the exchange of know-how about the processing of UV-glue for microfluidic devices with Marie-Caroline Jullien and Fabrice Monti of the group of Prof. Patrick Tabeling of the Microfluidics, MEMS and Nanostructures Laboratory at the ESPCI Paris, France.

I would also like to acknowledge Laure Aeschmann of NanoWorld for providing the nanostructures for the replication tests of our rapid prototyping method.

I also like to thank Laurent Perrenoud of the Swiss Laboratory for Doping Analyses (LAD) in Lausanne for the efficient collaboration for the cocaine reference measurements using their state of the art mass spectrometer. Thanks goes also to Christian Berchtold of the Institute of Chemistry of ETH in Zürich for further cocaine measurements and the development of a new detection routine.

Acknowledgements

Finally, I would like to thank all my friends and family for the unlimited support, the loyalty and abundance of patience throughout my years of study. My sister Claudine and my brother Michel particular for discussions prior to tough choices, for being close, even if being physically at the other end of the world. Special thank goes to my parents Irmgard and Georges, who support me, whenever and whatever I decide to do. I appreciate their infinite trust and the possibility to do, whatever I am up to. They managed to put me on a track; I am persuaded that it is still the right one.

Philip Wägli

Swiss, born 1983

philip.waegli@a3.epfl.ch

Education

- 06/2009 – 12/2012 **École Polytechnique Fédérale, Lausanne/Neuchâtel**
Doctoral School in Microsystems and Microelectronics
PhD student in The Sensors, Actuators and Microsystems Laboratory
project: IrSens – Integrated infrared sensing platform for liquids
Research on enhanced microfluidic liquid-liquid extraction systems
PhD Thesis: *"Integrated Microfluidic Liquid-Liquid Extraction for Detection of Cocaine in Human Saliva"*
- 10/2006 – 09/2008 **Eidgenössische Technische Hochschule, Zürich**
Master of Science ETH in Mechanical Engineering
Focus specialization in Micro-/Nanosystems and Biomedical Engineering
Master Thesis: *"Towards All-Polymer μ -TAS: Analysis of the Influence of Humidity, Varying Concentrations of Ethanol in Water, and Different Biomolecules on SU-8 Polymer Micro Resonators"*
Semester Thesis: *"DNA-Assisted Micro/Nano Pattern Reproduction Process"*
- 10/2002 – 07/2005 **Eidgenössische Technische Hochschule, Zürich**
Bachelor of Science ETH in Mechanical Engineering
Focus specialization in Micro-/Nanosystems
Bachelor Thesis: *"Fabrication and Characterization of Micromechanical Test Structures for the Determination of Intrinsic Thin Film Stress in Polyimide"*
- 08/1998 – 07/2002 **Gymnasium Kirchenfeld, Bern**
Matura in the department of math and natural science
Matura Thesis: *"Design and Visualization of a Building"*

Work Experience

- 02/2009 – 5/2009 **Chair of micro and Nanosystems ETHZ, Zürich**
project: WIPSS - wireless implantable passive strain sensor
Development of a fabrication process for polymer MEMS
- 01/2007 – 12/2007 **Micro- and Nanoscience Platform (MNSP), Zürich**
Build-up of a data base of leading companies in micro- and nanoscience
assistance for the conference "INDUSTRY DAY 2008"

Languages

- | | |
|---------|--|
| German | native language |
| English | conversational - around working knowledge, C1* |
| French | conversational, B2/C1* |
| Spanish | basic, A1* |
- *Common European Framework of Reference for Language

List of Publications

Publications related to this thesis

Y.-C. Chang, P. Wägli, V. Paeder, A. Homsy, L. Hvozدارa, P. van der Wal, J. Di Francesco, N.F. de Rooij and H.P. Herzig. Cocaine detection by a mid-infrared waveguide integrated with a microfluidic chip. *Lab on a Chip*, 12:3020–3023, 2012. doi:10.1039/C2LC40601B.

P. Wägli, A. Homsy and N.F. de Rooij. Norland optical adhesive (NOA81) microchannels with adjustable wetting behavior and high chemical resistance against a range of midinfrared-transparent organic solvents. *Sensors and Actuators B: Chemical*, 156(2):994–1001, 2011. doi: 10.1016/j.snb.2011.02.005.

P. Wägli, Y.-C. Chang, P.D. van der Wal, L. Hovzdara, A. Homsy, H.P. Herzig and N.F. de Rooij. Droplet based liquid-liquid extraction and on-chip IR-waveguide-spectroscopy detection of cocaine in human saliva. In *International Conference on Miniaturized Systems for Chemistry and Life Sciences (MicroTAS)*, Okinawa, Japan, 2012.

P. Wägli, A. Homsy and N.F. de Rooij. UV-curable adhesive as the low-cost material of choice for microfluidic forensic applications. In *International Meeting on Chemical Sensors (IMCS)*, Nürnberg, Germany, 2012. doi: 10.5162/IMCS2012/P1.9.5.

P. Jouy, Y. Bonetti, K. Hans, M. Gianella, M. Sigrist, M. Mangold, L. Emmenegger, P. Wägli, A. Homsy, Y.-C. Chang, J. Di Francesco, L. Hvozدارa, H.P. Herzig, H. Looser, D. Hofstetter, J. Faist and B. Tuzson. Liquid and gas spectroscopy platform with QCLs and QCDs. In *International Quantum Cascade Lasers School & Workshop*, Baden near Vienna, Austria, 2012.

P. Wägli, A. Homsy and N.F. de Rooij. Improved method for liquid-liquid extraction on lowcost polymer chips. In *Gordon Research Conference - Physics & Chemistry of Microfluidics*, Waterville Valley, USA, 2011.

P. Wägli, A. Homsy and N.F. de Rooij. UV-curable glue (NOA81) for fabrication of a closed microfluidic channel with hydrophilic and hydrophobic surfaces. In *Conference on Advances in Microfluidics and Nanofluidics & Asia-Pacific International Symposium on Lab on Chip*, Singapore, 2011.

List of Publications

Y.-C. Chang, V. Paeder, P. Wägli, L. Hvozدارa and A. Homsy. Mid-infrared waveguide evanescent field chemical sensor for liquids. In *Conference on Lasers and Electro Optics - European Quantum Electronics Conference (CLEO Europe)*, Munich, Germany, 2011.

Y.-C. Chang, V. Paeder, J.-M. Hartmann, P. Wägli and A. Homsy. Singlemode mid-infrared waveguide for evanescent sensor scheme in liquids. In *International Conference on Microtechnologies in Medicine and Biology (MMB)*, Lucerne, Switzerland, 2011.

P. Wägli, A. Homsy and N.F. de Rooij. Norland optical adhesive (NOA81) microchannels with adjustable surface properties and high chemical resistance against IR-transparent organic solvents. *Procedia Engineering*, 5:460–463, 2010. doi: DOI: 10.1016/j.proeng.2010.09.146.

P. Wägli, B. Guélat, A. Homsy and N.F. de Rooij. Microfluidic devices made of UV-curable glue (NOA81) for fluorescence detection based applications. In *International Conference on Miniaturized Systems for Chemistry and Life Sciences (MicroTAS)*, Groningen, Netherlands, 2010.

A. Homsy, L. Ribetto, B. Guélat, P. Wägli and N.F. de Rooij. Microfluidics. In *Concertation and Consultation Workshop on Micro-Nano-Bio Convergence Systems (MNBS)*, Neuchâtel, Switzerland, 2010.

Publications not related to this thesis

F. Umbrecht, P. Wägli, S. Dechand, F. Gattiker, J. Neuenschwander, U. Sennhauser and C. Hierold. Wireless implantable passive strain sensor: design, fabrication and characterization. *Journal of Micromechanics and Microengineering*, 20(8):085005, 2010.

S. Schmid, P. Wägli and C. Hierold. Biosensor based on all-polymer resonant microbeams. In *MEMS Conference*, Sorrento, Italy, 2009.

S. Schmid, P. Wägli and C. Hierold. All-polymer microstring resonant humidity sensor with enhanced sensitivity due to change of intrinsic stress. In *EUROSENSORS Conference*, Dresden, Germany, 2008.